CIVIL ENGINEERING STUDIES
Illinois Center for Transportation Series No. 11-092
UILU-ENG-2011-2018
ISSN: 0197-9191

TRANSFER AND DEVELOPMENT LENGTHS IN PRESTRESSED SELF-CONSOLIDATING CONCRETE BRIDGE BOX AND I-GIRDERS

Prepared By

Bassem Andrawes
Andrew Pozolo

University of Illinois at Urbana-Champaign

Research Report ICT-11-092

A report of the findings of
ICT-R27-56
Transfer and Development Lengths in Prestressed Self-Consolidating Concrete Bridge Box and I-Girders

Illinois Center for Transportation

September 2011

Technical Report Documentation Page

1. Report No.	2. Government Accession No.	3. Recipient's Catalog No.
FHWA-ICT-11-092		

4. Title and Subtitle	5. Report Date
Transfer & Development Lengths in Prestressed Self-Consolidating Concrete Bridge Box and I-Girders	September 2011
	6. Performing Organization Code
7. Author(s)	8. Performing Organization Report No.
Bassem Andrawes and Andrew Pozolo	ICT-11-092 UILU-ENG-2011-2018
9. Performing Organization Name and Address	10. Work Unit (TRAIS)
Illinois Center for Transportation Department of Civil and Environmental Engineering University of Illinois at Urbana-Champaign 205 N. Mathews Ave, MC 250 Urbana, IL 61801	11. Contract or Grant No. ICT R27-56
	13. Type of Report and Period Covered
12. Sponsoring Agency Name and Address	
Illinois Department of Transportation Bureau of Materials and Physical Research 126 E. Ash Street Springfield, IL 62704	14. Sponsoring Agency Code

15. Supplementary Notes

16. Abstract

Self-consolidating concrete (SCC) is a workable yet stable concrete which flows easily and consolidates under its own weight. Its unique properties can substantially reduce the labor required to pour complex or heavily-reinforced structural members. Over the past decade, the American precast industry has taken significant strides to adopt SCC in commercial projects, though concern about early-age bond behavior has limited the material's application in prestressed members. A general need remains for further research on the bond properties of SCC in full-scale prestressed members. The wide array of specimen types and SCC mixture designs utilized in practice further underscores this need.

To explore the application of SCC in Illinois bridge construction, the Illinois Department of Transportation (IDOT) and Illinois Center for Transportation (ICT) sponsored a three-phase study investigating the bond behavior of steel strands in pretensioned bridge box and I-girders. In the first phase, 56 pullout tests were conducted to compare the performance of seven-wire strands embedded in SCC to that of strands in normally-consolidated concrete (NCC) blocks. In the second phase, transfer lengths of prestressing strands in two 28-ft. SCC hollow box girders and two 48-ft. SCC I-girders were determined experimentally. In the third phase, development lengths of strands in the four girders were determined through a series of iterative flexural tests. This report details the experimental program for the study's three phases and compares results to current requirements of the American Concrete Institute (ACI) and the American Association of State Highway and Transportation Officials (AASHTO). The results of this study may prove fundamental to the safe application of SCC within the state of Illinois' prestressed concrete industry.

17. Key Words	18. Distribution Statement
Self-Consolidating Concrete, Full-scale Girders, Bond Behavior, Pullout Tests, Transfer Length, Development Length	No restrictions. This document is available to the public through the National Technical Information Service, Springfield, Virginia 22161.

19. Security Classif. (of this report)	20. Security Classif. (of this page)	21. No. of Pages	22. Price
Unclassified	Unclassified	101	

ACKNOWLEDGMENT / DISCLAIMER

This publication is based on the results of ICT-R27-56, **Transfer and Development Lengths in Prestressed Self-Consolidating Concrete Bridge Box & I-Girders**. ICT-R27-56 was conducted in cooperation with the University of Illinois at Urbana-Champaign; the Illinois Center for Transportation; the Illinois Department of Transportation, Division of Highways; and the U.S. Department of Transportation, Federal Highway Administration.

EXECUTIVE SUMMARY

Self-consolidating concrete (SCC) is a workable yet stable concrete which flows easily and consolidates under its own weight. Its unique properties can substantially reduce the labor required to pour complex or heavily-reinforced structural members. Over the past decade, the American precast industry has taken significant strides to adopt SCC in commercial projects, though concern about early-age bond behavior has limited the material's application in prestressed members. A general need remains for further research on the bond properties of SCC in full-scale prestressed members. The wide array of specimen types and SCC mixture designs utilized in practice further underscores this need. A thorough understanding of SCC's bond strength, including its impact on transfer and development lengths in prestressed members, is essential to safely implement the relatively new material in prestressed design.

To explore the application of SCC in Illinois bridge construction, the Illinois Department of Transportation (IDOT) and Illinois Center for Transportation (ICT) sponsored a three-phase study investigating the bond behavior of steel strands in pretensioned bridge box and I-girders. In the first phase, 56 pullout tests were conducted to compare the performance of seven-wire strands embedded in SCC to that of strands in normally-consolidated concrete (NCC) blocks. In the second phase, transfer lengths of prestressing strands in two 28-ft. SCC hollow box girders and two 48-ft. SCC I-girders were determined experimentally. In the third phase, development lengths of strands in the four girders were determined through a series of iterative flexural tests. Testing of hollow box girders was particularly notable because of their absence from previous large-scale studies on bond of SCC and their frequent use in bridge construction. Additionally, the design of hollow box girders is characterized by high strand concentration and low concrete cover, both of which may negatively impact bond.

This report details the experimental program for the study's three phases and compares results to current requirements of the American Concrete Institute (ACI) and the American Association of State Highway and Transportation Officials (AASHTO). The results of this study may prove fundamental to the safe application of SCC within the state of Illinois' prestressed concrete industry.

TABLE OF CONTENTS

CHAPTER 1 INTRODUCTION

1.1 MOTIVATION FOR RESEARCH PROJECT

Self-consolidating concrete (SCC) is a workable yet stable concrete which flows easily and consolidates under its own weight. Its unique properties can substantially reduce the labor required to pour complex or heavily reinforced structural members. Over the past decade, the United States (US) precast industry has taken significant strides to adopt SCC in commercial projects, recognizing its potential to reduce material costs, labor costs, and turn-over time. Concern about early-age bond behavior, however, has thus far limited the material's application in prestressed members. As studies assessing bond behavior in SCC have shown wide variability in their results, a general need remains for further research on the bond properties of SCC in full-scale prestressed members. The wide array of specimen types and SCC mixture designs utilized in practice further underscores this need. A thorough understanding of SCC's bond strength, including its impact on transfer and development lengths in prestressed members, is essential to safely implement SCC in prestressed design.

To explore the application of SCC in Illinois bridge construction, the Illinois Department of Transportation (IDOT) and Illinois Center for Transportation (ICT) sponsored a three-phase study investigating the bond behavior of steel strands in pretensioned bridge box and I-girders. In the first phase, 56 pullout tests were conducted to compare the performance of seven-wire strands embedded in SCC to that of strands in normally-consolidated concrete (NCC) blocks. In the second phase, transfer lengths of prestressing strands in two 28-ft. SCC hollow box girders and two 48-ft. SCC I-girders were determined experimentally. In the third phase, development lengths of strands in the four girders were determined through a series of iterative flexural tests. Testing of hollow box girders was particularly notable because of their absence from previous large-scale studies on bond of SCC and their frequent use in bridge construction. Additionally, the design of hollow box girders is characterized by high strand concentration and low concrete cover, both of which may negatively impact bond.

This report details the experimental program for the study's three phases and compares results to current requirements of the American Concrete Institute (ACI) and the American Association of State Highway and Transportation Officials (AASHTO). The results of this study may prove fundamental to the safe application of SCC within the state of Illinois' prestressed concrete industry.

1.2 REPORT OUTLINE

The primary goal of this research is to experimentally assess the bond behavior of prestressing strands in full-scale SCC members. This report presents results of pullout, transfer length, and development length tests conducted on steel strands in SCC specimens from 2008-2010 at the University of Illinois at Urbana-Champaign (UIUC).

Chapter 1 discusses the motivation for conducting large-scale tests on prestressed SCC bridge girders. The three phases of the IDOT-sponsored study are presented.

Chapter 2 succinctly discusses the properties of SCC, code requirements for transfer and development lengths, and results from recent studies concerned with bond behavior of prestressed SCC specimens. A more thorough review of said studies may be found in the synthesis review conducted by Andrawes et al. (2009) under ICT project R27-36.

Chapter 3 presents experimental results from pullout tests conducted on 0.5-in. diameter, low-relaxation seven-wire steel strands embedded in SCC and NCC blocks. The tests are used to characterize strand behavior in SCC as acceptable when compared to behavior in NCC.

Chapter 4 outlines the design, analysis, and fabrication of four full-scale SCC hollow box and I-girders. Theoretical prestress losses, shear capacities, and flexural capacities are presented.

Chapter 5 describes the transfer length measurements taken over 28 days for the four SCC girders. Experimental results are compared to ACI and AASHTO code requirements.

Chapter 6 details the flexural tests utilized to evaluate development length in the girders. Experimental results are compared to code requirements, and the girders' structural performance is compared to theoretical capacities.

Chapter 7 summarizes the major findings of the experimental program and provides possibilities for future work.

Four appendices follow the main text of this report. Appendix A contains the force-displacement responses from all 56 pullout tests. Appendix B provides fabrication drawings of the full-scale girder specimens; all pertinent reinforcement details and girder dimensions are included. Appendix C presents the surface strain profiles obtained for transfer length measurements in all four girders. Finally, Appendix D contains final damage and cracking patterns for flexural test specimens.

CHAPTER 2 LITERATURE REVIEW

2.1 BASICS OF SELF-CONSOLIDATING CONCRETE

Developed by researchers concerned with the durability of Japan's concrete infrastructure and the declining number of skilled laborers in Japan's workforce, self-consolidating concrete emerged as a structural material in the late 1980's (Okamura and Ouchi, 2003). By altering typical concrete mixture proportions and incorporating various chemical admixtures, researchers created a concrete which would easily flow and consolidate under its own weight, drastically reducing the labor required in the casting process. Japan and Europe soon began implementing SCC in large-scale applications, particularly in bridges (Ouchi et al. 2003). Over the past decade, the United States precast industry has taken significant strides to adopt the material in prestressed design, recognizing its tremendous potential to reduce fabrication time, labor, and cost.

2.1.1 Definition and Plastic Properties of SCC

The U.S. Precast/Prestressed Concrete Institute (PCI) defines SCC as "a highly workable concrete that can flow through densely reinforced or complex structural elements under its own weight and adequately fill voids without segregation or excessive bleeding without the need for vibration," (PCI 2003-a). The PCI classifies a concrete mixture as SCC if it meets specified requirements for three criteria: (1) filling ability, (2) passing ability, and (3) stability. Adequate filling ability ensures concrete can completely flow under its own weight without vibration into formwork. Adequate passing ability ensures concrete can flow through openings near the size of its coarse aggregate without experiencing blockage. Passing ability is particularly important in specimens with irregular shapes or dense reinforcement. Finally, stability refers to concrete's resistance to segregation, or its ability to retain homogenous characteristics during placement. Table 2.1 lists suggested test methods for evaluating plastic properties of SCC (PCI 2003-a).

Table 2.1. Test Methods for Determining SCC Plastic Properties

Test Method	Measured Characteristics
T_{50}	Relative viscosity
U-Box	Passing ability, self-consolidation
L-Box, J-Ring	Passing ability, fluidity
Visual Stability Index (VSI)	Segregation resistance
Slump Flow, Inverted Slump Flow	Flow separation resistance

The unique plastic characteristics of SCC are attained by altering the proportions of traditional concrete constituents including cement, water, coarse aggregate, and fine aggregate. A typical volume distribution of SCC mixture constituents is shown in Figure 2.1. When compared to NCC mixtures, SCC mixtures typically have lower aggregate volumes, smaller coarse aggregate sizes, and higher cementitious material contents. High-range water-reducers (HRWRs) or superplasticizers enhance the flow ability of SCC. Low aggregate volume and high flow ability would tend to promote segregation in the concrete; as such, mineral and chemical admixtures are incorporated to enhance segregation resistance. Mineral admixtures may include silica fume, fly ash, ground granulated blast-furnace slag, and pulverized limestone (Lange et al. 2008). Chemical additives designed to prevent segregation are known as viscosity modifying admixtures (VMAs).

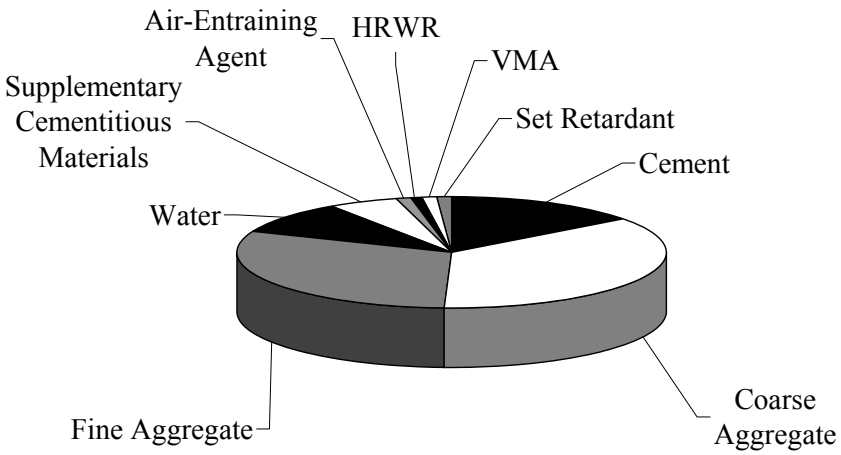

Figure 2.1. Typical SCC mixture constituents.

2.1.2 Hardened Properties of SCC

The primary advantages of SCC are clearly derived from its plastic properties; however, these benefits would be negated if the hardened properties of SCC could not match those of traditional concrete. Lower coarse aggregate volumes suggest that the modulus of elasticity in SCC would be lower than in similar strength NCC (Bonen and Shah, 2007). Additionally, aggregate significantly impacts long-term concrete shrinkage since it restrains volume change within the cement paste (Neville 1996). This could, in turn, affect prestress losses in SCC specimens. In a study by Schindler et al. (2007), hardened properties were measured experimentally on cylinders cast with twenty-one SCC mixtures with varying water/cement (w/c) ratios, sand-to-total aggregate ratios, and cementitious material types. The researchers concluded that 112-day drying shrinkage strains in the SCC mixtures were of the same order of magnitude or less than corresponding strains in control specimens cast with NCC. The sand-to-total aggregate ratios appeared to have no significant effect on 112-day drying shrinkage strains or concrete compressive strength at any age. Finally, the initial modulus of elasticity in SCC was less than that in control specimens with comparable initial strength. After 56 days, however, moduli in SCC and NCC were comparable.

2.2 TRANSFER AND DEVELOPMENT LENGTH DEFINITIONS

A pretensioned concrete specimen is fabricated by casting concrete around prestressed strands, allowing the concrete to harden, and then releasing the strands. Upon release, specimens rely on bond between strands and concrete in transfer zones of the specimen to develop the imparted prestress. Three factors which may contribute to bond are adhesion between steel and concrete, friction between steel and concrete, and mechanical interlock (Janney 1954; Hanson and Kaar, 1959). Since strands move relative to concrete upon release, it is generally accepted that bond due to pure adhesion is negligible; thus, friction and mechanical resistance are the primary contributors to bond. When strands are initially stressed, they constrict due to Poisson's effect; when released, they attempt to return to their original size, resulting in high radial pressure and frictional resistance. Additionally, the outer wires of helical strands tend to twist when released from tension; concrete surrounding the strands prevents twisting through mechanical interlock, thereby increasing bond. Specimens with adequate bond are able to reach their full shear and flexural design capacities without experiencing bond-slip failure at strand locations. Current design code requirements for transfer and development lengths were derived primarily from the work of Hanson and Kaar (1959).

The ACI defines transfer length as “the distance over which the strand must be bonded to the concrete to develop the effective prestress,” (ACI Committee 318, 2008). This distance is illustrated in Figure 2.2, which shows a theoretical strand stress profile at the end of a prestressed specimen. The AASHTO LRFD design specifications require transfer lengths equal to $60d_b$, where d_b is the diameter of the strand (AASHTO 2004). The Chapter 11 ACI shear design guidelines, meanwhile, require transfer lengths equal to $50d_b$ (ACI Committee 318). Additionally, ACI flexural guidelines calculate transfer length as in Equation 2-1, where f_{pe} is the effective prestress (ksi) and d_b is given in inches.

$$L_t = \frac{f_{pe} d_b}{3} \qquad \text{(Eq. 2-1)}$$

Development length is defined by the ACI as the transfer length plus “the additional length over which the strand must be bonded so that a stress f_{ps} may develop in the strand at nominal strength,” (ACI Committee 318). This is quantified in Equation 2-2, where f_{ps} is the stress in the prestressed reinforcement at nominal strength (ksi), and f_{pe} (ksi) and d_b (in.) were previously defined. The second term in Eq. 2-2 is deemed the flexural bond length and is illustrated in Figure 2.2.

$$L_d = \frac{f_{pe} d_b}{3} + \left(f_{ps} - f_{pe} \right) d_b \qquad \text{(Eq. 2-2)}$$

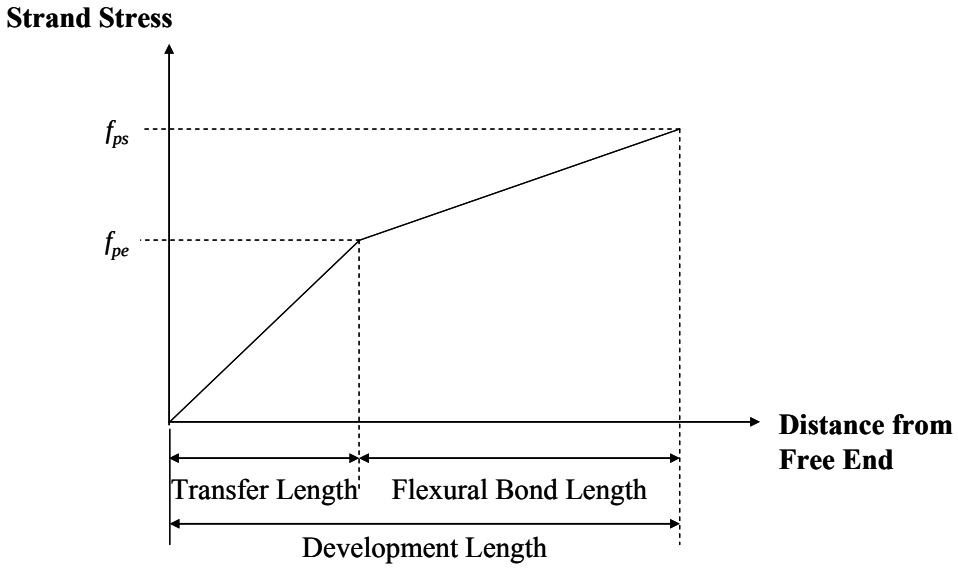

Figure 2.2. Strand stress variation along beam length.

Equation 2-2 was first incorporated in the 1963 ACI Building Code and was adopted by AASHTO in 1973 (Buckner 1995). Later, Cousins et al. (1986) completed a study in which experimental transfer and development lengths of coated, weathered strands were found to exceed standard design predictions by a significant margin. As a result of this study and recognizing code requirements for bond were based on tests using outdated materials, the US Federal Highway Administration (FHWA) issued a memorandum stating, among other items, that development length shall be taken as 1.6 times that which is determined by Equation 2-2. The 1.6 factor was formally presented at a joint meeting between the

AASHTO Technical Committee for Prestressed Concrete and PCI Bridge Committee and, at present, remains in the AASHTO LRFD (2004) specifications.

2.3 EXPERIMENTAL TEST METHODS

2.3.1 Slump Flow Test – ASTM C1611/C1611M-09b

The slump flow test is designed to assess filling and passing ability of SCC with coarse aggregate size no greater than one inch. The test uses the standard cone defined in Section 5 of ASTM C143/C143M-10, oriented in either the normal or inverted position and held firmly in place at the center of a smooth, non-absorbent, rigid board. The cone is filled with concrete in a continuous manner, and the SCC is not tamped or vibrated. The cone is raised over three seconds to a height of nine inches, during which time the fluid SCC expands outward from the board's center; this process is shown in Figure 2.3. Two diameter measurements are taken after the concrete stops flowing; the first is the largest diameter of the concrete patty, and the second corresponds to the diameter perpendicular to the first. The average of these two values is the slump flow, which should be reported to the nearest half-inch. SCC mixtures typically have slump flows between 22 in. and 30 in. If the two measured diameters are greater than two inches apart, the test must be repeated.

Figure 2.3. Slump flow test conducted on fresh SCC.

The T_{50} test noted in the Appendix of ASTM C1611/C1611M-09b may be performed in conjunction with the slump flow test to evaluate the relative viscosity of SCC. The T_{50} value is the time it takes for the outer edge of SCC to reach a diameter of 20 inches. Values typically range between 2-5 seconds (W.R. Grace & Co. 2005).

2.3.2 Visual Stability Index (VSI) Test

The VSI ranking for SCC mixtures is a subjective visual characterization of concrete stability based on surface bleeding, mortar halos, and aggregate distribution. The test method is described in the Appendix of ASTM C1611/C1611M-09b. The VSI assessment should be made immediately after SCC stops flowing in a slump flow test. A VSI ranking of 0 indicates high-quality SCC with no bleeding; a ranking of 1 indicates acceptable SCC with slight bleeding or surface sheen; a ranking of 2 indicates borderline SCC with a visible mortar halo and surface sheen; finally, a ranking of 3 implies unacceptable SCC with uneven aggregate distribution and visible mortar halo. A mixture with a VSI ranking of 2 should be retested and evaluated by quality control personnel to determine acceptability, while a mixture with a VSI ranking of 3 should be rejected.

2.3.3 J-Ring Test – ASTM C1621/C1621M-09b

Designed to measure the passing ability of SCC, the J-Ring test follows the same procedure as the slump flow test, albeit with a J-Ring placed at the center of the board surrounding the slump cone. The 12-inch diameter ring rests atop sixteen 0.625-in. diameter rods that mimic reinforcement through which SCC would pass in a structural member. Once filled, the cone is raised over three seconds to a height of nine inches, during which time the SCC expands outward and through the J-ring as shown in Figure 2.4. The J-Ring flow is taken as the average diameter of the concrete patty in the same manner as the original slump flow. J-Ring and original slump flows should be no greater than two inches apart.

Figure 2.4. J-Ring test conducted on fresh SCC.

2.3.4 L-Box Test

In the same spirit as the J-Ring test, the L-box test assesses the filling and passing ability of SCC. A typical L-box is shown in Figure 2.5 and comprises a vertical column separated from a horizontal box by a movable gate and reinforcement bars. The rebar configuration near the gate should represent the reinforcement expected in the specimens for which the SCC is being mixed. The horizontal portion of the L-box is approximately 32 inches long and 8 inches wide, while the vertical column is 4 inches wide. With the gate closed, the vertical L-box column is filled with concrete in a continuous manner; the concrete is not tamped or vibrated. After removing the gate, the concrete height at the end of the horizontal box is compared to the concrete height at the beginning of the horizontal box. The ratio between end and beginning heights should be greater than 75%. Visual inspection is also used to assess aggregate distribution and SCC passing ability.

Figure 2.5. L-box test conducted on fresh SCC.

2.3.5 Modified Moustafa Pullout Test

The PCI recommends the Moustafa pullout test to qualify bond characteristics of strands embedded in concrete as satisfactory (PCI 2003-a). Moustafa first performed pullout tests on lifting loop strands in 1974, considering 3/8-inch, 7/16-inch, and 1/2-inch diameter strands with embedment lengths between 12-30 inches (Moustafa 1974). Each strand was loaded by hydraulic jacks, and the relative displacement between concrete and strand was monitored throughout loading until failure occurred. Since no bond quality standard exists for prestressing strands, Moustafa's method was adopted with slight modifications in subsequent research by Rose and Russell (1996) and Logan (1997) to study bond performance of strands intended for pretensioned applications. For consistency, the latter studies utilized 1/2-inch diameter strands embedded 18 inches in large block specimens. The pullout test is attractive given its simplicity and relatively low cost.

The PCI (2003-a) directly refers to Logan (1997) for a detailed outline of the modified Moustafa method. In his study, Logan tested 1/2-inch diameter strands embedded in blocks cast with the conventional concrete mixture shown in Table 2.2. The strands were obtained from six different manufacturers. Logan found the pullout test to accurately predict transfer and development characteristics in pretensioned specimens. Based on experimental results, acceptable 1/2-inch diameter strands should be capable of resisting at least 16 kip prior to slip initiation and 36 kips prior to failure. A summary of recommendations and guidelines for conducting the modified pullout test is presented below:

a) The test is recommended for concrete with compressive strength between 3500-5900 psi. The concrete pullout block is typically 24 inches wide, 24 inches deep, and 36 inches long with strands embedded 18 inches. However, block dimensions are flexible and depend on the number of tested strands.

b) A hydraulic jack with a minimum travel length of 12 inches should be used to pull the strands. The maximum load shall not exceed 50 kips.

c) The jacking load is applied gradually (20 kip/min) until strand cannot carry additional load.

d) Four types of data should be recorded during the test: (1) maximum load capacity, (2) approximate load at first slip, (3) approximate pullout distance at maximum load, and (4) a general depiction of failure. Typically, poorly bonded strand would slip 8-10 inches before reaching its ultimate load, but well-bonded strand would slip only 1-2 inches.

e) The test should be repeated as many times as needed and the data obtained should be used to compute an average failure load and standard deviation for each strand group.

Table 2.2. Normally-Consolidated Concrete Mixture from Logan (1997)

Material	Quantity (per yd^3)
Type III Cement	660 lbs
Crushed Gravel	1900 lbs
Sand	1100 lbs
Water Reducer	26 oz.
Water	35 gal
W/C Ratio	0.44

2.3.6 Transfer Length via 95% Average Maximum Strain Method (95% AMS)

Two methods are commonly used to experimentally measure transfer length: (1) the "draw-in" or "end-slip" method, and (2) the 95% Average Maximum Strain method (Russell and Burns, 1993). The former method, which was not utilized in this study, calculates transfer length based on the relative displacement between strand and concrete after prestress release at the free ends of prestressed specimens; discussion of this method may be found in Balazs (1993) and Marti-Vargas et al. (2007). The latter method, which was utilized in this study, measures transfer length based on strain measurements throughout the transfer zone of a prestressed specimen. The procedure for the 95% AMS is detailed as follows:

a) Prior to prestress release, target points are affixed within a transfer zone of a specimen. The points are attached to the concrete surface at a depth equal to the strands' center of gravity. Initial measurements record the distance between each target point.

b) Immediately after prestress release and at any age thereafter, measurements are taken between all target points to determine the strain profile within the transfer zone.

c) Data may be smoothed by taking the strain at point "*a"* as the average of the strains at three adjacent points centered at "*a*" [e.g. $\varepsilon_{a,\,smooth} = 1/3 \cdot \sum (\varepsilon_{a-1}, \varepsilon_a, \varepsilon_{a+1})$]. An example of raw and smoothed strain data is shown in Figure 2.6.

d) The strain plateau region, or the distance over which strain is at a nearly constant maximum, is estimated visually. The average strain within the plateau is calculated. A line corresponding to 95% of this average strain is superimposed on the strain profile.

e) The intersection of the 95% AMS and the strain profile defines the transfer length (see Figure 2.6).

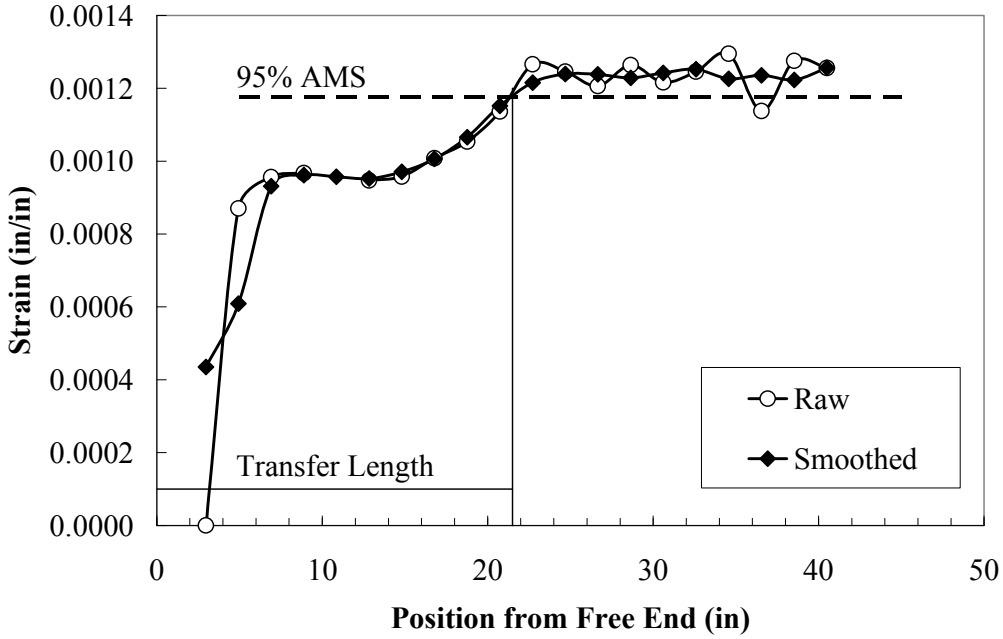

Figure 2.6. Example strain profile for determining transfer length using 95% AMS.

2.3.7 Development Length via Flexural Tests

An iterative sequence of flexural tests may be used to determine development length in full-scale prestressed concrete members. Specimens are subjected to either three- or four-point bending, with the position of applied load varying between test iterations. In the first trial, the distance from the applied load to the end of the specimen, or the strand embedment length, is taken equal to the development length predicted by design code criteria or external analyses. If the specimen fails due to bond-slip or fails in shear, embedment length for the next trial is increased; if the specimen fails in flexure, embedment length for the next trial is decreased. The procedure is repeated until determining the minimum embedment length at which flexural failure occurs; this embedment length is taken as the development length.

2.4 TRANSFER AND DEVELOPMENT LENGTH TESTS ON SCC SPECIMENS

Recent large-scale studies investigating bond behavior in prestressed SCC members have focused on comparing experimental data from SCC specimens to data from NCC specimens and current code provisions. The rest of this chapter summarizes the pertinent findings of these studies. A more extensive literature review of these studies was previously conducted by Andrawes et al. (2009).

2.4.1 Kansas State University

Sponsored by the Kansas Department of Transportation, this project aimed to characterize properties of pretensioned SCC bridge girders via pullout tests, transfer length tests, and development length tests (Larson et al. 2007). Pullout tests were conducted on 0.5-in. diameter strands embedded in blocks cast with a conventional concrete mixture utilized by Logan (1997). Meeting Logan's suggested criteria, the strands were deemed adequate for use in flexural test specimens.

The study considered small-scale rectangular beams with one bottom strand or one top strand, as well as 21-in. deep T-beams, all of which were cast with SCC. Span lengths for the rectangular and T-beams were 13.2 ft. and 15.5 ft., respectively. Transfer lengths were obtained using the end-slip method immediately after strand release, 18 days after release, and on the flexural testing day for each specimen. Average transfer lengths in the three specimen types were below the AASHTO requirement at all ages. However, average transfer lengths in top strand beams and T-beams exceeded the ACI requirement for measurements taken after 18 days past prestress release.

Four-point bending tests were conducted to determine the flexural behavior of the beams. Strand embedment lengths equal to the code-predicted development length produced flexural failures. Subsequent flexural failures using shorter embedment lengths demonstrated that development lengths in the small-scale SCC specimens were 80% of the ACI/AASHTO predictions. No top-strand effect was observed in development length tests.

2.4.2 Lehigh University

Sponsored by the Pennsylvania Department of Transportation, this project had three objectives: (1) Investigate the material characteristics of SCC and conventional high early strength concrete (HESC), (2) Evaluate the transfer length, maximum moment, and maximum shear force of full-scale bulb-tee girders cast with SCC and HESC, and (3) Investigate the characteristics of bond between concrete and prestressing strands (Naito et al. 2006). The target compressive concrete strengths at 24 hours and 28 days were 6800 psi and 8000 psi, respectively. At 24 hours, both concretes had attained over 90% of their 28-day target strength.

To qualify the study's strands as acceptable, pullout tests were conducted on 0.5-in. diameter strands embedded in concrete similar to the mixture utilized by Logan (1997). At

the test date, the concrete compressive strength was 4,000 psi. Although the average maximum pullout load was 31.5 kips, below the recommended 36 kips, researchers decided the strands were acceptable for the study based on past engineering experience.

The study considered 30-ft. long bulb-tee girders; two specimens were cast for each SCC and HESC. Transfer lengths obtained via the 95% AMS were 15.8 in. and 15.7 in., respectively, for HESC and SCC specimens; hence, experimental values met requirements of both the ACI and AASHTO design codes. No significant difference was observed between transfer lengths in the SCC and HESC girders.

2.4.3 Michigan State University

This study investigated the effect of SCC mixture proportioning on bond behavior and the bond-related parameters of transfer and development lengths (Burgueno and Haq, 2007). Researchers conducted strand pullout tests to evaluate bond strength, concrete surface strain calculations and end-slip measurements to characterize transfer length, and flexural tests to determine development lengths. Specimens were cast with three types of SCC and one conventional concrete, and the study considered variability in SCC composition by utilizing different amounts of VMA and HRWR admixtures. When strands utilized in the first phase of the project (Phase 1) were found to be unacceptable, a second phase (Phase 2) was added to the project scope; results from both phases are presented herein.

In both project phases, large-block pullout tests were conducted on 0.5-in. diameter strands with 18-in. embedment. The strands in Phase 1 were of poor quality, and those embedded in NCC were rusted. In Phase 2, strands were pre-qualified and clean in both SCC and NCC. Rust was estimated to increase bond strength by 30%. The effect of poor quality strand was highlighted by comparing the behavior of strands in SCC in both phases; poor quality strand was found to have 103% lower bond strength than the pre-qualified strand. Removing the effects of rust and poor quality, researchers observed lower bond strength in SCC than in NCC.

All girders utilized for transfer and development length tests were 38-ft. long T-beams with two 0.5-in. diameter low-relaxation bottom strands. Researchers used the 95% AMS and end-slip methods to evaluate transfer length. By comparing results from the two project phases, poor strand quality was estimated to increase transfer length by 17%. The effect of rust on transfer length was negligible. On average, SCC mixtures yielded transfer lengths which were 36% longer than in the NCC, though they were less than the value required by the ACI.

Iterative flexural tests were conducted to determine the development length of strands in the girders. Because trials were limited, an ideal development length was linearly extrapolated for each concrete mix using test results and the beams' nominal moment capacities. Again, effects of rust and strand quality were removed prior to comparing results from both phases. Development lengths in SCC specimens were approximately 3% longer than those in NCC specimens; excluding one value, they all met ACI criteria. Additionally, the effect of SCC mixture proportioning was clear; the SCC with the highest fine aggregate content and lowest w/c ratio had the worst bond performance, while the SCC with the highest coarse aggregate content and highest w/c ratio had the best bond performance.

2.4.4 North Carolina State University

Sponsored by the North Carolina Department of Transportation, this study measured transfer length and compared load-deformation characteristics in full-scale SCC and NCC specimens (Zia et al. 2005). Researchers utilized three 54.8-ft. long AASHTO Type III girders, two of which were cast with SCC and one of which was cast as a control specimen with NCC. The girders had 18 straight 0.5-in. low-relaxation strands. Researchers used the

end-slip method as well as embedded steel bars instrumented with strain gauges to measure transfer lengths at ends of the three specimens. Using the end-slip method, transfer lengths in the SCC girders were found to be 32.3 in. and 50 in. In the control NCC girder, transfer length was estimated as 44.1 in. These values were approximately 40% greater than the AASHTO requirement of $60d_b$, or 30 in. Researchers were unable to determine transfer lengths using the embedded gauges since many were damaged during specimen production; however, the gauges which remained indicated that transfer lengths in both top and bottom strands were between 30 in. and 40 in. The researchers attributed the lower bond strength to porous and soft fine aggregate utilized in all three concrete mixtures.

2.4.5 South Dakota State University

Research was conducted to investigate the performance of full-scale prestressed bridge girders cast with SCC containing limestone aggregates, which are commonly used in South Dakota concretes (Wehbe et al. 2009). The investigation entailed analyses of transfer length, prestress losses, flexural strength, and shear strength. The study considered three 40-ft. long MnDOT 36M girders, two of which were cast with SCC and one of which was cast as a control specimen with conventional concrete. Each specimen contained twelve straight 0.6-in. diameter low-relaxation strands within the bottom flange. Both concrete mixtures had target strengths of 6,500 psi and 7,000 psi at release and 28 days, respectively.

Researchers planned to measure transfer lengths via surface strain measurements and strain gauges attached to strands. However, surface strain measurements were highly erratic and were not used to estimate transfer lengths. From the strain gauges attached to strands, transfer lengths were determined to be 30 in., 34.5 in., and 25.2 in., respectively, for the NCC, SCC1, and SCC2 specimens. Only the 34.5 in. value exceeded the $50d_b$ ACI requirement. The researchers concluded the structural performance of the prestressed SCC girders was comparable to that of the control specimen, and equations currently utilized to determine strength and stiffness of prestressed NCC girders are applicable to prestressed SCC girders.

2.4.6 University of Arkansas at Fayetteville

This project evaluated the transfer lengths of prestressing strands in SCC beams and compared them to ACI and AASHTO recommended values and transfer lengths in conventional concrete (Staton et al. 2009). The study utilized high strength SCC with target strengths of 7000 psi at prestress release and 12000 psi at 28 days. Twelve 18-ft. long prestressed beams with rectangular cross-sections were cast; half used SCC and half used conventional concrete. Each beam had two 0.6-in. diameter bottom strands.

Researchers used the 95% AMS method to measure transfer length. Additionally, vibrating wires were placed between the strands at each end of the beam to confirm the results from the strain gauges. A 2-10% difference was observed between the 95% AMS readings and the vibrating wire results. The measured transfer lengths in all six beams cast with SCC satisfied the ACI code requirement by a margin of 33% and the AASHTO code requirement by a margin of 44%. Transfer lengths did not vary significantly over time after 3 days of prestress release; thus, the researchers suggested compressive strength had minor impact on transfer length.

2.4.7 University of Florida

The Florida Department of Transportation sponsored a research project to compare the structural performance of six 42-ft. long AASHTO Type II bridge girders cast with SCC to those cast with conventional concrete (Labonte and Hamilton, 2005). The project entailed analyses of production methods, plastic and hardened mixture properties, transfer length,

and shear and flexural behavior. Three of the girders were cast with SCC and three were cast with NCC; both concretes had a 28-day target compressive strength of 8500 psi.

Prestressing strands were released from tension by cutting in order to evaluate the impact cutting had on transfer length. Researchers estimated transfer lengths in two specimens using a slightly modified version of the 95% AMS method because they observed higher variation in strain readings than is typical. In the modified version, transfer length was determined using the intersection of the 95% AMS and a best-fit line through the origin and the first two data points of the strain profile. Experimental transfer lengths in the control specimen were determined to be 12.1 in. and 15.5 in. at the cutting and free ends, respectively; this yields a 28% difference. In the SCC specimen, transfer lengths were found to be 15.0 in. and 13.0 in. at the cutting and free ends, respectively; this yields a 15% difference. All experimental transfer lengths were well below ACI and AASHTO requirements, and the results revealed no significant difference between transfer lengths of strands in SCC girders and those of strands in conventional concrete girders.

2.4.8 University of Nebraska-Lincoln

The Nebraska Department of Roads sponsored a research project to assess bond strength of SCC and transfer length of strands in pretensioned SCC bridge girders (Girgis and Tuan, 2005). Researchers considered concrete mixtures and girder specimens used in three bridge projects; Mix #1 was an SCC used in the Oak Creek Bridge in Lancaster, NE, Mix #2 was an SCC used in the Clarks South Bridge in Merrick, NE, and Mix #3 was a conventional concrete used in the North Broadway Bridge in Sedgwick, KS.

The research team conducted Moustafa pullout tests on 0.6-in. diameter strands embedded 18-in. in large block specimens cast with the three concretes. At early ages, Mix #1, Mix #2, and Mix #3 had 43.4-kip, 54.2-kip, and 48-kip maximum pullout forces, respectively. At 28 days, Mix #2 and Mix #3 had maximum pullout loads of 65.7 kips and 63.1 kips, respectively. To compare results to the 36-kip minimum proposed by Logan (1997) for 0.5-in. diameter strands, researchers adopted a multiplier based on the ratio of strand diameters. This resulted in a benchmark pullout value of 43.2 kip, which all pullout loads exceeded.

The study utilized the 95% AMS method to evaluate transfer lengths in three specimens. The first specimen was a 72.5-ft. long NU1100 I-beam cast with Mix #1; the second specimen was a 90.2-ft. long NU900 I-beam cast with Mix #2; and the third specimens was a 124-ft. long NU1350 I-beam cast with Mix #3. Data was acquired from both sides of both ends of the girders at the bottom flanges. Average transfer lengths within Mix #1 and Mix #2 specimens were determined to be 36 in. and 43 in., respectively, which exceeded the 30-in. transfer length required by the ACI. The average transfer length in Mix #2 also exceeded the 36 in. transfer length required by AASHTO. The 20-in. average transfer length in the girder cast with conventional concrete met all code requirements. As such, transfer lengths of strands in the SCC girders were greater than those of strands in the conventional concrete girder by approximately 98%.

2.4.9 Virginia Polytechnic Institute and State University

The Shockey Precast Group of Winchester, VA sponsored research to investigate bond strength, transfer length, and development length of strands in SCC girders (Trent 2007). The study considered three concrete mixtures, two of which were SCC (S1CCM, S1CCM2) and one of which was conventional concrete (S1CRM). All concretes had target compressive strengths of 3500 psi at 12 hours and 6500 psi at 28 days.

The 95% ASM method was utilized to determine transfer lengths in three prestressed specimens (one for each concrete mixture). The specimens had 6-in. square cross-sections with a single 9/16-inch diameter, 270-ksi low relaxation strand. Upon prestress release, the

two edge specimens (S1CRM and S1CCM2) absorbed most of the energy before force transferred gradually to the middle specimen (S1CCM). Experimental transfer lengths were compared to values recommended by ACI ($50d_b$ = 28.1 inches) and AASHTO ($60d_b$ = 33.7 inches). Results indicated two of three specimens (S1CRM and S1CCM) yielded acceptable transfer lengths. However, transfer lengths in the third specimen (S1CCM2) exceeded ACI requirements at 7 and 28 days after transfer. The transfer length values of the strands used in the SCC specimens were greater than those of strands in the conventional concrete specimen.

Twelve 24-ft. long T-beam development length specimens were cast with the three concrete mixtures (four specimens per mixture). An iterative scheme in which both ends of the specimens were subjected to flexural testing produced 10 bond failures and 14 flexural failures. Development lengths in the specimens cast with either SCC mixture were approximately 80%-83% of recommended ACI/AASHTO values. The study failed to determine a development length for the members cast with conventional concrete.

2.4.10 SCC Mix Designs from Previous Large-Scale Studies

U.S. State Departments of Transportation are continually establishing guidelines for proper material proportioning to ensure adequate plastic and hardened behavior of new SCC mixtures. However, these requirements may significantly vary between institutions. As a result, the nine aforementioned studies in Section 2.4 tested specimens with fourteen different SCC mix compositions. The SCC mixture designs are summarized in Table 2.3; constituents are shown as required for one cubic yard of concrete. Nine of the mixtures in the table contained Type III cement, two contained Type I/II cement, and three contained Type I cement. Type III cement is commonly used in prestressed members because its high early strength permits quick turnover times in fabrication plants. Four of the SCC mixtures also incorporated supplementary cementitious materials such as fly ash and ground granulated blast-furnace slag.

The chemical additives included in the mixes in Table 2.3 varied considerably. For instance, in the nine mixtures which utilized an air-entraining agent (AEA), the volume of AEA ranged from 1.8 oz. to 22.3 oz. per cubic yard. In seven mixtures the volume of VMA ranged from 10 oz. to 108 oz. per cubic yard. The amount of VMA is significant as it may adversely affect bond (Girgis and Tuan, 2005). Finally, the amount of superplasticizer in the mixes varied from 14 oz. to 224 oz. per cubic yard. Where a dash is present in the table, either the SCC did not contain a particular material or the literature did not report a specific value for that material (i.e. the amount was indeterminate or varied between specimens and no range was presented).

Using results from earlier studies to predict bond adequacy of a proposed SCC mixture may be unsound when the studies' mixtures do not comply with standards applicable to the proposed SCC. If compared to current provisions set forth by the IDOT Bureau of Materials and Physical Research (2007), ten mixtures reported in the Table 2.3 would exceed the maximum cement factor of 705 lbs per cubic yard, eight would exceed the 50% limit for fine-to-total aggregate proportions, and three would have w/c ratios outside an allowable 0.32-0.44 range. Acknowledging this and recognizing the general need for further research on large-scale prestressed SCC specimens, the IDOT sponsored this study exploring the bond behavior of strands in prestressed bridge girders cast with SCC adhering to current IDOT provisions.

Table 2.3. SCC Mixture Designs from Studies on Prestressed SCC Specimens

Constituent	Units	A	B	C				D
Cement	Type	III	III	III	III	III	III	III
	lbs	750	849	750	700	700	700	810
Fly Ash	lbs	-	-	-	-	-	-	-
Coarse Agg.	lbs	1360	1651	1479	1380	1380	1435	1330
Fine Agg.	lbs	1500	1283	1628	1426	1426	1275	1300
Fine/Total Agg.		0.52	0.44	0.52	0.51	0.51	0.47	0.49
Water	gal.	27	33	31	33	33	37	41
W/C Ratio		0.30	0.32	0.34	0.39	0.39	0.44	0.42
AEA	oz.	5.0	2.0	13.1	5.3	12.3	22.3	2.4
HRWR	oz.	70	136	97	102	84	108	81
VMA	oz.	-	16	-	49	13	108	-
Set Retardant	oz.	-	-	525	-	410	327	32

Constituent	Units	E	F	G	H		I	
Cement	Type	I/II	I	I/II	III	III	I	I
	lbs	800	950	752	800	632	750	745
Fly Ash	lbs	-	-	168	150	100	-	-
Coarse Agg.	lbs	1454	1350	1307	1282	1311	1625	1650
Fine Agg.	lbs	1343	1474	1414	1417	1449	1340	1308
Fine/Total Agg.		0.48	0.52	0.52	0.53	0.53	0.45	0.44
Water	gal.	29	34	31	35	35	34	34
W/C Ratio		0.33	0.30	0.34	0.36	0.46	0.38	0.38
AEA	oz.	15.0	-	1.8	-	-	-	-
HRWR	oz.	224	105	64	14	14	-	-
VMA	oz.	-	19	-	10	10	-	-
Set Retardant	oz.	24	-	14	5	5	-	-

Notes	
(a)	Exceeds 705 lbs/cy cement factor
(b)	W/C ratio outside range of 0.32 - 0.44
(c)	Fine/total agg. ratio exceeds 50%
(d)	Mix contains 25 lbs of slag

Legend	
A	Larson et al. 2007
B	Naito et al. 2006
C	Burgueno and Haq, 2007
D	Zia et al. 2005
E	Wehbe et al. 2009
F	Staton et al. 2009
G	Labonte and Hamilton, 2005
H	Girgis and Tuan, 2005
I	Trent 2007

CHAPTER 3 PULLOUT TESTS

Modified Moustafa pullout tests (see Section 2.3.5) were conducted to evaluate the bond characteristics of the seven-wire strands intended for use in this study's large-scale specimens. The tests method was utilized to verify comparable bond behavior between strands and SCC than between strands and a conventional concrete of similar design. The pullout test was attractive given its simplicity and relatively low cost. A total of 56 pullout tests were performed on 0.5-in. diameter, seven-wire low-relaxation strands embedded in SCC and NCC blocks. The strands had 270 ksi tensile strength and a modulus of elasticity equal to 28700 ksi. Concrete compressive strengths and the strands' force-slip responses were recorded at curing ages of 1, 3, 7, and 28 days.

3.1 PULLOUT BLOCK SPECIMENS

Four pullout block specimens and 32 6 in. x 12 in. cylinder specimens were cast simultaneously on February 2, 2009. Half the specimens used SCC and half used NCC; details of the mixture compositions are presented at the end of this section. Each block was 24 in. x 24 in. x 66 in. and contained fourteen 0.5-in. diameter strands with 18 in. embedment. All block dimensions including strand spacing, longitudinal reinforcement, and clear cover are shown in Figure 3.1. Embedded strands were not tied to any of the nominal reinforcement which was utilized to control cracking and shrinkage. Strands extended 36 in. above the block surface to accommodate the pullout loading apparatus. Concrete was cast outdoors in a single casting bed with temperatures above the IDOT minimum of 25 degrees Fahrenheit. Space heaters were placed around the specimens and the casting bed was covered to ensure adequate overnight curing conditions. Specimens were shipped the following day to the Newmark Structural Testing Laboratory at UIUC for 24-hr. tests.

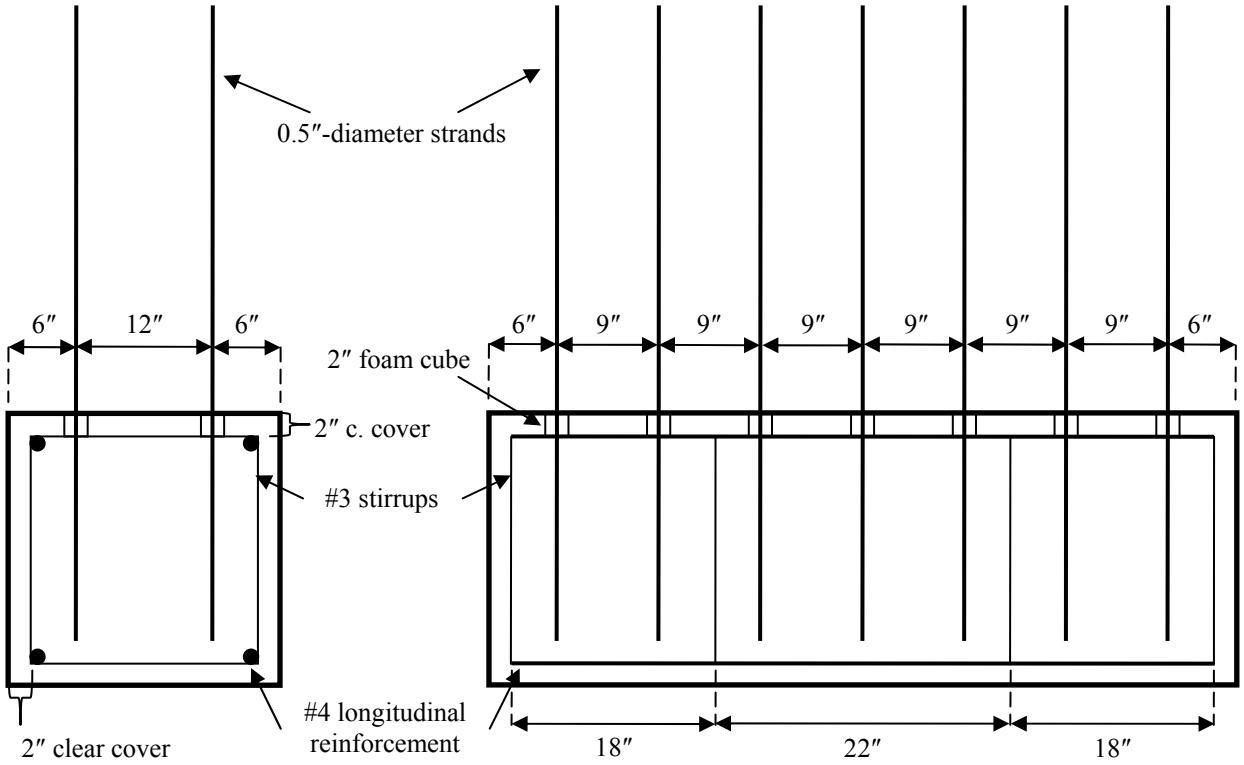

Figure 3.1. Pullout specimen design with dimensions in inches.

Figure 3.2. Formwork for pullout specimens on casting day.

Figure 3.3. Casting of pullout block specimen.

Figure 3.4. Pullout block specimens after delivery to UIUC.

The actual constituent proportions for the two concrete mixtures used in pullout block specimens are presented in Table 3.1. Pullout specimens were cast using one batch of SCC and one batch of NCC, both of which were 2 cubic yards in volume. Both mixtures contained Type III cement, coarse aggregate with maximum 0.5-in. nominal size, and natural sand fine aggregate. Use of a HRWR and an AEA ensured proper workability for each mixture. The amount of AEA was half the design volume because an issue with dosing equipment during specimen fabrication resulted in actual dosages which were half the values output on the batch tickets. The concretes contained no VMA, though the HRWR was promoted by the manufacturer as a single-component admixture having properties to improve segregation resistance. The SCC adhered to all current IDOT standards for precast/prestressed specimens (IDOT 2007).

Table 3.2 summarizes the results for plastic property tests conducted on pullout specimen concrete. A standard slump test was performed on the fresh batch of NCC, which had a 7-in. slump. Standard slump flow, J-Ring, L-box, and VSI tests were conducted for fresh pullout specimen SCC. Table 3.2 shows the SCC utilized in the blocks had moderate passing ability, moderate filling ability, and minimal segregation.

Table 3.1. Actual NCC and SCC Mixture Proportioning for Pullout Specimens

Mix Constituent	Units	Pullout NCC	Pullout SCC
Type III Cement	lbs/cy	670	662
Coarse Aggregate	lbs/cy	1849	1607
Fine Aggregate	lbs/cy	1180	1441
AEA	oz/cy	11	14
HRWR	oz/cy	45	81
Water	gal/cy	27	22
W/C	-	0.33	0.28
Coarse/Fine Aggregate	-	1.57	1.12
Fine/Total Aggregate	-	0.39	0.47

Table 3.2. Fresh Mixture Properties for Pullout Specimen Concrete

		Pullout SCC	Pullout NCC
Temperature	°F	63	62
Entrained Air	%	5.7	6.3
Spread	in.	22.0	-
J-Ring Spread	in.	20.0	-
L-Box Ratio	%	75	-
Slump	in.	-	7

3.2 PULLOUT TEST SETUP

The servo-controlled assembly in Figure 3.5 was utilized to apply load to strands in the pullout tests. The 120-kip capacity hydraulic ram had a 13-in. stroke, a 6.25-in. outer diameter, and a 3-in. bore diameter. A linear variable differential transducer (LVDT) attached to the ram's cylinder monitored displacement of an aluminum plate secured to the top of the piston. Strands were loaded at a constant displacement-controlled rate of 0.4 in/min, resulting in loading rates below the maximum 20 kip/min as set forth by Logan (1997). Load was applied continuously until strands were completely pulled out or fractured. Five criteria were obtained for each pullout test: (1) First slip load, (2) Peak pullout load, (3) Displacement at first slip, (4) Displacement at peak load, and (5) Depiction of failure. The

former four criteria were taken from the force-displacement response for each strand, while the latter criterion was made by visual observation.

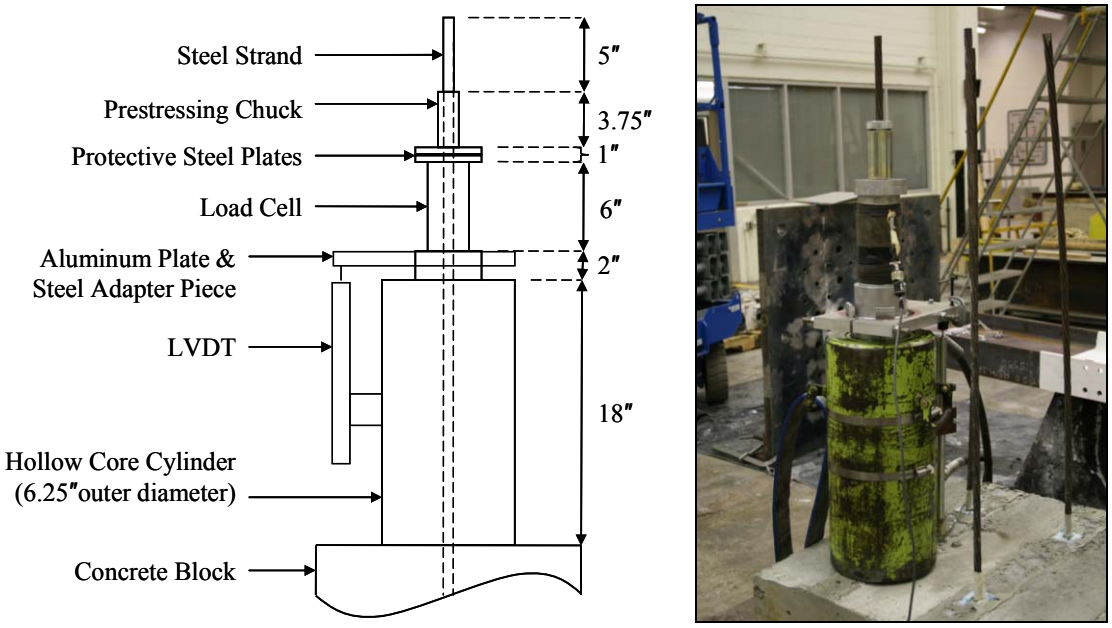

Figure 3.5. Servo-controlled assembly utilized to perform pullout tests.

3.3 PULLOUT TEST RESULTS

Fourteen pullout tests were conducted on each testing date (1, 3, 7, 28 days after casting); half the tests were on SCC specimens and half were on NCC specimens. Each strand was assigned a label corresponding to the day of testing and the type of concrete in which the strand was embedded; for example, the label “S3-A” corresponds to the first (“A”) of seven strands embedded in SCC (“S”) tested three days (“3”) after concrete placement. The force-displacement responses for all tests are presented in Appendix A.

For discussion purposes, Figure 3.6 displays the responses of the seven strands embedded in SCC tested three days after concrete placement. Each response in the figure shows regions of linear and nonlinear behavior typical of all the results regardless of concrete age or type. Linear behavior was observed when a strand remained fully bonded to concrete and steel deformed elastically. Localized bond failure then brought about a reduction in pullout stiffness at the point when a strand first slipped relative to concrete (“first slip” point). Progressive bond failure caused a gradual reduction in pullout stiffness until the strand reached a maximum capacity (“peak pullout” point). After reaching this maximum load, one of two types of behavior were observed: (1) load resistance gradually declined, indicating a bond failure, or (2) load resistance abruptly dropped, indicating the fracture of one or more of the wires in the steel strand.

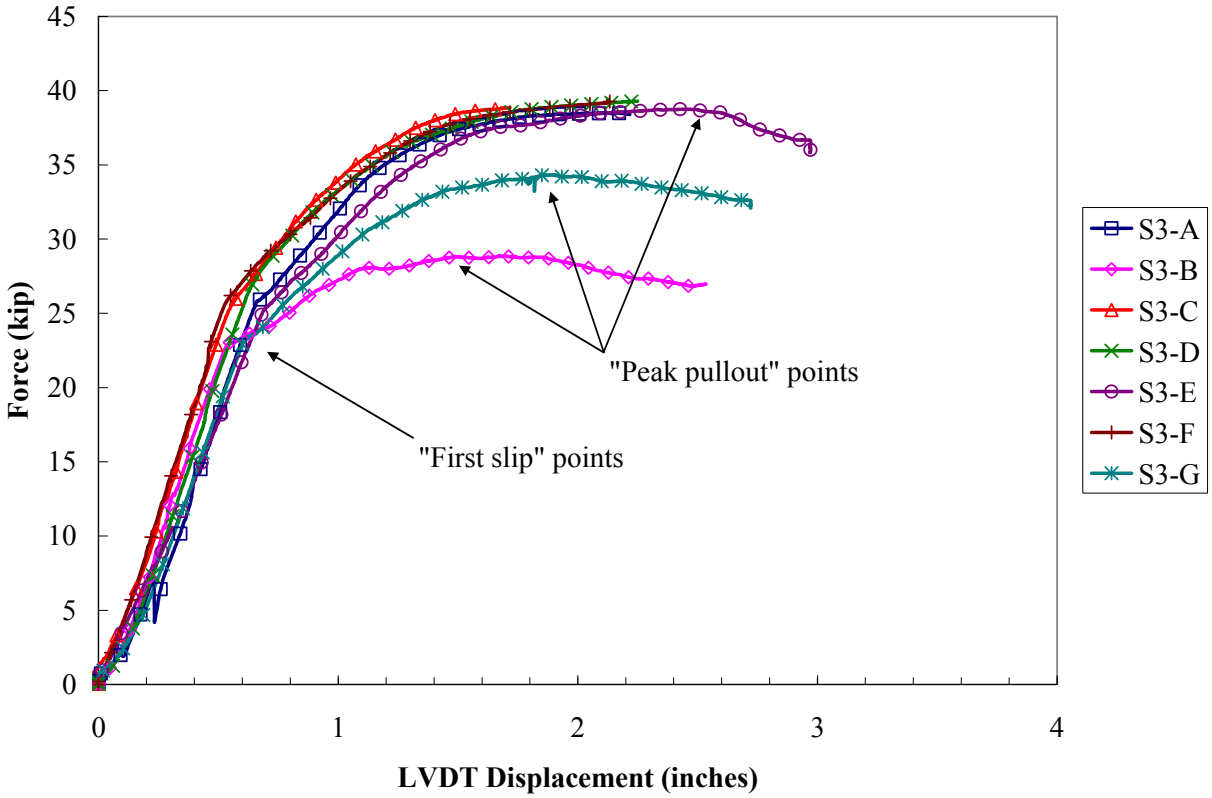

Figure 3.6. Force-displacement responses for strands in SCC 3 days after casting.

Table A.1 in Appendix A contains the first slip loads and peak pullout loads for all tested strands. One strand (N3-E) yielded no data because the LVDT became dislodged during testing, requiring an abrupt stop of the loading mechanism; the LVDT and load cell were recalibrated prior to testing the next strand. Figure 3.7 shows the average absolute first slip and peak pullout loads at all ages with an assumed error of ±one standard deviation. Average absolute first slip loads increased over time, ranging in SCC from 23.8-25.3 kips and in NCC from 23.5-26.3 kips. Average absolute peak loads also increased over time, ranging in SCC from 36.1-38.3 kips and in NCC from 30.4-36.2 kips

Considering normalization techniques is prudent when comparing bond strength in different concretes. Numerous studies on bond behavior have shown a correlation between bond strength and $(f_c)^{1/2}$, where f_c is the concrete compressive strength (Chan et al. 2003; Esfahani et al. 2008). ACI provisions, moreover, state development lengths of reinforcing bars are inversely proportional to $(f_c)^{1/2}$, which implies a linear relationship between bond strength and $(f_c)^{1/2}$ (ACI Committee 318). However, methods of normalization vary among studies depending upon the concrete strength range, confinement within specimens, and country in which testing occurs. Previous research and most European design codes consider bond strength to vary proportionally with $(f_c)^{1/3}$ (Mitchell and Marzouk, 2007). Other studies have found a more precise correlation between bond strength and $(f_c)^{1/4}$ (Darwin et al.1996). Based on similarities to the studies discussed in Section 2.4, the current study assumes a linear relationship between bond strength and $(f_c)^{1/2}$, and Figure 3.8 shows first slip and peak pullout loads normalized using $(f_c)^{1/2}$ to better assess the bond behavior of SCC and NCC using a common datum.

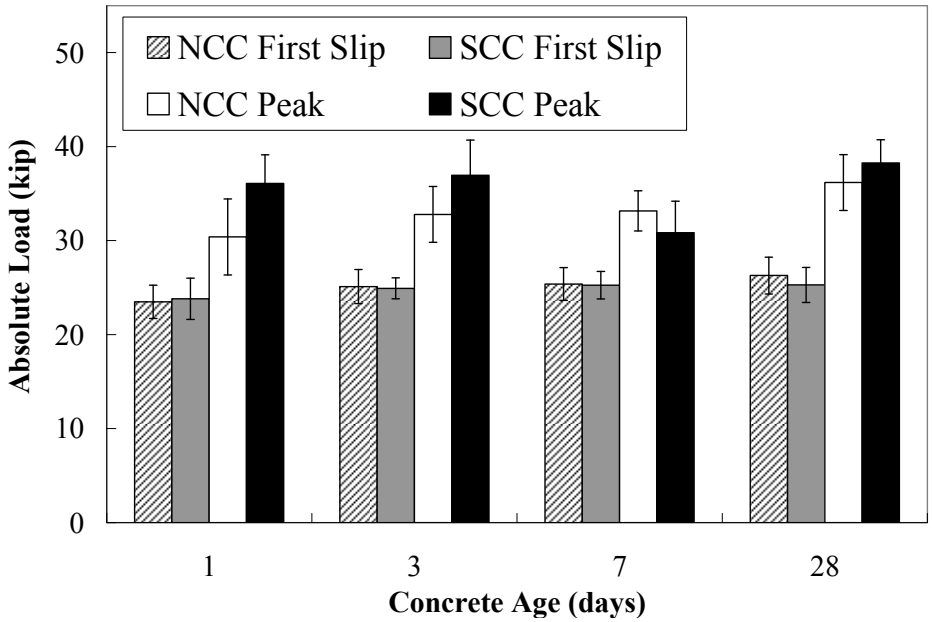

Figure 3.7. Average absolute first slip and peak pullout loads at various ages.

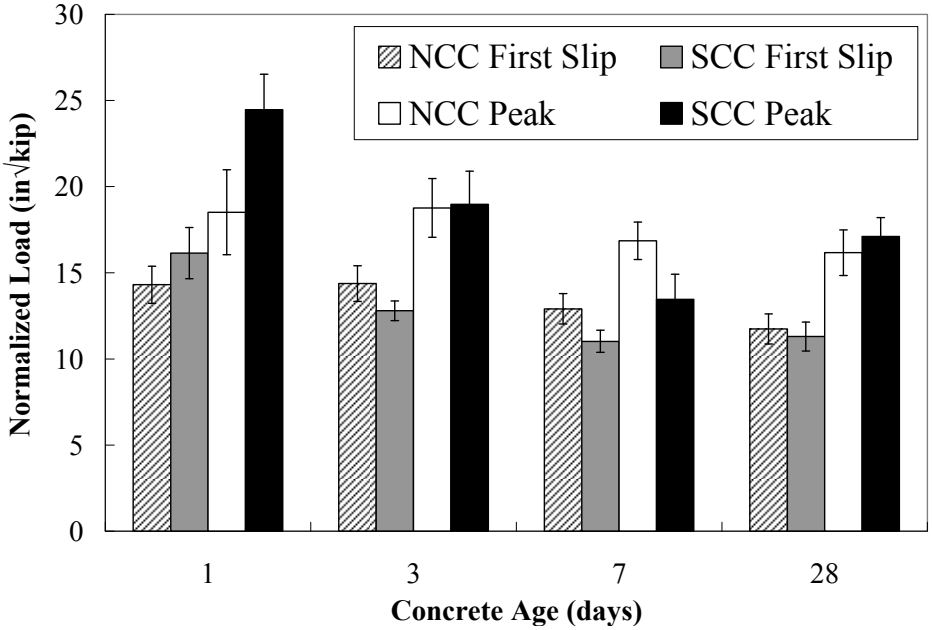

Figure 3.8. Average normalized first slip and peak pullout loads at various ages.

The average compressive cylinder strengths for both concretes at various testing ages are shown in Figure 3.9 with an assumed error of ±one standard deviation. Both concretes achieved adequate strength for initial tests and strengthened over time, exceeding 5 ksi after 28 days. It should be noted, however, that individual cylinder specimens for either concrete type showed wide variability in strength at the same age. Indeed, cylinder strengths reported for both concrete types prior to shipping pullout specimens to UIUC were greater than 4 ksi. Normalized first slip loads differed between SCC and NCC by an average of 10% for all tests. Only the 1-day tests showed first slip normalized loads in SCC higher than those in NCC (see Figure 3.8). Normalized pullout loads differed between SCC and NCC by as much as 25% at 1 day and as little as 1% at 3

days. Only the 7-day tests produced lower normalized pullout loads in SCC than in NCC. From the pullout capacities, it was concluded that the strands in this study displayed sufficient bond to SCC; therefore, they were utilized in subsequent full-scale girder testing.

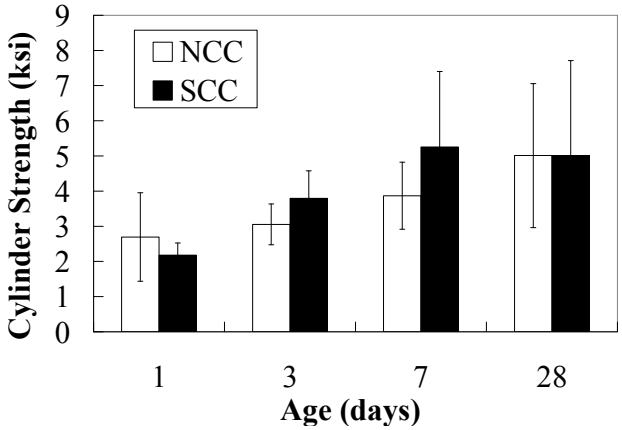

Figure 3.9. Average compressive cylinder strengths for pullout specimens at various ages.

CHAPTER 4 FULL-SCALE GIRDER DESIGN AND ANALYSIS

This chapter contains all design, analysis, and fabrication information for the four SCC girders cast for transfer and development length tests. Results of transfer length tests are discussed in Chapter 5, and results of development length tests are discussed in Chapter 6. This chapter details the design loading conditions, design capacities, and predicted development lengths within the girder specimens.

4.1 SPECIMEN FABRICATION AND DESCRIPTION

Two full-scale hollow box girders and two full-scale I-girders were cast for transfer and development length tests using the same SCC and strands as in the pullout blocks. The girder types were selected for their frequent use in Illinois bridge construction. Box girders were 28 ft. long and 27 in. deep, and each was prestressed with sixteen strands. All strands were straight, fully bonded to concrete, and stressed to 202 ksi prior to casting. The cross-section and strand configuration for the box girders are provided in Figure 4.1. Low concrete cover (1.75 in.) and high stress concentration at the middle strands were primary concerns, as both tend to negatively impact bond. The center hollow in each girder was formed by a 23-ft. long Styrofoam® block; for 30 in. from either end, the cross-section was not hollow. Fabrication drawings showing reinforcement, lifting loops, and other pertinent details are included in Appendix B. Shear reinforcement within the box girders comprised overlapping #4 stirrups spaced every 9 in. throughout the center span and every 6 in. at the beam ends.

The two I-girders were 48 ft. long and 42 in. deep, and each was prestressed with twelve strands. Strands were straight, fully bonded to concrete, and stressed to 202 ksi prior to casting. The I-girder cross-section and strand configuration are shown in Figure 4.2. Again, fabrication drawings showing all pertinent specimen details may be found in Appendix B. Transverse reinforcement comprised #4 stirrups throughout the web and bent #3 bars in both flanges; stirrups were spaced every 12 in. throughout the center span and every 6 in. at the beam ends. Additional overlapping #4 stirrups were placed within the end zones to prevent shear failure.

All four girders were cast sequentially on August 26, 2009 using eight batches of SCC; actual constituent proportions for each batch are shown in Table 4.1. All batches were 3 cubic yards in volume except for the Batch 8, which was 0.5 cubic yards. Proportioning of the AEA required modification throughout casting but did not affect overall mixture acceptability. Table 4.2 summarizes the results for plastic property tests for girder specimen concrete. Standard slump flow, J-Ring, L-box, and VSI tests were conducted for the first batch of SCC. Results showed the SCC had good passing ability, good filling ability, and minimal segregation. For subsequent batches, only the slump flow test was performed. Temperature and entrained air were checked for all batches of SCC.

The casting bed configuration for the girders is provided in Figure 4.3. Per the figure, Box-1 and Box-2 hereafter refer to the box girder specimens, and I-1 and I-2 hereafter refer to the I-girder specimens. Box-1 was cast first with Batches 1-2 (see Table 4.1); then, Box-2 was cast with Batches 2-4, I-1 was cast with Batches 4-6, and I-2 was cast with Batches 6-8. Box girders were cast monolithically starting at their south ends; the I-girders were cast starting at their north ends. A monolithic pour of a hollow girder is typically more problematic when using conventional concrete than when using SCC because formwork for the center void obstructs the flow of concrete. No mechanical vibration or tamping was utilized during casting. Casting and strand release locations were noted in order to analyze whether they affected transfer length at either girder end. All girders had a specified 5000 psi release strength and 6000 psi 28-day target strength at 28 days. Seventy 4 in. x 8 in. cylinders were

cast during fabrication to determine concrete compressive strength at later ages. Figures 4.4 through 4.15 illustrate the fabrication process for the four girders.

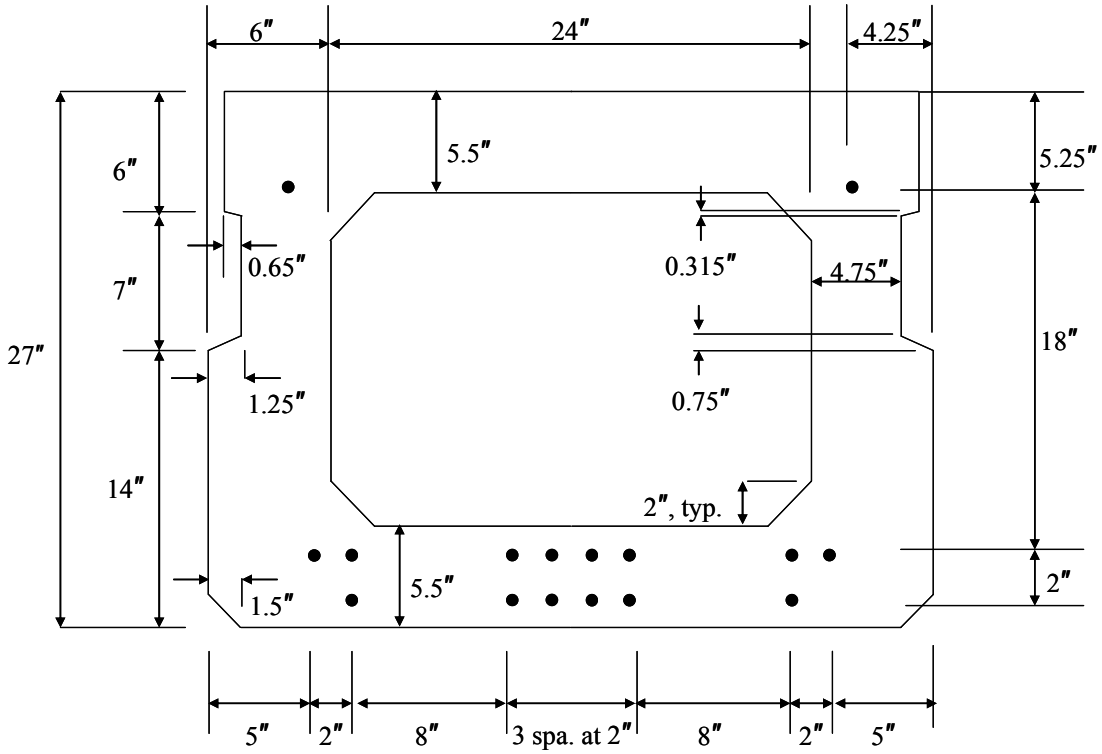

Figure 4.1. Cross-sectional geometry and strand configuration for box girders.

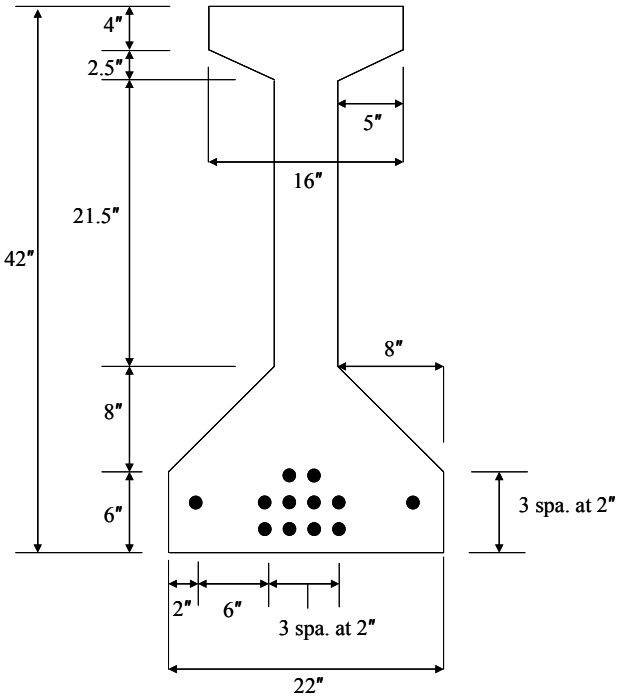

Figure 4.2. Cross-sectional geometry and strand configuration for I-girders.

Table 4.1. Actual Mixture Proportioning for Batches of Girder Specimen SCC

Constituent	Units	1	2	3	4	5	6	7	8
Type III Cement	lbs/cy	660	660	660	660	660	660	660	664
Coarse Agg.	lbs/cy	1578	1581	1577	1569	1571	1585	1571	1714
Fine Agg.	lbs/cy	1420	1420	1420	1420	1420	1422	1421	1476
AEA	oz/cy	17	20	25	28	32	32	32	32
HRWR	oz/cy	80	80	80	80	80	80	80	84
Water	gal/cy	31	30	31	30	30	31	31	30
W/C	-	0.39	0.38	0.39	0.39	0.39	0.39	0.39	0.38
Coarse/Fine Agg.	-	1.11	1.11	1.11	1.11	1.11	1.12	1.11	1.16
Fine/Total Agg.	-	0.47	0.47	0.47	0.48	0.47	0.47	0.47	0.46

Table 4.2. Fresh Mixture Properties for Batches of Girder Specimen SCC

		1	2	3	4	5	6	7	8
Temperature	°F	69	70	71	70	72	70	70	70
Entrained Air	%	4.0	4.0	5.2	5.2	5.4	6.2	6.0	3.8
Spread	in.	25.8	23	24.5	23	22.9	24	23.3	25.5
J-Ring Spread	in.	25.4							
L-Box Ratio	-	0.92							

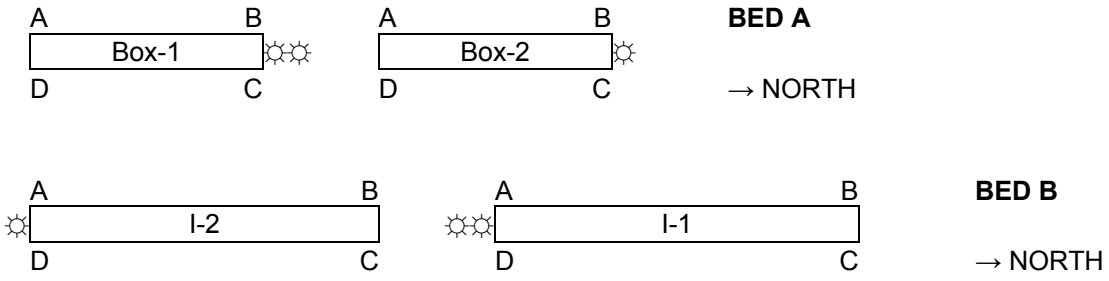

Box-1	Started casting at A-D	Strands first cut at ☼, then cut at ☼☼
Box-2	Started casting at A-D	
I-1	Started casting at B-C	Strands first cut at ☼, then cut at ☼☼
I-2	Started casting at B-C	

Figure 4.3. Diagram showing casting locations, cutting locations, and beam orientation.

Figure 4.4. Box girder formwork prior to casting.

Figure 4.5. End zone of box girder.

Figure 4.6. Box girder half-filled during casting.

Figure 4.7. Completely filled box girder.

Figure 4.8. Box girders covered overnight.

Figure 4.9. Box girders removed from bed.

Figure 4.10. I-girder formwork prior to casting.

Figure 4.11. End zone of I-girder before casting.

Figure 4.12. Partially filled I-girder.

Figure 4.13. Completely filled I-girder.

Figure 4.14. I-girders covered overnight.

Figure 4.15. I-girders removed from bed.

Specimens were shipped to UIUC approximately one month after casting, after transfer length measurements had been completed. Prior to flexural tests, composite SCC slabs were cast atop the I-girders to simulate the effective portion of a bridge deck. The slab for girder I-1 was cast on April 23, 2010, and the slab for girder I-2 was cast on April 28, 2010. Provided by a local fabricator, the slab SCC differed slightly from the concrete utilized to cast the girders, though the 28-day target strength remained the same. The actual constituent proportions for the deck SCC are provided in Table 4.3. As shown, the concrete incorporated Type I/II cement, unlike the girders which utilized Type III cement for rapid strength gain. The AEA manufacturer differed between mixtures; only 5 oz. per cubic yard was required for the deck concrete. The brand of HRWR also differed between mixtures, but the required quantity remained the same. Each deck was cast using a single, 7-cubic yard batch of concrete. No mechanical vibration or tamping was utilized during casting.

The slabs were 8 in. x 30 in., extended the entire length of the specimens, and utilized nominal reinforcement to meet temperature and shrinkage requirements. The transverse reinforcement in the slabs comprised #4 bars spaced every 12 in. Longitudinal reinforcement comprised five #3 bars throughout the full deck, spliced appropriately. Slab dimensions were selected to ensure strands would yield prior to concrete crushing during flexural tests. Figures 4.16 through 4.21 show the deck fabrication process; decks were allowed to cure, covered with tarps, for one week prior to formwork removal.

Table 4.3. Actual SCC Mixture Proportioning for I-Girder Decks

Mix Constituent	**Units**	**SCC**
Type I/II Cement	lbs/cy	658
Coarse Aggregate	lbs/cy	1557
Fine Aggregate	lbs/cy	1489
AEA	oz/cy	5
HRWR	oz/cy	91
Water	gal/cy	30.1
W/C	-	0.38
Coarse/Fine Aggregate	-	1.05
Fine/Total Aggregate	-	0.49

Figure 4.16. Formwork for I-girder deck.

Figure 4.17. Reinforcement for I-girder deck.

Figure 4.18. Casting of I-girder deck.

Figure 4.19. Leveling surface of I-girder deck.

Figure 4.20. Completely filled deck formwork.

Figure 4.21. Composite girder.

4.2 SECTION PROPERTIES

This section briefly summarizes the geometrical properties used in the analysis of each specimen type. Table 4.4 contains the properties of both the hollow and filled cross-sections within the box girder. As shown in the fabrication drawings in Appendix B, the box girder cross-section is hollow for only 25 ft. within the specimen; for 30 in. from wither end, the section is completely filled. Table 4.5 contains I-girder properties with and without the composite deck. For simplicity, the concrete in the girder and slab comprising the composite section were assumed to have the same strength; hence, no transformed moment of inertia or section properties are presented. Volume-to-surface (V/S) ratios utilized in calculating prestress losses are also listed in the tables.

Table 4.4. Box Girder Section Properties

Hollow Section Properties		
A_c	568.8	in
h_t	27.0	in
d_p	21.5	in
e_o	8.04	in
y_t	13.29	in
y_b	13.71	in
I_g	49684	in^4
Z_b	3739	in^3
Z_t	3624	in^3

Filled Section Properties		
A_c	896.8	in
h_t	27.0	in
d_p	21.5	in
e_o	8.12	in
y_t	13.63	in
y_b	13.37	in
I_g	57452	in^4
Z_b	4297	in^3
Z_t	4215	in^3

Strand Properties		
# Strands	16	
CG Strands	5.25	in
A_{ps}	2.448	in^2

Girder Properties		
Surface Area	65074	in^2
Volume	210780	in^3
V/S Ratio	3.24	

Table 4.5. I-Girder Section Properties

Original Section Properties		
A_c	464.5	in
h_t	42	in
d_p	38.3	in
e_o	14.0	in
y_t	24.35	in
y_b	17.65	in
I_g	90822	in^4
Z_b	5145.1	in^3
Z_t	3730.2	in^3

Section Properties with Deck		
A_c	704.5	in
h_t	50	in
d_p	46.3	in
e_o	23.6	in
y_t	22.7	in
y_b	27.3	in
I_g	219262	in^4
Z_b	8028.8	in^3
Z_t	9663.2	in^3

Strand Properties		
# Strands	12	
CG Strands	3.67	in
A_{ps}	1.836	in^2

Girder Properties (without deck)		
Surface Area	79265	in^2
Volume	267552	in^3
V/S Ratio	3.37	

4.3 PRESTRESS LOSSES

Throughout the life of a prestressed concrete member, the stress in its prestressing strands decreases in an asymptotic manner. This reduction in tensile stress is termed “prestress losses.” The combined effects of concrete and steel behavior over time, as well as mechanical action during specimen fabrication, equate to the total losses within a specimen. Losses may occur during three stages of the specimen’s life: (1) prior to transfer, (2) at transfer, and (3) after transfer. Prior to transfer, steel relaxation induces losses in pretensioned members. A number of one-time, instantaneous losses occur at transfer. In pretensioned members, instantaneous losses result from elastic shortening of concrete. Finally, steel relaxation, concrete creep, and concrete shrinkage continue to reduce tensile strand stress after transfer and throughout the lifespan of the specimen. Proper estimation of prestress losses will accurately predict the effective prestress f_{pe} utilized in design. The effective prestress directly relates to transfer and development length; as such, this study utilized four methods to predict f_{pe} values after all losses within the girders: (1) AASHTO

approximate lump sum method, (2) AASHTO refined method, (3) PCI method (PCI 2004), and (4) ACI Committee 209 (2008) method.

The AASHTO approximate lump sum method estimates the combined effect of all time-dependent losses based on specimen and strand type. For box girders with Grade 270 strands, the upper bound estimate of time-dependent losses Δf_{pTD} is taken per Equation 4-1, where *PPR* is the partial prestressing ratio. For low-relaxation strands, AASHTO permits the reduction of Eq. 4-1 by 4 ksi. For I-girders with Grade 270 strands, the average estimate of time-dependent losses is calculated using Equation 4-2, which may be reduced by 6 ksi for low-relaxation strands. Both equations are valid for pretensioned members cast with normal-weight concrete, stressed after reaching 3.5-ksi strength, and either steam or moist cured.

$$\Delta f_{pTD} = 21.0 + 4.0PPR \quad \text{(Eq. 4-1)}$$

$$\Delta f_{pTD} = 33\left[1 - 0.15\left(\frac{f_c' - 6}{6}\right)\right] + 6PPR \quad \text{(Eq. 4-2)}$$

The AASHTO refined method, PCI method, and ACI method provide refined estimates for elastic shortening and individual components of time-dependent losses including concrete shrinkage, concrete creep, and steel relaxation. The procedures for the methods may be found in appropriate references but are not presented herein. The PCI (2004) handbook also states typical prestress losses range from 25 ksi to 50 ksi in normal-weight concrete members, and from 30 ksi to 55 ksi in lightweight concrete members. According to ACI Committee 209, correlation between measured and computed prestress losses is reasonable but not accurate; calculated losses may be expected to correlate to actual losses within 15-20%. A more rigorous method of computing prestress losses is the time-step method, where time-dependent losses are evaluated at successive intervals over a specified length of time. In doing so, the interdependent effects of relaxation, creep, and shrinkage, all of which occur at different rates, are included in analysis. However, since the estimated long-term losses using the aforementioned methods were reasonable, the time-step method was not utilized in this study.

Table 4.6 lists the effective prestress in the girders calculated using various methods. Values were calculated using the actual release and 28-day concrete strengths. The difference in design and actual concrete strengths had little impact on calculated effective prestress (less than 2 ksi difference). For the box girders, effective prestress from the ACI and AASHTO methods were reasonably precise; however, these were approximately 6 ksi lower than values from the PCI method. Much greater variability is seen in the values for the I-girders; nearly a 15 ksi difference exists between predictions from the AASHTO approximate lump sum and PCI methods.

Table 4.6. Effective Prestress within Girders using Various Prediction Methods

	Box-1	**Box-2**	**I-1**	**I-2**
1-Day Strength (psi)	5660	5460	4880	4710
28-Day Strength (psi)	7500	7010	6870	6740
AASHTO Approx.	168.0	168.0	159.2	159.1
AASHTO Refined	166.1	166.1	166.9	166.9
PCI	172.2	171.6	173.8	173.6
ACI 209	166.5	166.2	165.8	165.5

4.4 DEVELOPMENT LENGTH PREDICTIONS

Predicted development lengths in the four specimens were calculated using Eq. 2-2. Both the effective prestress f_{pe} and the nominal strand stress f_{ps} may vary depending on method of calculation. Effective prestress was calculated using four different methods (Section 4.3). The nominal strand stress was calculated using two methods, the first of which was an AASHTO code approximation. The second, iterative method utilized constitutive stress-strain material properties of Grade 270 prestressing strand; in the method, three strain components are calculated for an assumed nominal stress f_{ps}; if the sum of the three strains is within reasonable tolerance of the corresponding strain on the strand's stress-strain curve, the f_{ps} is acceptable. The first strain is due to the effective prestressing load, without self-weight; the second strain is due to the load required to negate the effect of camber; the third strain is the additional strain required to reach ultimate failure. Only the third strain depends on the assumed nominal stress.

Nominal stress predictions from the two methods differed by no greater than 4 ksi. Development lengths calculated using various effective prestress values and nominal stress from the stress-strain (SS) and AASHTO methods are shown in Table 4.7. Specific values are presented only for one specimen per type of beam because differences in predictions for two specimens of the same beam type were negligible. For the box girder, development length predictions ranged between 68.6 in. and 72.4 in; for the I-girder, predictions ranged from 73.9 in. to 81 in. The development length predictions did not incorporate the 1.6 multiplier specified by the FHWA and AASHTO (see Section 2.2).

Table 4.7. Development Lengths Calculated using Various Methods

Box Girder 1	**Actual f'_c = 7.5 ksi**		
Methods	*SS*	*AASHTO*	
AASHTO Approx.	70.0	71.8	
AASHTO Refined	70.6	72.4	
PCI	68.6	70.3	
ACI 209	70.4	72.2	**Range**
Minimum	68.6	70.3	**68.6**
Average	69.9	71.7	**70.8**
Maximum	70.6	72.4	**72.4**

I-Girder 1	**Actual f'_c = 6.9 ksi**		
Methods	*SS*	*AASHTO*	
AASHTO Approx.	81.0	78.8	
AASHTO Refined	78.5	76.2	
PCI	76.3	73.9	
ACI 209	78.8	76.5	**Range**
Minimum	76.3	73.9	**73.9**
Average	78.7	76.4	**77.6**
Maximum	81.0	78.8	**81.0**

4.5 DESIGN CAPACITIES

The full-scale specimens were designed per AASHTO design specifications (AASHTO 2004). Flexural capacity was calculated using the AASHTO f_{ps},and was found to be 1035 kip-ft and 1800 kip-ft for the box and I-girder, respectively. Figures 4.23 and 4.24 also display as-built sectional shear capacities for each specimen; shear capacities were

calculated using both ACI and AASHTO methods, and all calculations utilized the 6000 psi design
strength.

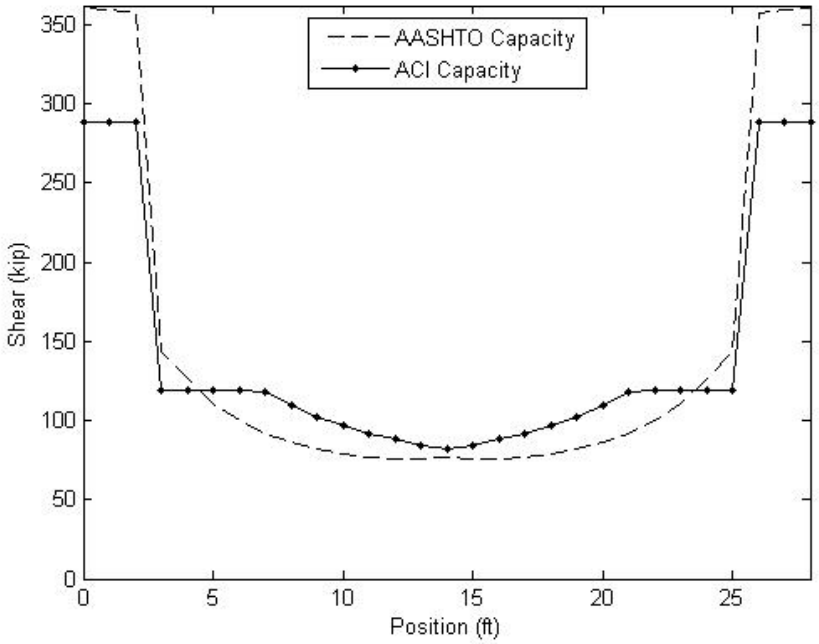

Figure 4.23. Shear capacity for box girders.

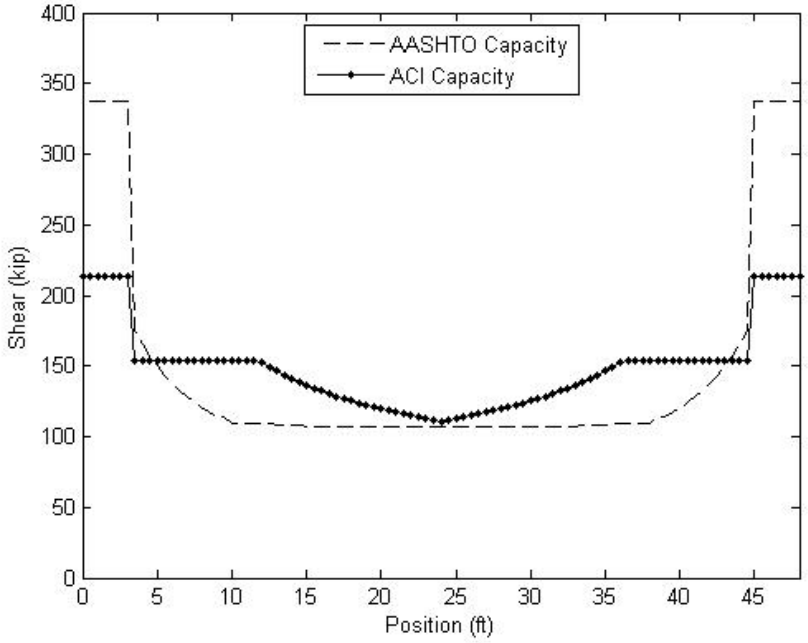

Figure 4.24. Shear capacity for I-girders.

As seen in Figure 4.23, the box beam is most critical in shear at the interface of the hollow and filled cross-sections, 30 in. from either girder end. Shear capacity at the interface was calculated as 145 kip and 207 kip using ACI and AASHTO methods. The difference in

the two capacities resulted from the methods' assumptions regarding compressive crack angles. Capacities in Figure 4.24 were calculated using the composite girder with a 6-ksi strength 8 in. x 30 in. slab. As shown, the I-girder is most critical in shear approximately 4 ft. from either end of the specimen, where stirrup area decreases from 0.8 in^2 to 0.4 in^2 and stirrup spacing increases from 6 in. to 12 in. on center.

4.6 CFRP SHEAR REINFORCEMENT

As shown in Figure 4.23, the box girders were adequately designed for typical AASHTO load conditions. However, the purpose of flexural tests in this study was to develop the maximum design moment as near to the specimen's end as possible; the applied load required to attain this moment would result in shear demand exceeding the design shear capacity. While it was decided to test three ends of the box girders as built, Carbon Fiber Reinforced Polymer (CFRP) sheets were wrapped around one end of specimen Box-2 to enhance its shear performance prior to flexural testing. Fiber reinforced polymers have been proven effective in strengthening concrete members in shear (Norris et al. (1997) and Kachlakev and McCurry (2000)).

To prevent premature shear failure during the first flexural test on Box-2, an 18-in. wide CFRP wrap was applied at one end of the specimen. Coupon tests were conducted to evaluate the tensile modulus and strength of the composite formed with unidirectional carbon fabric and a saturating epoxy resin. Coupons were 0.6 in. x 14 in., and each had 4-in. long perforated plastic tabs at either end for gripping within the loading apparatus. The specimens were formed by saturating two 0.014-in. thick layers of carbon fabric with an epoxy resin designed to have a 120-minute pot life. Specimens were cured for 36 hours prior to testing. The average tensile modulus and ultimate strength of the composite coupons were 19694 ksi and 284 ksi, respectively. The coupon specimens consistently failed at the location of grips due to high stress concentration or fracture of the plastic tabs; therefore, the average modulus and strength values were probably conservative.

Following the ACI Committee 440 design procedure, it was determined that two layers of carbon fabric wrapped entirely around an 18-in. section of the beam would provide sufficient shear strength. In this configuration, the CFRP would not interfere with plastic hinge development under the load, nor would it cover the specimen where shear capacity was adequate. The 18-in. section was prepared by roughening the smooth concrete surface with a diamond-toothed grinder to facilitate adhesion between the CFRP and concrete. After the roughened surface had been cleaned, a first coat of epoxy resin was applied directly to the concrete. Then, the first layer of carbon fabric was pressed onto the epoxy and held in place. An absorbent roller was utilized to impregnate the fabric with another layer of resin. The process was repeated for the second layer of fabric. Care was taken to ensure fabric was completely saturated, and excess resin was removed by pulling a rubber squeegee along the contour of the beam. The CFRP wrapping procedure is shown in Figure 4.25.

Figure 4.25. Application of CFRP wrap to specimen Box-2.

CHAPTER 5 TRANSFER LENGTH

After fabrication, transfer lengths in the four full-scale girders were measured between August 27, 2009 and September 28, 2009. Measurements were taken at 16 locations to obtain average transfer lengths for the eight girder ends and each girder as a whole. Experimental data was compared to ACI and AASHTO requirements.

5.1 MEASUREMENTS

After 20 hours of moist curing, forms for all girders were removed to provide access for attaching surface-strain target points, which were used to obtain longitudinal strain profiles at the ends of specimens. For each girder, 0.39-in. diameter stainless steel target points were glued to each side of both ends at a depth corresponding to strands' center of gravity; five-minute metal-concrete epoxy was used, and concrete surfaces were wiped clean prior to application. Figure 5.1 shows targets attached to specimens Box-1 and I-1. Targets were spaced 2 in. apart on specimens Box-1 and I-1, 4 in. apart on specimens Box-2 and I-2, and were extended approximately 45 in. from the end of each beam. Prior to releasing the pretensioned strands, initial distance measurements were taken between each pair of target points using a mechanical gauge with 4-in. length.

Strands were released after 24 hours of curing; Box-1 and Box-2 had reached 5660 psi and 5460 psi strengths, respectively, while I-1 and I-2 had reached 4880 psi and 4710 psi strengths, respectively. Although the latter two girders did not meet the specified 5000 psi release strength, it was deemed appropriate to release all four specimens so that subsequent measurements could proceed on the same day. Strands were flame-cut (see Figure 4.3 for cutting locations), and distances between target points were measured immediately after release. In conjunction with the initial target point measurements, these readings were then used to develop a strain profile for all sides and ends of the beams. The specimens were moved from their casting beds to the fabrication plant yard after 1-day measurements were complete. The beams remained unmoved in the yard for measurements taken 3, 7, 14, and 28 days after concrete placement.

For each day of transfer length measurements, seven compressive cylinder tests were performed to determine concrete strength. The top and bottom cylinder surfaces were made smooth with an electric grinder prior to testing. One cylinder each from SCC Batches 1-3 and SCC Batches 5-8 (see Tables 4.1 and 4.2) were tested, and beam strengths were determined based according to batch distribution within the beams. The resultant concrete strengths over time for each beam are listed in Table 5.1. The 6000-psi design strength was reached by the box girders within 3 days and by the I-girders within 14 days.

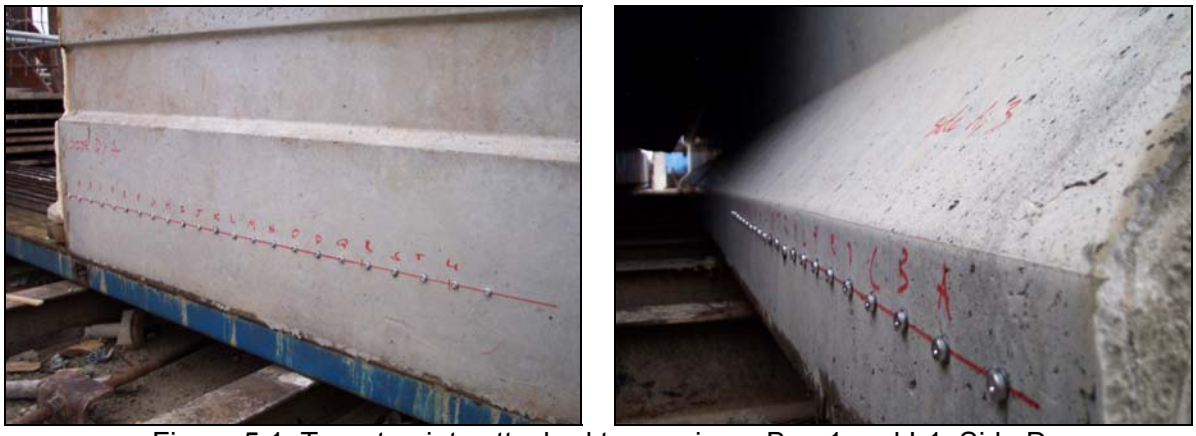

Figure 5.1. Target points attached to specimen Box-1 and I-1, Side D.

Table 5.1. Girder Specimen Strength as Determined by Compressive Cylinder Tests

Age (days):	1	3	7	14	28
Box-1	5660	6140	6680	7460	7500
Box-2	5460	6300	6760	7450	7010
I-1	4880	5480	5940	6550	6870
I-2	4710	5470	5980	6590	6740

5.2 DISCUSSION OF TRANSFER LENGTH RESULTS

The 95% AMS method (see Section 2.3.6) was utilized to determine experimental transfer lengths via surface strain measurements. Strain profiles obtained for all 16 transfer length locations (refer to Figure 4.3) are presented in Figures C.1-C.16 in Appendix C. An example set of strain profiles is shown in Figure 5.2 for the far end of specimen I-1 at Location D. At various ages, individual transfer lengths were obtained for both sides of both ends of each girder. Then, average transfer lengths were calculated for the eight end locations ($L_{t\text{-}end}$) and for each girder as a whole ($L_{t\text{-}avg}$). At the far end of specimen I-2, no transfer lengths were obtainable at Location A since strain profiles showed no distinct plateau (see Figure C.15). However, readings at Location D (see Figure C.16) at the same end clearly displayed plateau regions. $L_{t\text{-}end}$ values reported for I-2's far end, therefore, were based solely on measurements at Location D.

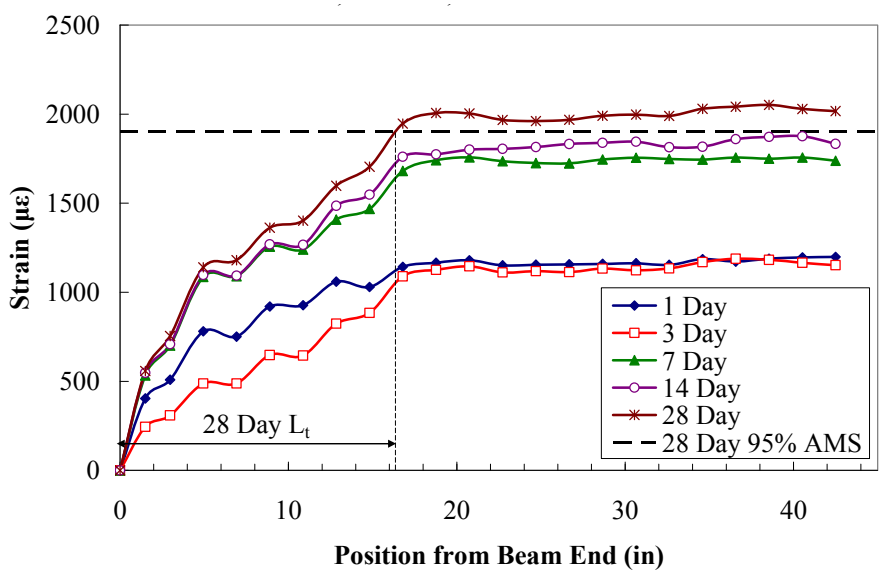

Figure 5.2. Strain profiles for the far end of specimen I-1 at Location D.

Table 5.2 contains all $L_{t\text{-}end}$ values obtained in the study. At seven of eight ends, transfer lengths consistently met ACI and AASHTO code requirements. However, at I-2's far end, transfer lengths exceeded the ACI $50d_b$ provision at all ages by up to 30% and exceeded the AASHTO $60d_b$ provision at 1-day and 3-day measurements by up to 8.3%. No 28-day data was available for I-2's far end because strain readings at Location D were incomplete due to human error. A bolded value in Table 5.2 indicates the end at which transfer length was largest within a girder at each age.

A number of factors acting in combination could have produced different transfer lengths at two ends of the same beam: concrete casting location, strand cutting location, and, because beams were cast with multiple batches of concrete, compressive strength at

transfer. The far ends of Box-2 and I-2 experienced the most immediate force transfer due to strand cutting and had the lowest concrete compressive strengths within their respective girder types. Accordingly, transfer lengths at the far ends of Box-2 and I-2 were longer than those at their opposite ends by 11% and 57%, respectively. The effects of cutting location and concrete strength were not considered independently; however, their combined action appeared to significantly impact transfer length. Table 5.2 also contains ratios between $L_{t\text{-}end}$ values at starting and far ends for each girder. Average "Starting/Far" ratios ranged from 0.63 in specimen I-2 to 1.19 in specimen I-1, suggesting transfer length is independent of casting location. The $L_{t\text{-}end}$ values are also shown over time in Figure 5.3. No consistent increase in transfer length was observed as concrete aged.

Table 5.2. Transfer Lengths at all Beam Ends ($L_{t\text{-}end}$, in inches)

	Age (days):	**1**	**3**	**7**	**14**	**28**
Box-1	Starting End	18.1	18.9	18.1	19.3	20.3
	Far End	**24.5**	**20.2**	**24.0**	**19.6**	**24.1**
	Starting/Far	0.74	0.94	0.75	0.98	0.84
Box-2	Starting End	19.8	19.3	18.7	17.7	18.1
	Far End	**21.6**	**20.6**	**19.8**	**20.0**	**21.4**
	Starting/Far	0.92	0.94	0.94	0.89	0.84
I-1	Starting End	**24.6**	**23.1**	**22.4**	**22.6**	**21.8**
	Far End	18.6	19.5	19.1	19.6	19.5
	Starting/Far	1.32	1.19	1.17	1.16	1.12
I-2	Starting End	18.5	19.6	20.6	19.8	21.0
	Far End	**32.3**	**32.5**	**29.7**	**29.9**	-
	Starting/Far	0.57	0.60	0.69	0.66	-

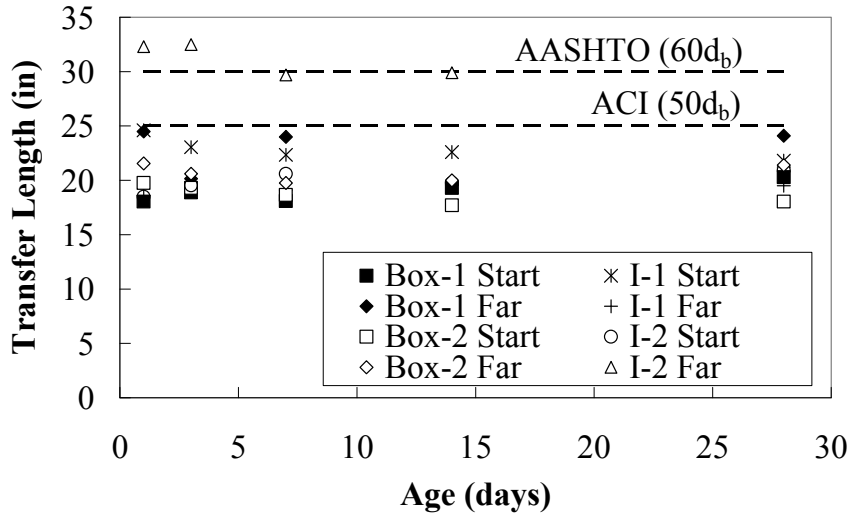

Figure 5.3. $L_{t\text{-}end}$ values at various ages compared to ACI and AASHTO requirements.

At all ages, the average transfer length ($L_{t\text{-}avg}$) for each girder was calculated by taking the average of the girder's two $L_{t\text{-}end}$ values presented in Table 5.2. $L_{t\text{-}avg}$ values are presented in Table 5.3 for comparison to ACI and AASHTO provisions. No 28-day $L_{t\text{-}avg}$ value was calculated for specimen I-2 because data for its far end was not available, as previously mentioned. Ratios $L_{t\text{-}avg}/50d_b$, $L_{t\text{-}avg}/(f_{pe}d_b/3)$, and $L_{t\text{-}avg}/60d_b$ in Table 5.3 with

values less than unity indicate adequate transfer lengths with respect to code requirements. The ratio $L_t/(f_{pe}d_b/3)$ was calculated using experimental data only from 28-day tests, since the ACI Code prediction utilizes the effective prestressing force after all prestress losses.

As seen in the table, average transfer lengths in three of the four specimens consistently met the most stringent transfer length requirement ($50d_b$). However, average transfer lengths within specimen I-2 exceeded $50d_b$ prior to 14-day measurements. This is attributed to the unusually large transfer lengths obtained at the specimen's far end, for reasons suggested previously. Overall, experimental transfer lengths were 86% of $50d_b$, 72% of $60d_b$, and 69% of $f_{pe}d_b/3$. Therefore, it is reasonable to presume the bond properties of the tested SCC are sufficient to meet current design requirements; the final phase of this project described in Chapter 6 seeks to confirm this presumption. Data in Table 5.2 and Table 5.3 shows no correlation between transfer length and girder type.

Table 5.3. $L_{t\text{-}avg}$ Values at Various Ages Compared to ACI and AASHTO Requirements

			ACI ($50d_b$)	**ACI ($f_{pe}d_b/3$)**	**AASHTO ($60d_b$)**
	Age (days)	**$L_{t\text{-}avg}$ (in)**	**$L_{t\text{-}avg}/L_{t\text{-}calc}$**	**$L_{t\text{-}avg}/L_{t\text{-}calc}$**	**$L_{t\text{-}avg}/L_{t\text{-}calc}$**
Box-1	1	21.3	0.85	-	0.71
	3	19.5	0.78	-	0.65
	7	21.1	0.84	-	0.70
	14	19.5	0.78	-	0.65
	28	22.2	0.89	0.73	0.74
Box-2	1	20.7	0.83	-	0.69
	3	20.0	0.80	-	0.67
	7	19.2	0.77	-	0.64
	14	18.9	0.75	-	0.63
	28	19.7	0.79	0.65	0.66
I-1	1	21.6	0.86	-	0.72
	3	21.3	0.85	-	0.71
	7	20.7	0.83	-	0.69
	14	21.1	0.84	-	0.70
	28	20.7	0.83	0.68	0.69
I-2	1	25.4	1.02	-	0.85
	3	26.0	1.04	-	0.87
	7	25.2	1.01	-	0.84
	14	24.8	0.99	-	0.83
	28	-	-	-	-
Box Beam Average:			**0.81**	**0.69**	**0.67**
I-Beam Average:			**0.92**	**0.68**	**0.77**
Overall Average:			**0.86**	**0.69**	**0.72**

CHAPTER 6 DEVELOPMENT LENGTH

After completion of the final 28-day transfer length tests, the four girders were transported to the Newmark Structural Engineering Laboratory at UIUC. An iterative test method was employed to determine the development length of strands within the two types of beams (see Section 2.3.7). Due to scheduling conflicts, the first flexural test on specimen Box-1 was conducted April 12, 2010. A total of eight flexural tests were executed; concrete cracking, concrete strain, deflection, and strand end-slip were monitored throughout each test; web strains and deck slip were also monitored during I-girder tests. This chapter details the flexural test procedure, observations, and results, comparing experimental development lengths to code requirements and experimental strengths to theoretical predictions.

6.1 THREE-POINT FLEXURAL TEST SETUP

6.1.1 Loading Frame

A structural loading frame was designed to apply forces up to 600 kip to the girders. The frame components are shown in Figure 6.1, with pertinent dimensions called out in the elevations shown in Figures 6.2 and 6.3. The centerline-to-centerline (CL-to-CL) distance and shear span, as indicated in Figure 6.2, changed for each test. In addition, for the I-girder tests the entire frame assembly was raised 24 in. from the position shown in Figure 6.3 to accommodate the height differential between girder types.

The four built-up columns were bolted to the structural testing floor. Two pairs of channels extended between the columns, and a stiffened I-beam extended between the channels. The I-beam was oriented in the longitudinal direction of the test specimens. Attached to the I-beam were two manually-controlled hydraulic rams with 300-kip capacity each. Load cells were secured to the rams' pistons by threaded rods and were protected by aluminum caps. When activated, the rams pressed the cells onto a bearing block resting atop a pinned support beneath the load point, per Figure 6.4. For each test, a pinned support was placed beneath the end of the girder nearest the applied load, while a roller support was placed at the opposite end; supports are shown in Figure 6.5. The bottom bearing plates on either end were affixed to reaction blocks utilized to prevent damage to the structural testing floor. The fully assembled testing frame may be seen in Figure 6.6.

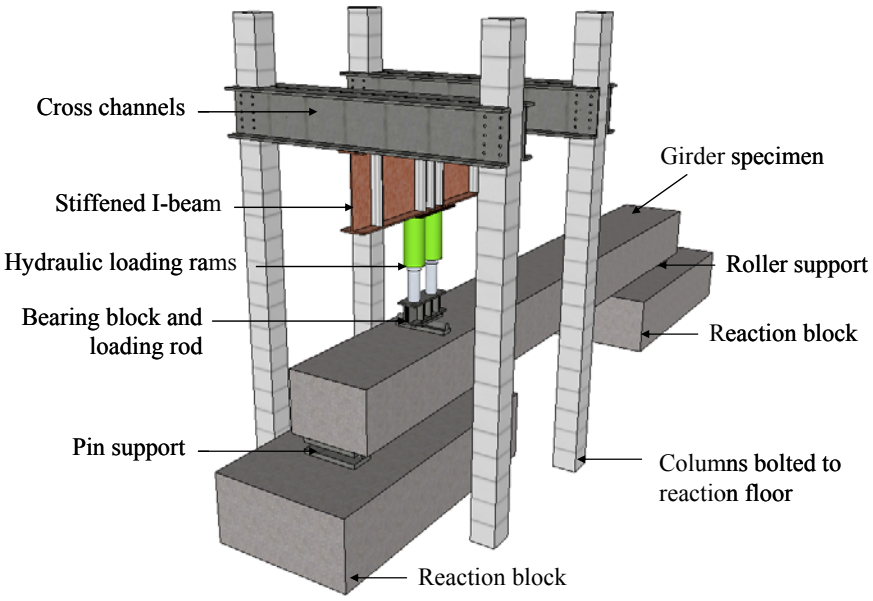

Figure 6.1. Schematic of loading frame components and assembly for flexural tests.

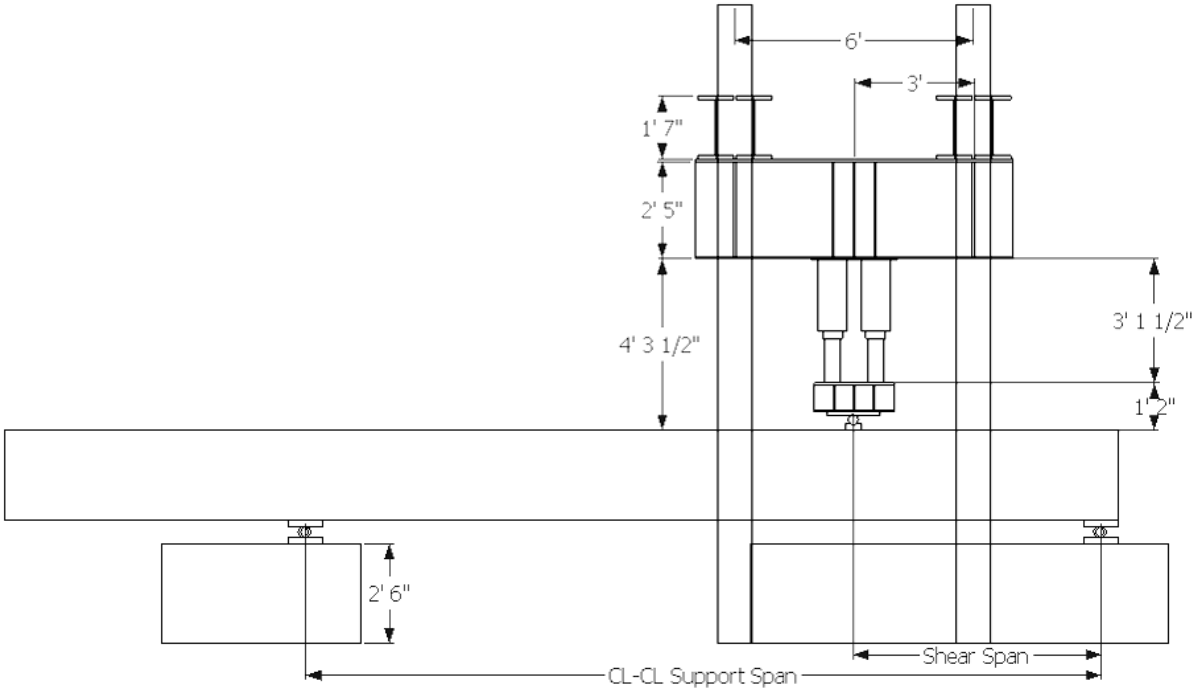

Figure 6.2. East-West elevation of flexural test loading frame.

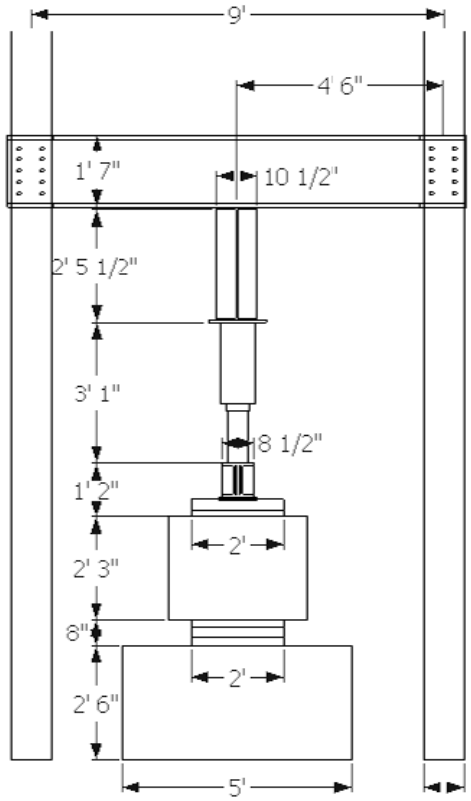

Figure 6.3. North-South elevation of flexural test loading frame.

Figure 6.4. Bearing block and pinned support at point of loading.

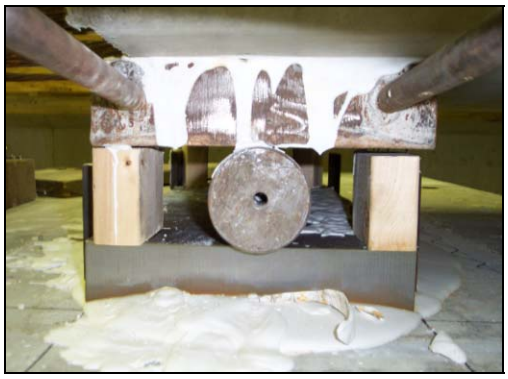

Figure 6.5. Roller (left) and pin (right) support in flexural test setup.

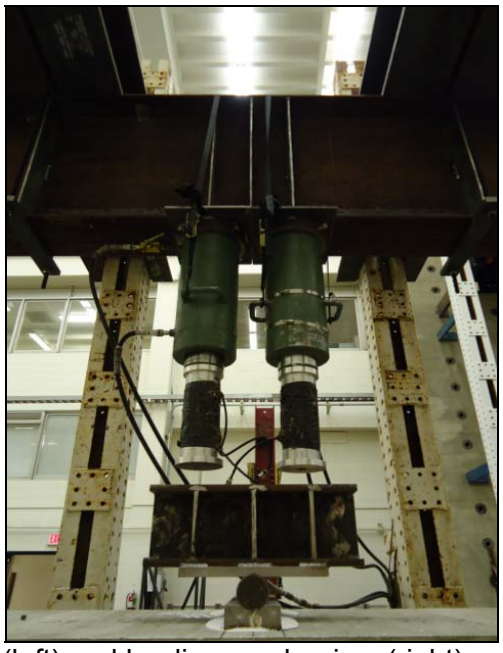

Figure 6.6. Fully assembled testing frame (left) and loading mechanism (right).

6.1.2 Instrumentation

For each test, instrumentation was set in place to measure the applied load, strand end-slip, concrete strain, and beam deflection. End-slip was continuously monitored via LVDTs attached to prestressing strands at the specimen end nearest the applied load. LVDT configurations for the box and I-girders are shown in Figure 6.7. LVDTs #1-3 had a range of ±0.10 in. and were affixed to strands using aluminum angles and hose clamps. LVDTs #4-8 had a range of ±0.50 in. and were affixed using wooden connector pieces and hose clamps; both attachments are shown in Figure 6.8.

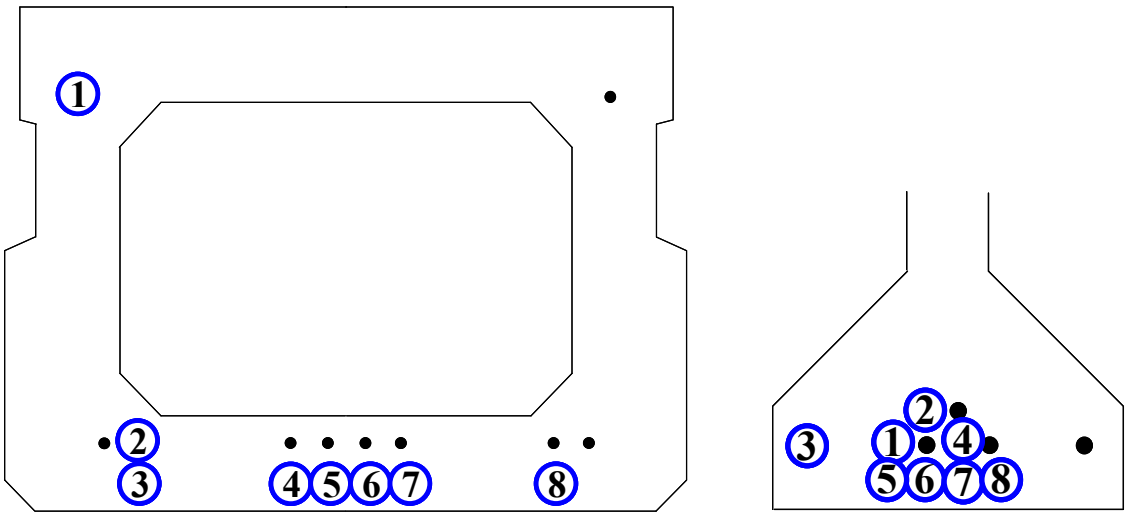

Figure 6.7. End-slip LVDT configuration for box girder (left) and I-girder (right) tests.

Figure 6.8. Spring-loaded ±0.10 in. (left) and guided ±0.50 in. (right) LVDTs.

All tests utilized concrete surface strain gauges with 3.54 gauge length and 2% strain limit to obtain experimental strain profiles under the point of loading, as shown in Figure 6.9. Vertical deflection was measured beneath the applied load and at the midpoint between supports by LVDTs with ±3 in. range. Both were attached to the beam using high-strength epoxy paste, per Figure 6.9.

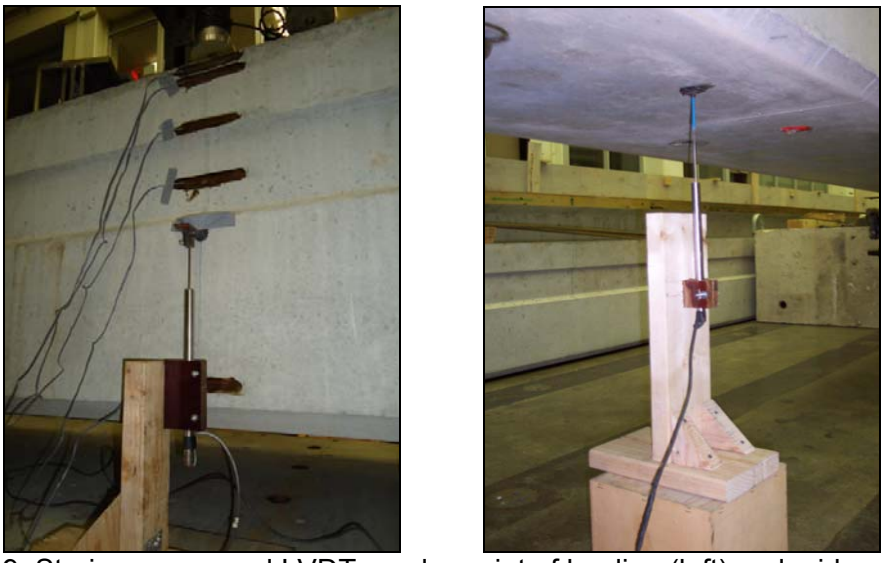

Figure 6.9. Strain gauges and LVDTs under point of loading (left) and midspan (right).

For each I-girder flexural test, an LVDT with ±1 in. range was attached at the end of each I-girder to monitor horizontal slip between the deck and girder. Additionally, three LVDTs with ±1 in. range were attached in a rosette configuration to the web of the girder, as shown in Figure 6.10. Thin rods were utilized to extend the horizontal and vertical LVDTs to a desired 17-in. gauge length and the diagonal LVDT to a desired 24 in. gauge length. The center of the rosette configuration was positioned at the middle of the shear span and middle of the web, per Figure 6.10. The LVDTs were attached such that they could pivot at either end. Strains calculated using output from the rosette configuration were utilized to determine principle compression angles, principal strains, and strain in vertical stirrups.

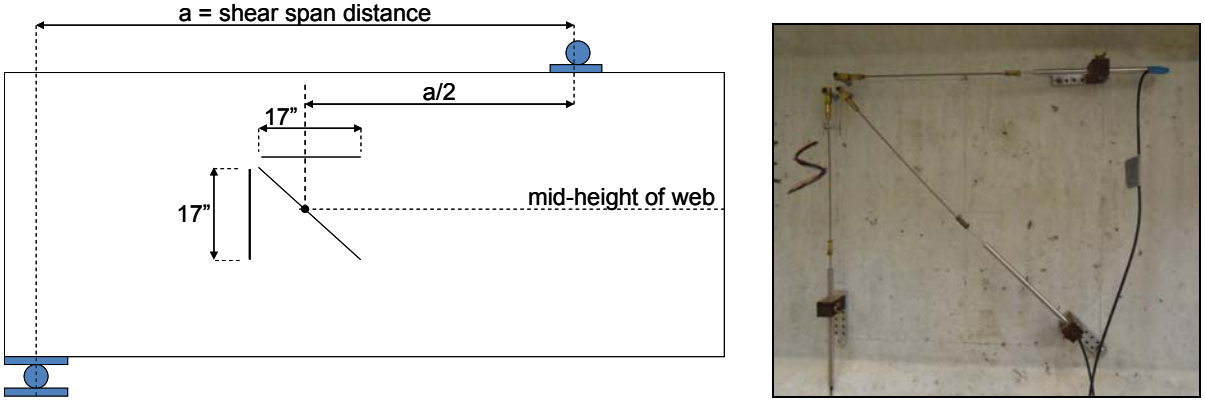

Figure 6.10. Rosette configuration of web LVDTs for I-girder flexural tests.

6.2 DEVELOPMENT LENGTH TESTS

Each girder was tested twice under three-point bending. Strand embedment for each test was controlled by varying the location of bearing supports relative to the loading frame, which remained stationary and bolted to the reaction floor. For the first test on each girder, the pinned support was set nearly flush with the loaded end of the specimen. At the opposite end, the roller support was placed nearly flush with the specimen edge for box girders and 12 ft. from the edge for I-girders. After a specimen’s first test, the partially damaged girder was removed from the testing frame and rotated 180 degrees. The reaction block furthest from the loading frame was shifted to prevent the damaged portion of the specimen from

bearing on the support. Finally, the girder was placed under the frame for its second flexural test. The location of the supports and point of loading for each test are shown in Figures 6.11 and 6.12 for box and I-girders, respectively.

An electric pump was utilized to advance the two hydraulic rams until the bottom load cell caps were in contact with the bearing block. To afford better control throughout testing, the rams were disconnected from the electric pump and reconnected to a manual pump; both the electric and manual pumps had 10,000 psi capacity. The hydraulic system was connected in parallel to ensure rams advanced at the same rate. The rams were advanced continuously until the applied load was within 50 kips of the predicted flexural cracking load, unless shear cracking initiated sooner. Then, specimens were loaded in 6-kip increments until cracking initiated. After crack initiation, specimens were loaded in 3-kip increments and time was allotted between load steps to monitor crack formation and allow load to settle.

Care was taken to monitor end-slip, cracking patterns, and load resistance to determine the most probable failure mode in each test. Shear failure was characterized by prominent diagonal cracking within the shear span and abrupt decreases in load capacity. Flexural failure was characterized by symmetric cracking about the point of load, concrete crushing and high strain in the compression flange under the applied load. Constant load resistance and steadily increasing strand end-slip were indicative of bond failure. When embedment in a specimen approached the development length, the specimen displayed characteristics of more than one failure mechanism; such behavior was termed flexure-shear, flexure-slip, or shear-slip failure. Tests were stopped once a dominant failure mechanism was evident.

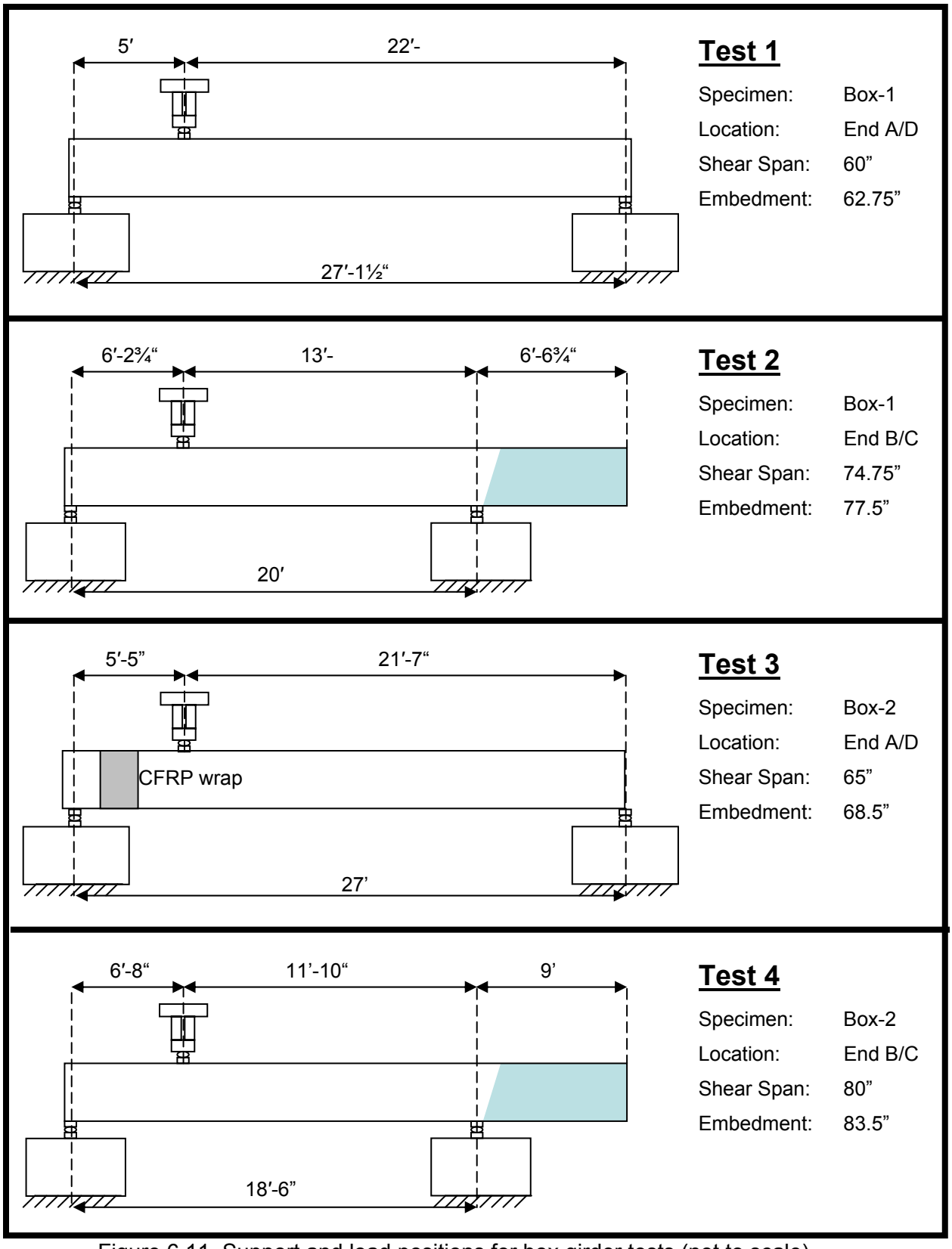

Figure 6.11. Support and load positions for box girder tests (not to scale).

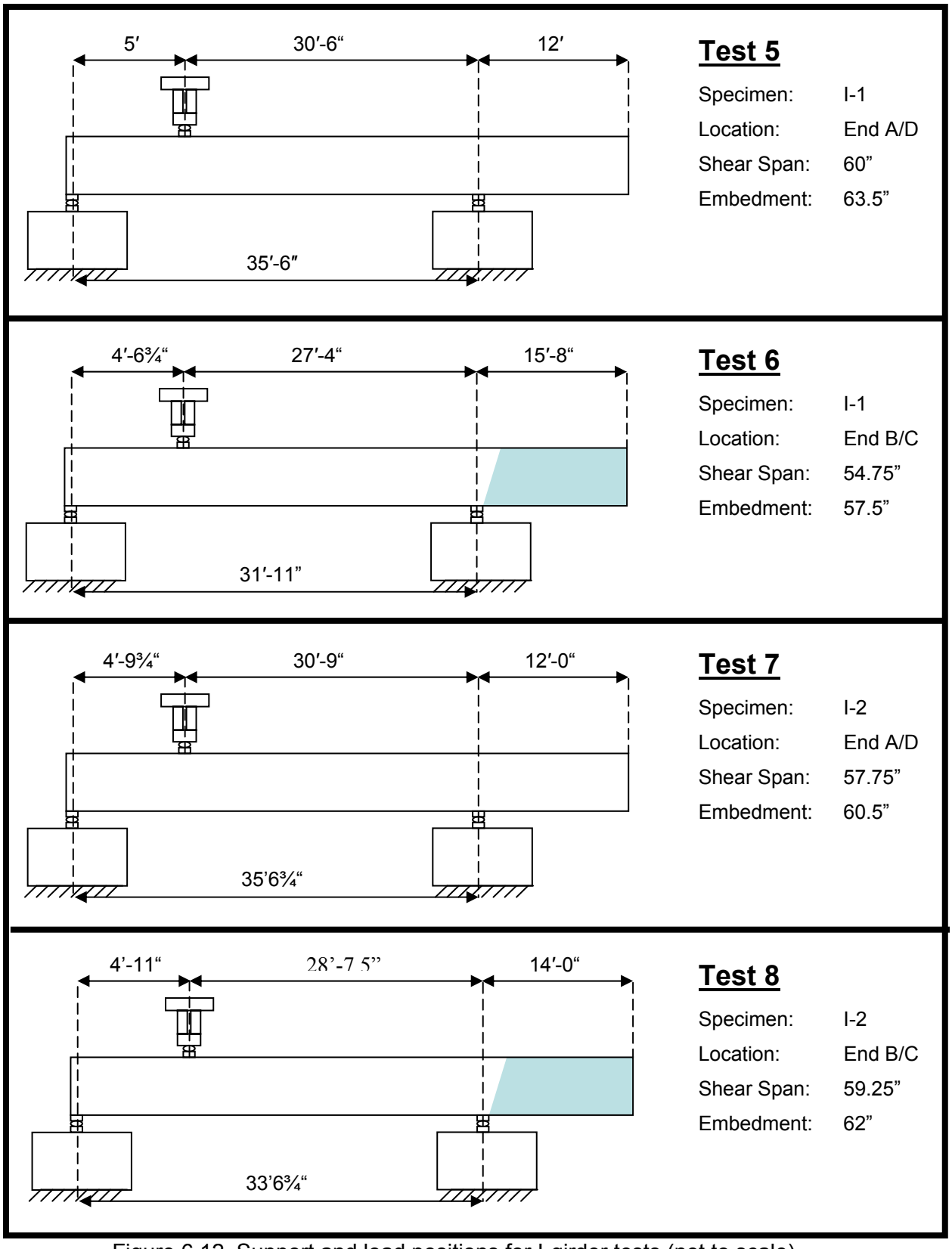

Figure 6.12. Support and load positions for I-girder tests (not to scale).

6.2.1 Test 1: Specimen Box-1, South End (A/D)

The first flexural test was performed on April 12, 2010; 229 days after casting. The total CL-to-CL distance between supports was 27.13 ft. The beam was placed under the loading frame such that the shear span was 5 ft. The embedment was taken as the distance from the beam end to the face of the loading plate; in this case, 62.75 in. The loading protocol for the test was previously described in Section 6.2. The first visible cracks, both shear and flexural, occurred at an applied load of 165 kip. Shear cracking became dominant at 176 kip, after which flexural cracks did not significantly propagate. The maximum resisted load was 197.4 kip, which corresponds to a maximum experimental moment of 841.1 kip-ft. Though the beam remained capable of resisting load, the test was stopped when end-slip of the bottom strands exceeded 0.2 in.

The load-deflection response for the specimen is shown in Figure 6.13. The flexural cracking observed visually corresponded well with the onset of nonlinear behavior in the figure. Deflection at the point of loading was 0.47 in. when the peak load was reached; however, the maximum deflection at the conclusion of the test was 0.76 in. The final cracking pattern for the first test may be seen in Figures D.1 and D.2 in Appendix D. Only three flexural cracks formed throughout the test. Two primary shear cracks formed in the web and propagated diagonally upward toward the point of loading and downward toward a point 30 in. from the end of the specimen, where the hollow within the beam ended. Strand slip occurred only after shear cracks had propagated across the strands in the tension flange. The maximum end-slip of any strand with respect to the applied load is illustrated in Figure 6.14. The term “significant shear cracking” in the figure refers to the load at which shear became the prominent failure mode. The maximum end-slip values for individual strands are shown in Table 6.1.

Longitudinal strain was monitored throughout the test at five locations under the point of loading. The strain output, adjusted for the initial strain in the concrete due to self-weight and the effective prestress, is shown in Figure 6.15. The distances listed in the legend indicate the location of each strain gauge with respect to the bottom fiber of the beam. Using a linear strain assumption, the maximum compressive strain at the top concrete fiber was 942 microstrain.

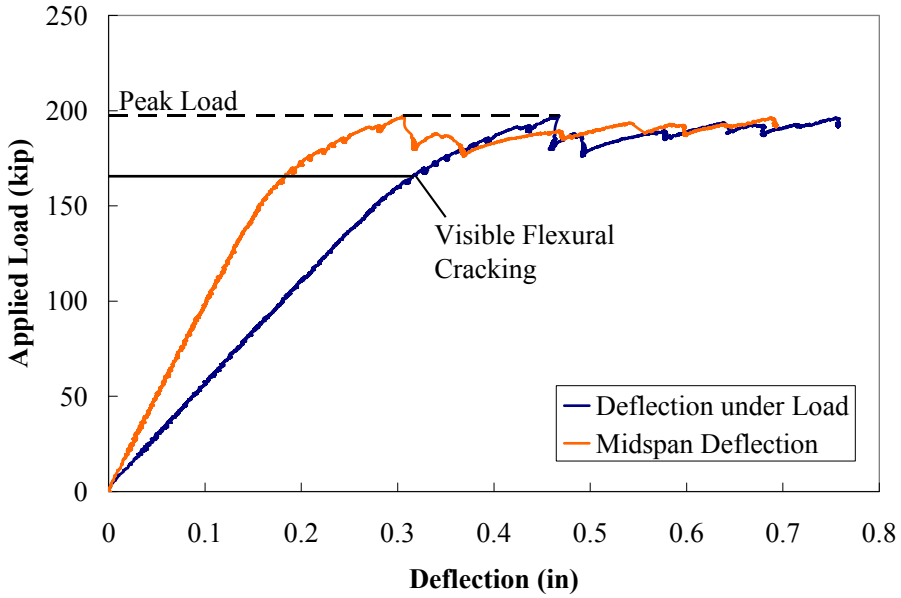

Figure 6.13. Load-deflection response for Box-1, South End.

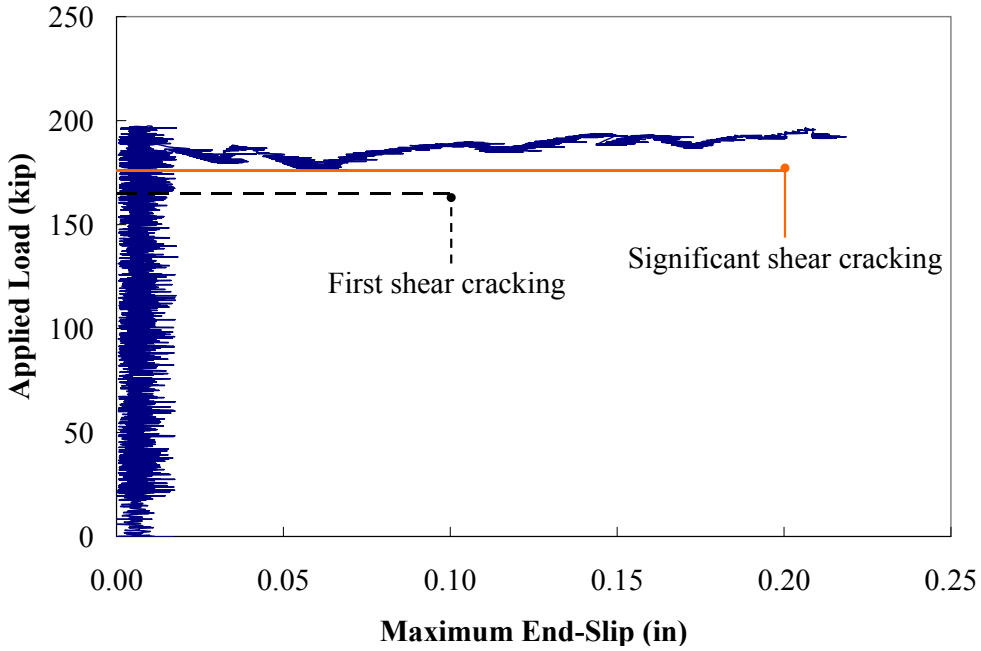

Figure 6.14. Maximum end-slip of any strand for Box-1, South End.

Table 6.1: Maximum End-Slip of Individual Strands for Box-1, South End.

Strand	End-Slip (in)
1	0.017
2	0.209
3	0.194
4	0.191
5	0.212
6	0.208
7	0.219
8	0.167
Bottom Strands	**0.198**
Outer Strands (3 & 8)	**0.180**
Center Strands (4-7)	**0.207**

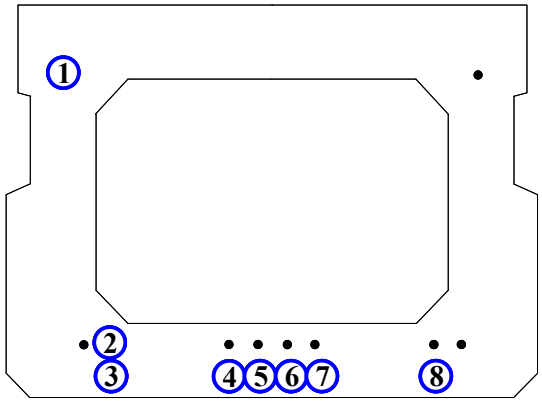

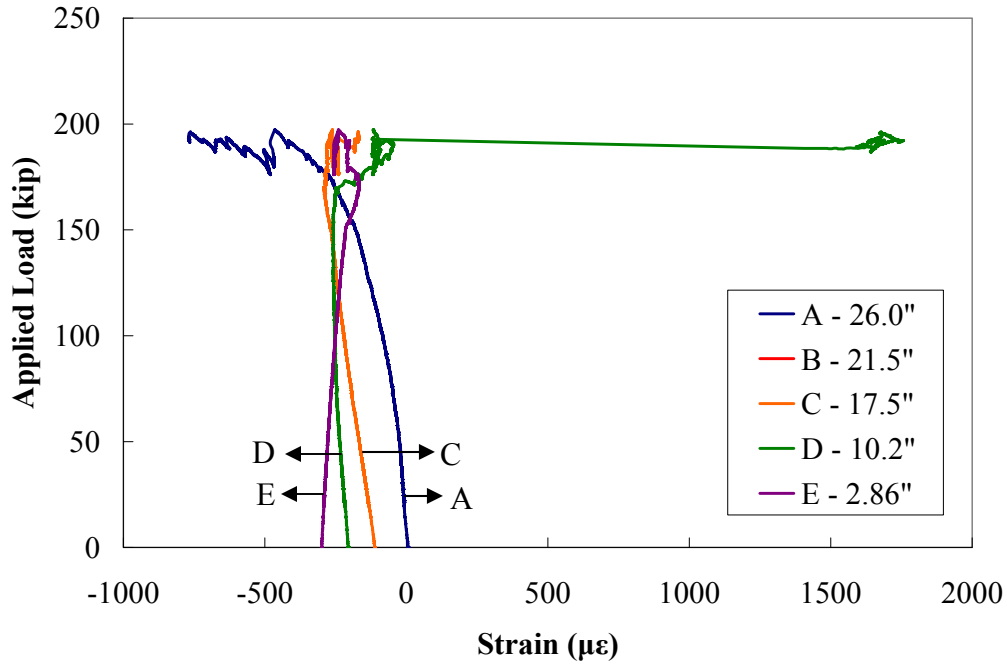

Figure 6.15. Longitudinal strains under loading for Box-1, South End.

6.2.2 Test 2: Specimen Box-1, North End (B/C)

The second development length test was performed April 26, 2010; 243 days after casting. The total CL-to-CL distance between supports was 20 ft. The beam was placed under the loading frame such that the shear span was 6.23 ft. The 77.5 in. embedment for this iteration was selected based on the shear-slip failure observed in the first test.

The first visible flexural cracks occurred at an applied load of 149 kip. The behavior of the beam remained heavily flexural until shear cracking initiated under 218-kip loading. The specimen reached a peak load of 227 kip, which corresponds to a maximum experimental moment of 995.7 kip-ft. The load-deflection response for the specimen is shown in Figure 6.16. As shown in the figure, after reaching the maximum load, resistance declined due to flexural cracking, shear cracking, and strand-slip. The hydraulic rams were pushed downward, though the beam could not again attain the maximum load; the specimen failed abruptly in shear at a load of 218 kip. Deflection under the point of loading was 0.85 in. at the peak load; however, the maximum deflection at failure was 1.41 in.

The flexural cracking pattern is clearly visible in Figure D.3 (see Appendix D), which shows Side C of the specimen immediately prior to failure. Figure D.4 shows the same location after abrupt shear failure occurred in the following load step. As in the first trial, the primary shear crack extended from the point of loading to the point where the hollow within the beam terminated. Had the beam's shear capacity been sufficient for laboratory test load conditions, the specimen would likely have failed in flexure. Akin to the behavior observed in the first test, strand slip occurred only after cracking had propagated across the strands in the tension flange. The maximum end-slip of any strand with respect to the applied load is shown in Figure 6.17, with end-slip values for individual strands shown in Table 6.2.

The longitudinal strain was monitored throughout the test at five locations under the point of loading. The strain output, adjusted for the initial strain in the concrete due to self-weight and the effective prestress, is shown in Figure 6.18. Using a linear strain assumption, the maximum compressive strain at the top concrete fiber was 2257 microstrain.

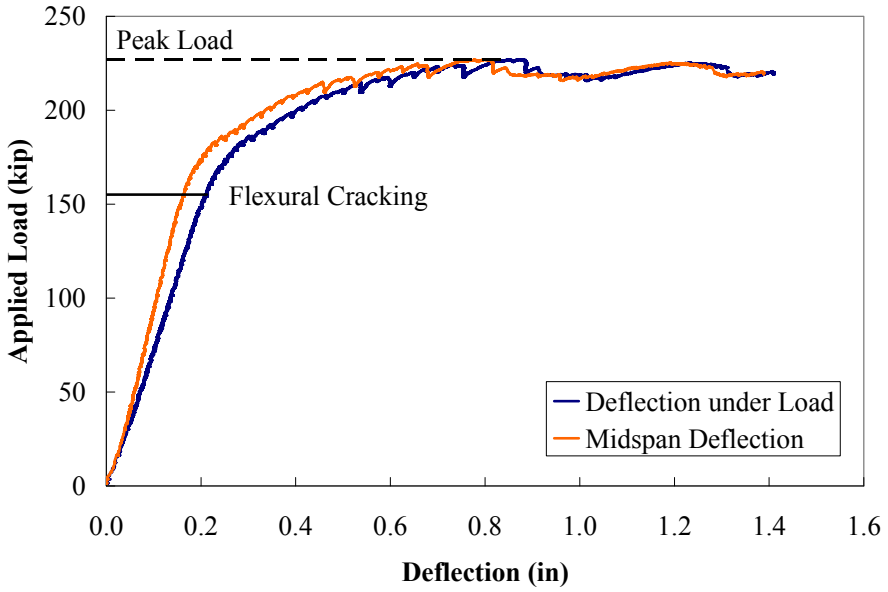

Figure 6.16. Load-deflection response for Box-1, North End.

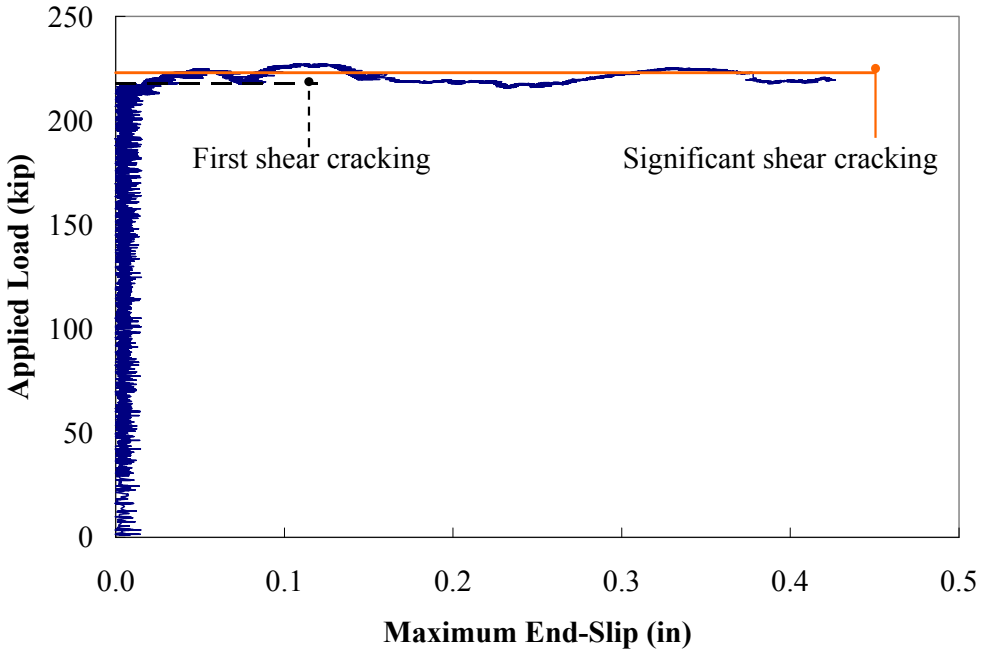

Figure 6.17. Maximum end-slip of any strand for Box-1, North End.

Table 6.2. Maximum End-Slip of Individual Strands for Box-1, North End

Strand	End-Slip (in)
1	0.001
2	0.229
3	0.241
4	0.406
5	0.427
6	0.354
7	0.425
8	0.367
Bottom Strands	**0.370**
Outer Strands (3 & 8)	**0.304**
Center Strands (4-7)	**0.403**

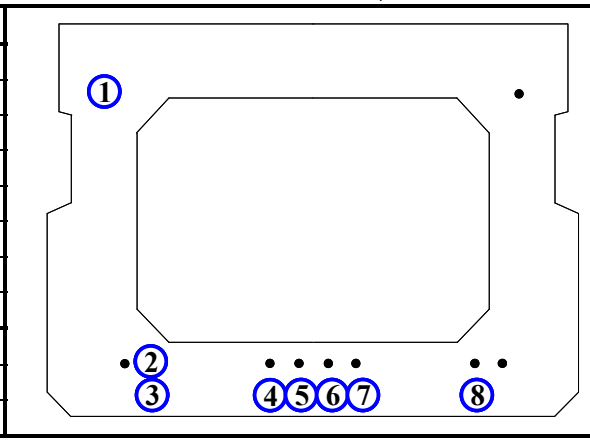

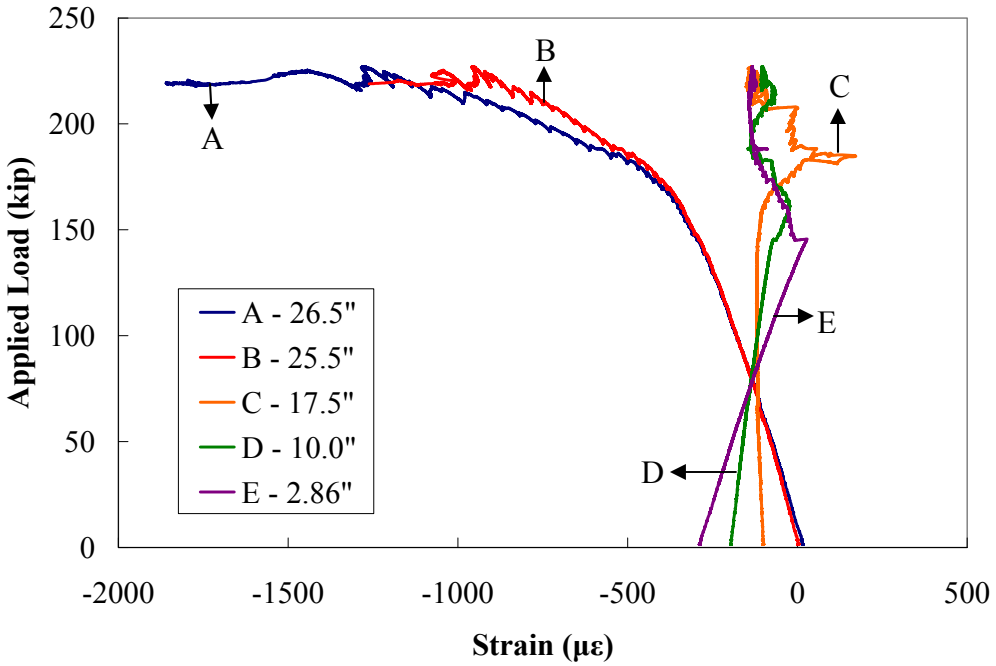

Figure 6.18. Longitudinal strains under loading for Box-1, North End.

6.2.3 Test 3: Specimen Box-2, South End (A/D)

The third development length test was performed on June 21, 2010; 299 days after casting. The total CL-to-CL distance between supports was 27 ft. The beam was placed such that the shear span was 5.42 ft. and the embedment was 68.5 in. As discussed in Section 4.6, an external CFRP wrap was placed around an 18-in. wide section of the beam to provide additional shear reinforcement. It was anticipated that the beam's shear capacity would then be sufficient to withstand the reaction required to reach the theoretical moment capacity; hence, the selected embedment was less than in the preceding test.

Two unforeseen complications during the third test hindered the acquisition of digital data. At an applied load of 184 kip, the manual pump advancing the hydraulic rams failed to develop any further pressure in the system. It was later determined that the pump's oil had been depleted. The beam was unloaded, the data acquisition system was stopped, and the rams were disconnected from the manual pump. In order to proceed with the third test on

the same day, the rams were reconnected to an electric pump. The test was restarted; however, at the conclusion of the test, it was discovered that the data acquisition system failed to record anything during this second trial. It was determined that an internal limit within the logger's code had been exceeded. As a result of these complications, no end-slip or strain readings from the second trial of test three are represented graphically, and data reported for loads greater than 184 kip was obtained through notes taken during the test. For reference, the load-deflection response prior to 184 kip is shown in Figure 6.19.

The first visible flexural cracks occurred at an applied load of 149 kip. Shear cracking initiated at 188 kip and was accompanied by local de-bonding of the CFRP in the web of the beam. At a load of 208 kip, part of the CFRP had become fully delaminated from the side of the specimen. Also, from notes taken during the 208-kip load step, the strain gauge nearest the top of the beam had reached a value of 2040 microstrain. The specimen failed abruptly in shear at a maximum 217-kip load, which corresponds to a maximum experimental moment of 977.6 kip-ft. At failure, CFRP on one side of the beam completely de-bonded after fracturing at the corner of the beam; CFRP on the opposite side de-bonded only across the web. The progression of CFRP failure is illustrated in Figure 6.20.

The final cracking pattern for the third test may be seen in Figures D.5 and D.6 in Appendix D. While significant flexural cracks had developed, the ultimate failure mode paralleled what had been observed in the first two tests. In this case, however, the specimen was able to sustain considerable additional load past the point when shear cracking became prevalent. The external CFRP acted to effectively confine the concrete when diagonal cracking would tend to split the specimen. As before, strand slip occurred only after shear cracks had propagated across the strands in the tension flange; however, exact end-slip data is unavailable for loads greater than 184 kip.

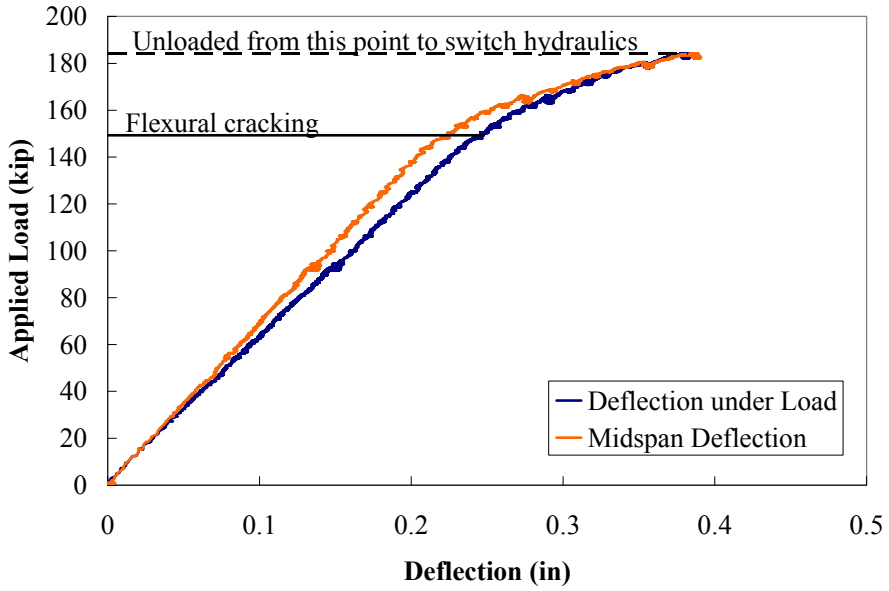

Figure 6.19. Partial load-deflection response for Box-2, South End.


Figure 6.20. Initial peeling (left) and final CFRP failure on Side D (middle) and Side A (right).

6.2.4 Test 4: Specimen Box-2, North End (B/C)

The fourth and final box girder test was performed on June 30, 2010; 308 days after casting. The total CL-to-CL distance between supports was 18.5 ft. The beam was placed under the loading frame such that the shear span was 6.67 ft. and embedment was 83.5 in. No external CFRP was utilized since analysis predicted the beam's shear capacity would be adequate for the given shear span.

The first visible flexural cracks occurred at an applied load of 161 kip, and shear cracking did not initiate until 235 kip. The specimen was not loaded until failure; rather, it was loaded until the induced moment exceeded the beam's theoretical moment capacity. The maximum load was 253 kip, which corresponds to a maximum experimental moment of 1095 kip-ft. The load-deflection response for the specimen is shown in Figure 6.21. The maximum deflection under the point of loading was 0.94 in.

The final cracking pattern for the fourth box girder test may be seen in Figures D.7 and D.8 in Appendix D. Cracking followed a flexural failure pattern and was symmetric about the point of loading. One significant shear crack was observed on only one side of the beam. The end-slip recorded for this test was minimal, even after the shear crack had propagated through the tension flange. The maximum end-slip of any strand with respect to the applied load is illustrated in Figure 6.22, and maximum end-slip values for individual strands are listed in Table 6.3.

The longitudinal strain was monitored throughout the test at five locations under the point of loading. The strain output, adjusted for the initial strain in the concrete due to self-weight and the effective prestress, is shown in Figure 6.23. Using a linear strain assumption, the maximum compressive strain at the top concrete fiber was 1941 microstrain. For scaling purposes, tensile strain readings exceeding 4000 microstrain are not plotted.

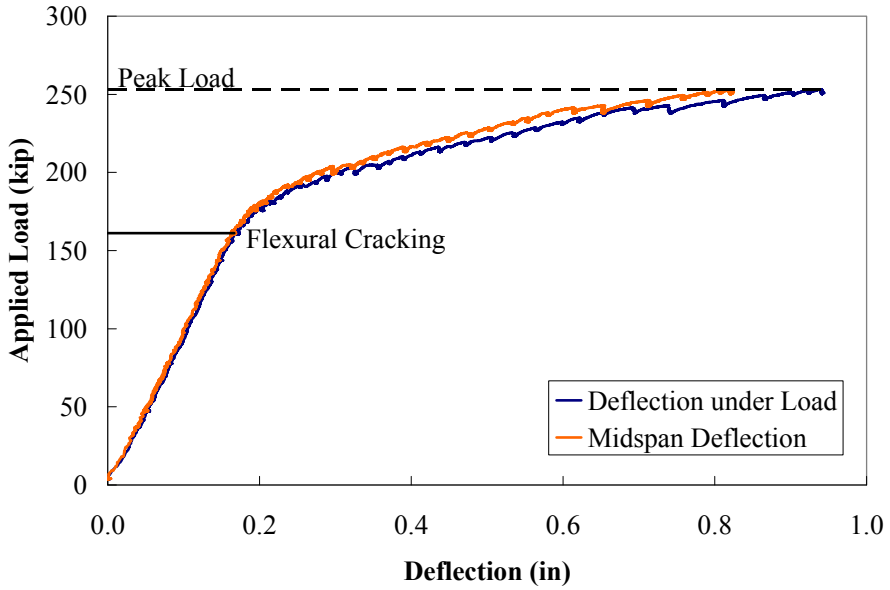

Figure 6.21. Load-deflection response for Box-2, North End.

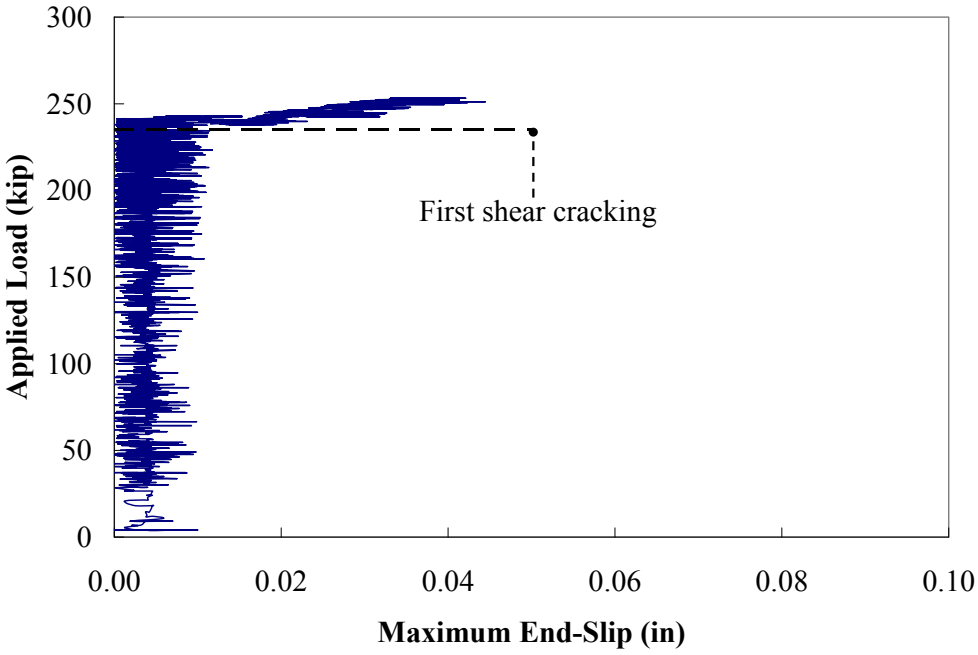

Figure 6.22. Maximum end-slip of any strand for Box-2, North End.

Table 6.3. Maximum End-Slip of Individual Strands for Box-2, North End

Strand	End-Slip (in)
1	0.000
2	0.005
3	0.001
4	0.035
5	0.012
6	0.038
7	0.044
8	0.001
Bottom Strands	**0.022**
Outer Strands (3 & 8)	**0.001**
Center Strands (4-7)	**0.032**

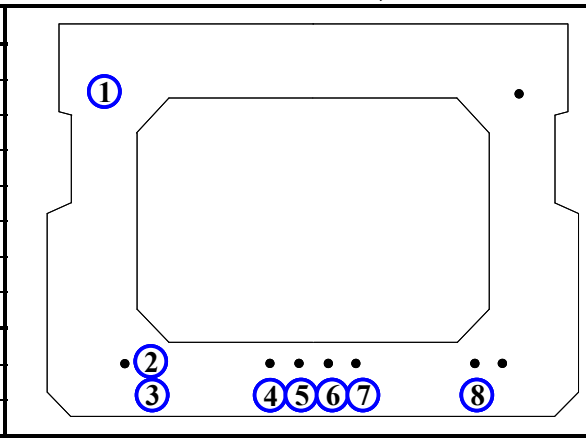

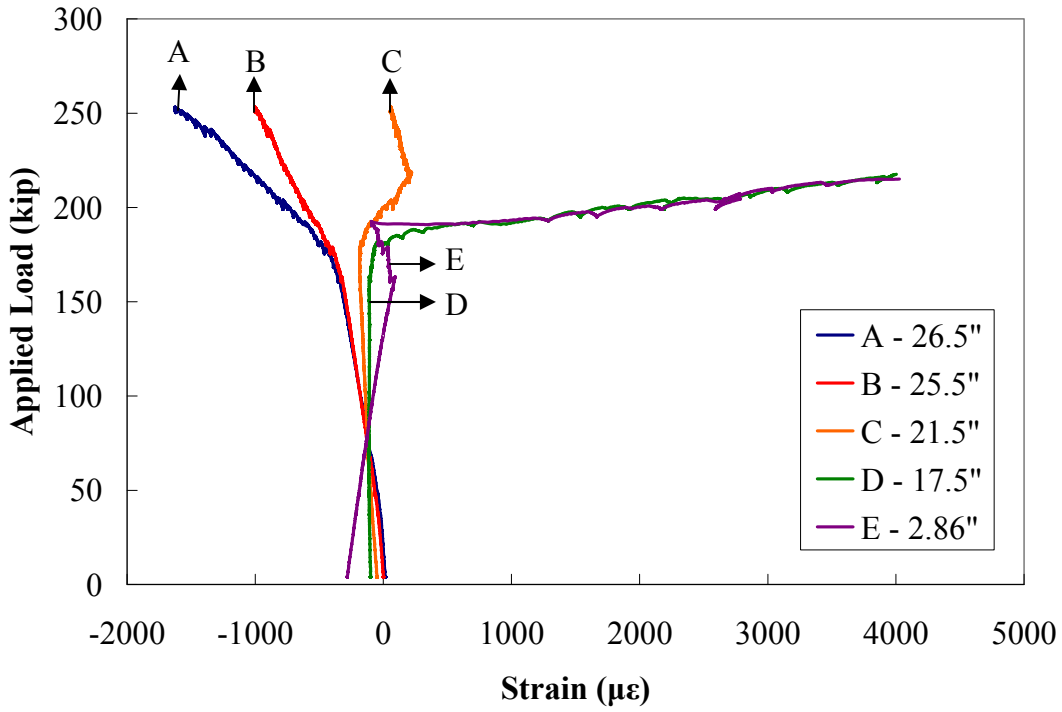

Figure 6.23. Longitudinal strains under loading for Box-2, North End.

6.2.5 Test 5: Specimen I-1, South End (A/D)

The first I-girder flexural test was performed on July 15, 2010, when girder concrete was 323 days old and deck concrete was 83 days old. The beam was placed under the loading frame such that the shear span was 5 ft. and embedment was 63.5 in. Two trials were necessary to conduct the test. In the first trial, the specimen was loaded to 345 kip when an electrical shortage stopped and cleared the data logger. After unloading the beam and resetting the data acquisition system, the second trial was executed.

The first shear cracking occurred at an applied load of 178 kip. The shear cracks formed in the web and propagated through the shear span toward the support. Flexural cracking initiated at 295 kip. As load increased, shear cracks continued to widen, though

flexural cracking governed and occurred at progressively further distances from the applied load. The final cracking pattern may be seen in Figures D.9 through D.12 in Appendix D. The specimen was not loaded until ultimate failure; rather, it was loaded until the induced moment exceeded the beam's design moment capacity. The maximum load was 427 kip, which corresponds to a maximum experimental moment of 1882 kip-ft.

The load-deflection response for the specimen is shown in Figure 6.24. The maximum deflection under the point of loading was 0.8 in. As flexural failure progressed away from the load, deflection at midspan eventually exceeded deflection under the load; the maximum midspan deflection was 0.83 in. Minimal end-slip was recorded as flexural cracking progressed. The maximum end-slip of any strand with respect to the applied load is illustrated in Figure 6.25, and maximum end-slip values for individual strands are listed in Table 6.4. The amount of end-slip was not significant enough to classify a bond failure. The maximum compressive strain recorded at the top concrete fiber under the point of load was 900 με. However, as the heaviest flexural damage occurred approximately 1.5 ft away from the load, the strain reading was not interpreted as an accurate representation of failure.

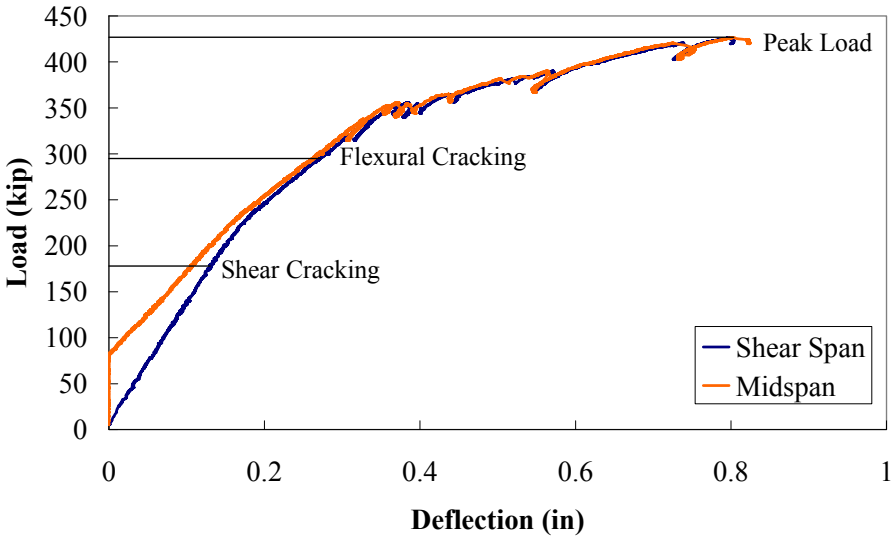

Figure 6.24. Load-deflection response for I-1, South End.

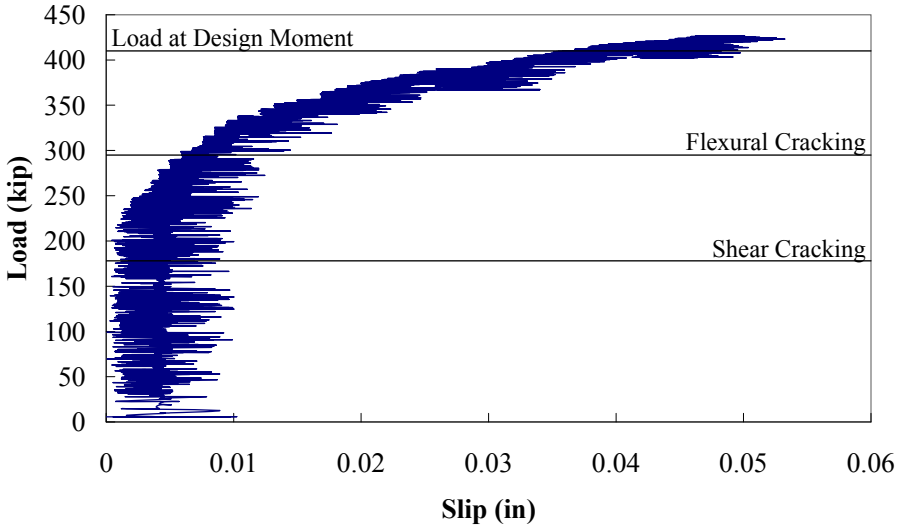

Figure 6.25. Maximum end-slip of any strand for I-1, South End.

Table 6.4. Maximum End-Slip of Individual Strands for I-1, South End

Strand	End-Slip (in)
1	0.038
2	0.047
3	0.046
4	0.047
5	0.046
6	0.052
7	0.053
8	0.051
Bottom Strands	0.051
Outer Strand	0.046
Center Strands	0.048

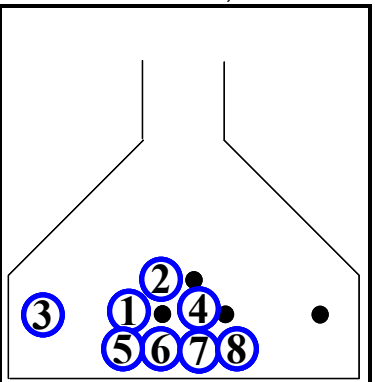

As stated previously, LVDTs in a rosette configuration were utilized to determine strains within the web of the girder. Using the rosette data, the compression strain angle was calculated as 39.8 degrees; physically measured angles after the test were on average 42 degrees.

6.2.6 Test 6: Specimen I-1, North End (B/C)

The second I-girder test was performed on Jul7 28, 2010, when girder concrete was 336 days old and deck concrete was 96 days old. The beam was placed under the loading frame such that the shear span was 4.6 ft. and embedment was 57.5 in. The first shear cracking occurred at an applied load of 177 kip. As in the previous test, shear cracks formed in the web and propagated through the shear span toward the support. Flexural cracking initiated at 290 kip and occurred at progressively further distances from the applied load as load increased. The specimen ultimately failed in shear at a load of 484 kip, which corresponded to a maximum moment of 1925 kip-ft. The final cracking pattern may be seen in Figures D.13 through D.16 in Appendix D.

The load-deflection response for the specimen is shown in Figure 6.26. The maximum deflection under the point of loading was 0.86 in., and the maximum midspan deflection was 0.88 in. The maximum end-slip of any strand with respect to the applied load is illustrated in Figure 6.27, and maximum end-slip values for individual strands are listed in Table 6.5. Minimal end-slip was recorded as flexural cracking progressed. The amount of end-slip was not significant enough to classify a bond failure. The maximum compressive strain recorded at the top concrete fiber under the point of load was 1300 με.

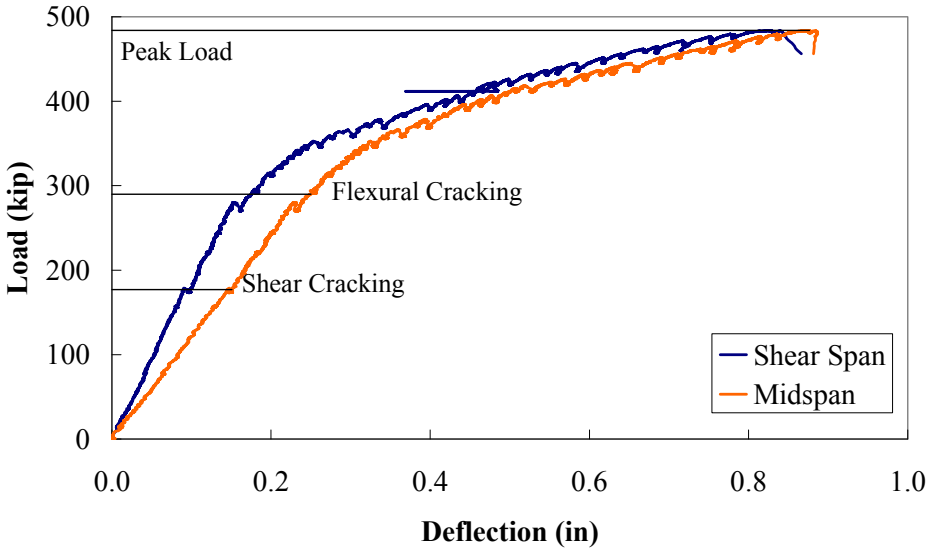

Figure 6.26. Load-deflection response for I-1, North End.

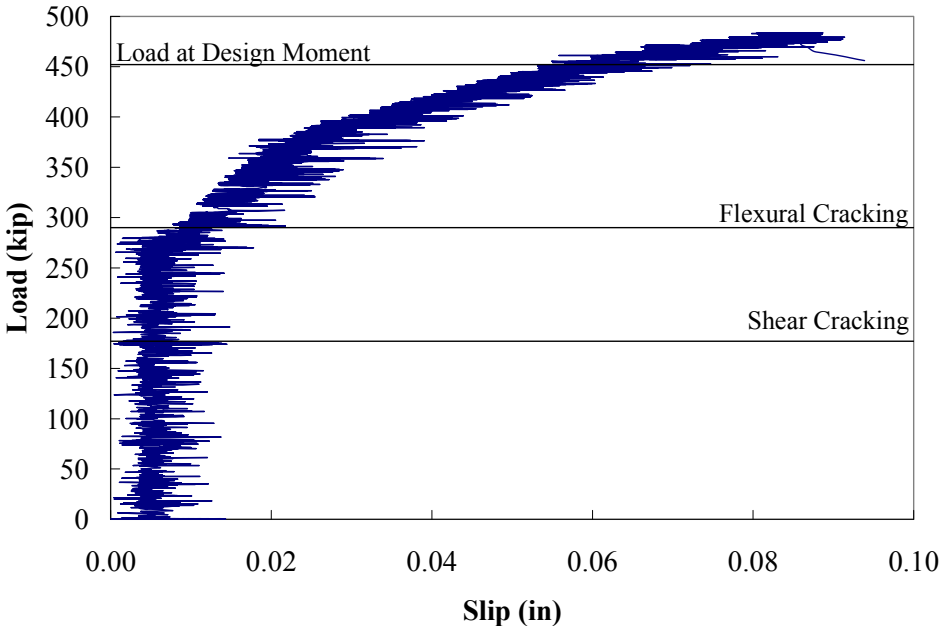

Figure 6.27. Maximum end-slip of any strand for I-1, North End.

Table 6.5. Maximum End-Slip of Individual Strands for I-1, North End

Strand	End-Slip (in)
1	0.050
2	0.094
3	0.066
4	0.057
5	0.041
6	0.047
7	0.091
8	0.028
Bottom Strands	**0.052**
Outer Strand	**0.066**
Center Strands	**0.058**

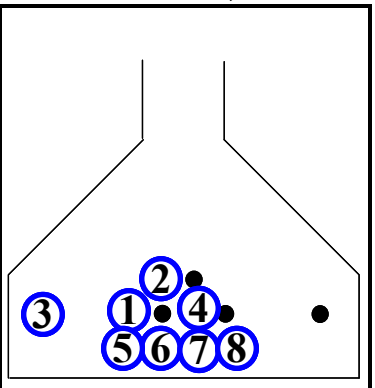

6.2.7 Test 7: Specimen I-2, South End (A/D)

The third I-girder test was performed on Aug 30, 2010; the girder concrete was 369 days old and deck concrete was 124 days old. The beam was placed under the loading frame such that the shear span was 4.8 ft. and embedment was 60.5 in.

The first shear cracking occurred at an applied load of 150 kip. Flexural cracking initiated at 290 kip. The specimen was loaded until the induced moment exceeded the design moment capacity. The maximum load was 439 kip, which corresponds to a maximum experimental moment of 1818 kip-ft. The load-deflection response for the specimen is shown in Figure 6.29. The maximum deflection under the point of loading was 0.74 in. The deflection at midspan was 0.73 in. Minimal end-slip was recorded as flexural cracking progressed. The maximum end-slip of any strand with respect to the applied load is illustrated in Figure 6.30, and maximum end-slip values for individual strands are listed in Table 6.6. The final cracking pattern for the third I-girder test may be seen in Figure D.9 in Appendix D.

The longitudinal strain was monitored throughout the test at five locations under the point of loading. The strain output, adjusted for the initial strain in the concrete due to self-weight and the effective prestress, is shown in Figure 6.30. Using a linear strain assumption, the maximum compressive strain at the top concrete fiber under the point of load was 600 με.

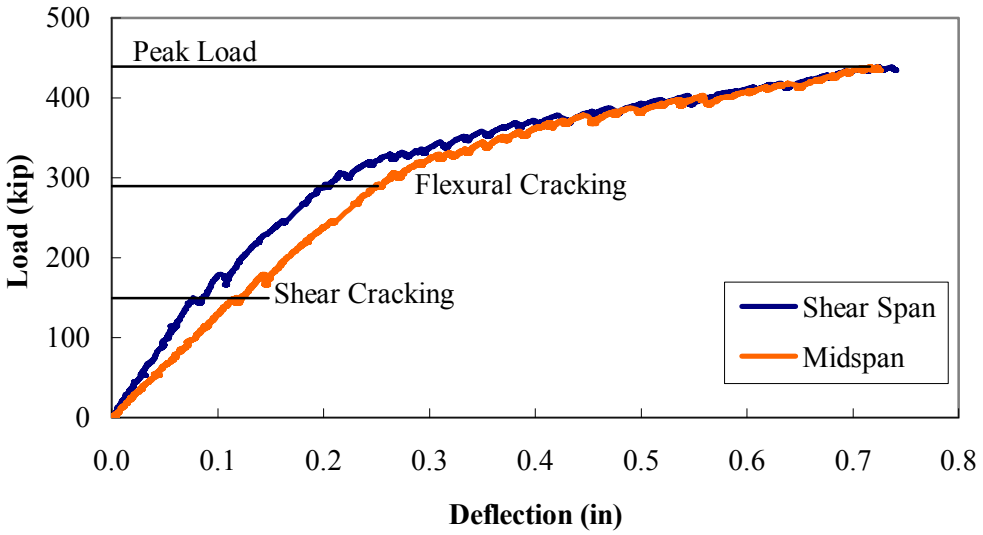

Figure 6.29. Load-deflection response for I-2, South End.

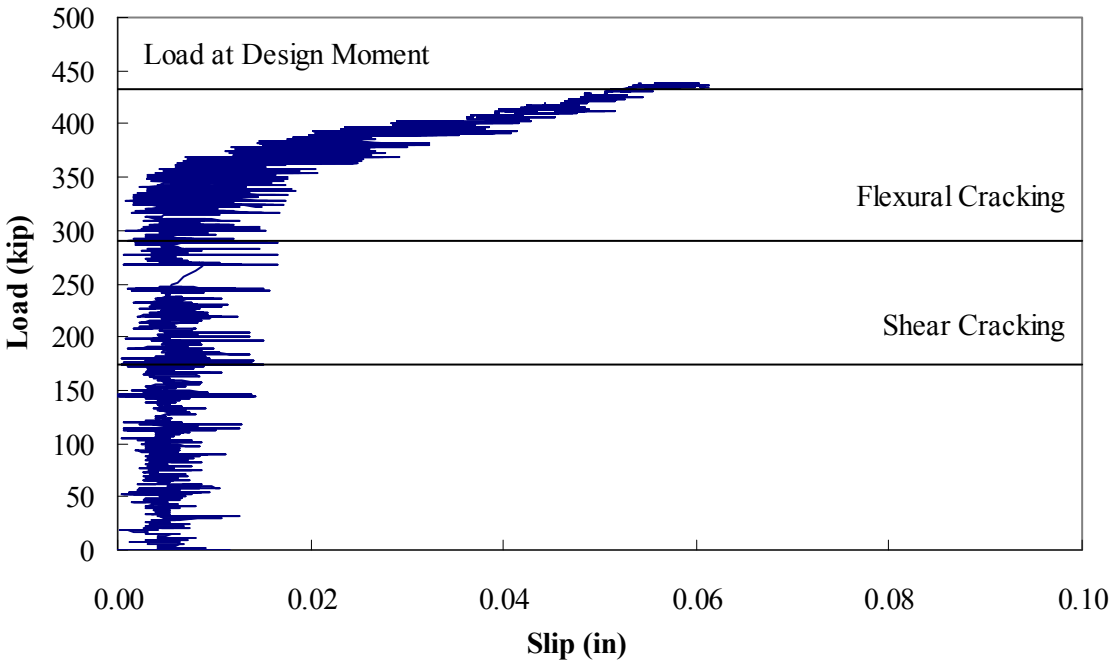

Figure 6.30. Maximum end-slip of any strand for I-2, South End.

Table 6.6. Maximum End-Slip of Individual Strands for I-2, South End

Strand	End-Slip (in)
1	0.015
2	0.061
3	0.031
4	0.009
5	0.061
6	0.037
7	0.007
8	0.006
Bottom Strands	**0.028**
Outer Strand	**0.031**
Center Strands	**0.028**

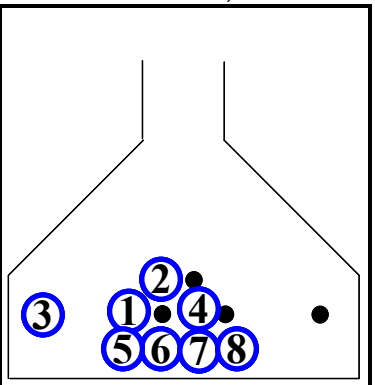

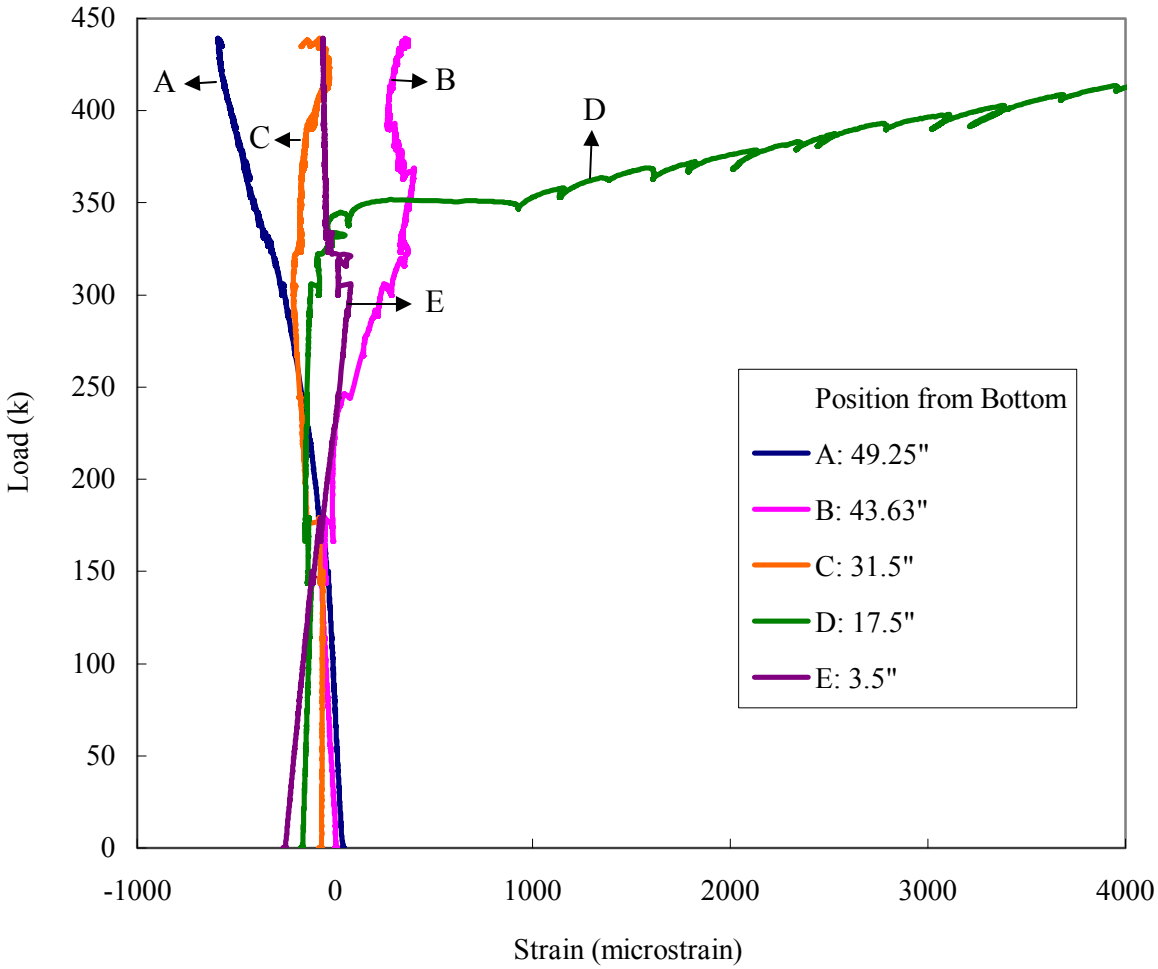

Figure 6.30. Longitudinal strains under loading for I-2, South End.

6.2.8 Test 8: Specimen I-2, North End (B/C)

The final flexural test was performed on Nov. 5, 2010; the girder concrete was 436 days old and deck concrete was 191 days old. The total CL-to-CL distance between supports was 33.56 ft. The beam was placed under the loading frame such that the shear span was 4.92 ft. and embedment was 62 in.

The first shear cracking occurred at an applied load of 152 kip. The shear cracks formed in the web and propagated through the shear span toward the support. Flexural cracking initiated at 295 kip. As load increased, shear cracks widened, though flexural cracking occurred at progressively further distances from the applied load. The final cracking pattern may be seen in Figure D.10 in Appendix D. The specimen was not loaded until ultimate failure; rather, it was loaded until the induced moment exceeded the beam's design moment capacity at the design 28-day strength of concrete of the girder. The maximum load was 426 kip, which corresponds to a maximum experimental moment of 1835 kip-ft.

The load-deflection response for the specimen is shown in Figure 6.31. The maximum deflection under the point of loading was 0.88 in. The maximum midspan deflection was 0.83 in. Minimal end-slip was recorded as flexural cracking progressed. The maximum end-slip of any strand with respect to the applied load is illustrated in Figure 6.32, and maximum end-slip values for individual strands are listed in Table 6.7. The amount of end-slip was not significant enough to classify a bond failure.

The longitudinal strain was monitored throughout the test at five locations under the point of loading. The strain output, adjusted for the initial strain in the concrete due to self-weight and the effective prestress, is shown in Figure 6.33. Using a linear strain assumption, the maximum compressive strain at the top concrete fiber was 1337 microstrain.

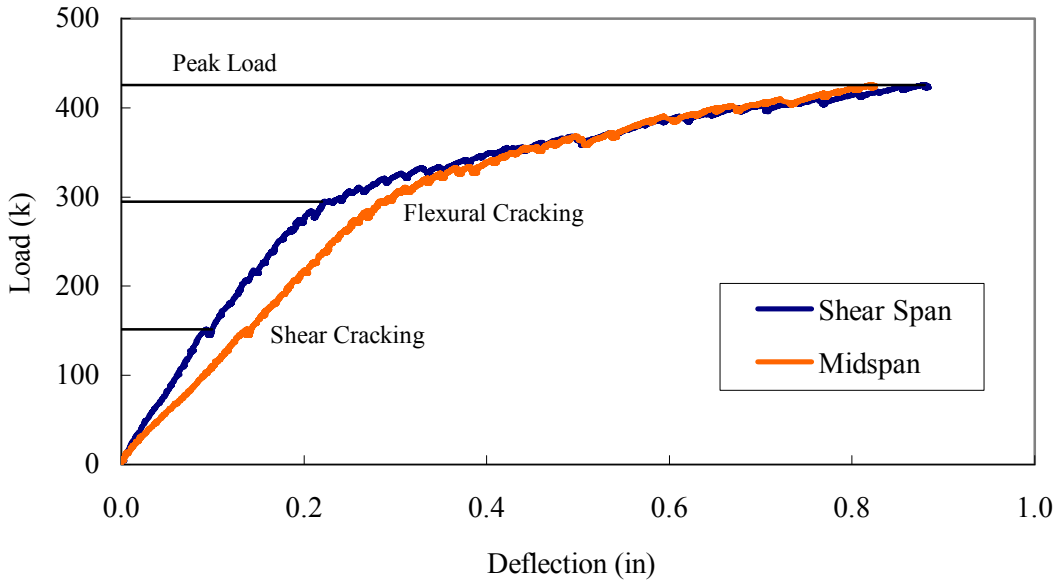

Figure 6.31. Load-deflection response for I-2, North End.

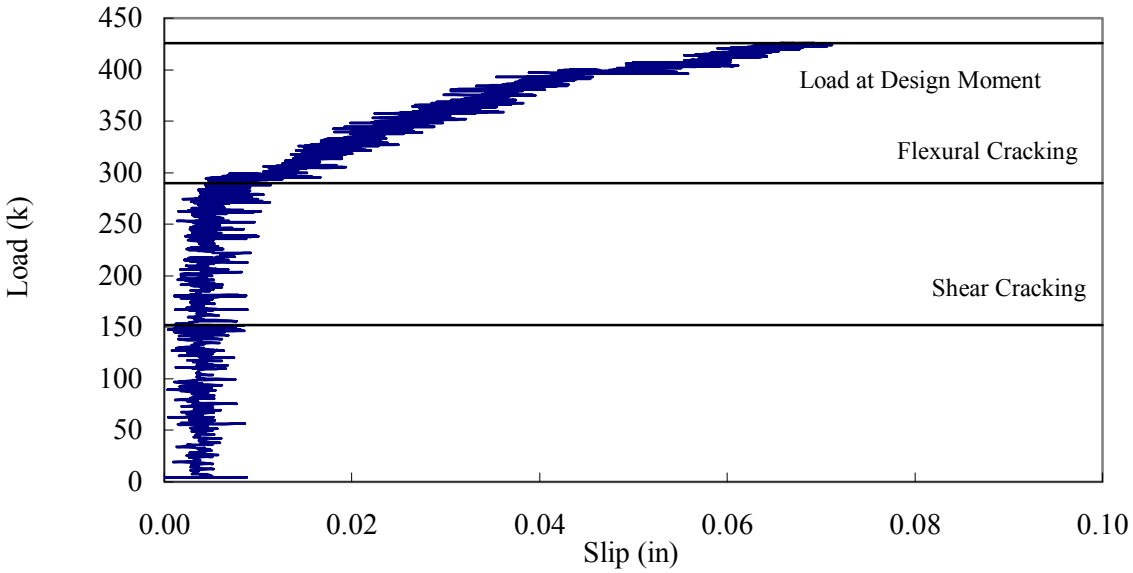

Figure 6.32. Maximum end-slip of any strand for I-2, North End.

Table 6.7. Maximum End-Slip of Individual Strands for I-2, North End

Strand	End-Slip (in)
1	0.06
2	0.01
3	0.04
4	0.04
5	0.04
6	0.04
7	0.03
8	0.01
Bottom Strands	**0.03**
Outer Strand	**0.03**
Center Strands	**0.04**

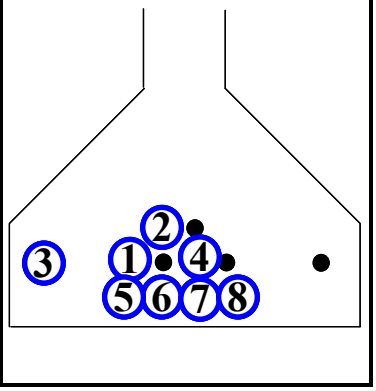

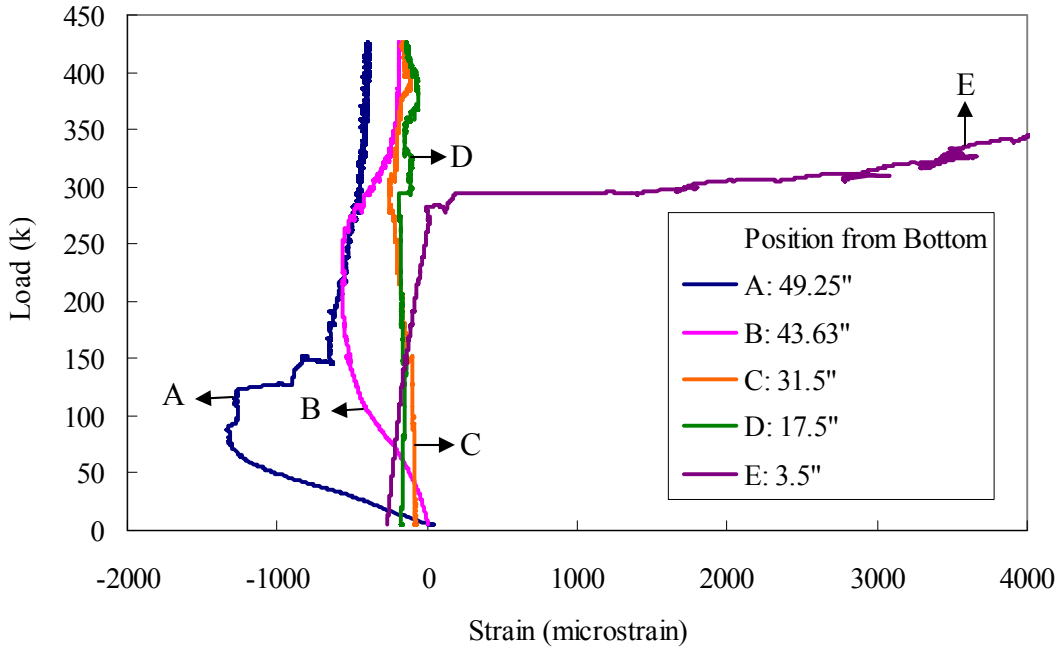

Figure 6.33. Longitudinal strains under loading for I-2, North End.

6.3 DISCUSSION OF DEVELOPMENT LENGTH RESULTS

This section summarizes the results of eight flexural tests performed on the full-scale SCC box and I-girders. First, the effective prestress in the specimens at the time of loading is calculated using initial cracking loads. This permits comparison to prestress losses calculated in Section 4.3. Then, experimental shear and moment capacities are compared to the sectional capacities calculated in Section 4.5. The effectiveness of external CFRP reinforcement in shear strengthening is also evaluated. Finally, ranges for development length in the box and I-girders are established.

6.3.1 Effective Prestress from Initial Cracking

The effective prestress at the time of flexural testing may be back-calculated using the initial cracking load and relationships of mechanics. Two variables in the calculation varied between tests: (1) the experimental cracking moment and (2) the concrete modulus of rupture. The modulus of rupture in all calculations was taken as $7.5\sqrt{f_c}$. The compressive strengths for SCC batches at the time of testing are shown in Table 6.8. Note that no cylinders were cast or tested for Batch 4. It was assumed that any increase in concrete strength between flexural test iterations was negligible. The table also shows corresponding girder strengths. As illustrated in the table, the compressive strength of the concrete at the day of flexural testing was in some cases significantly higher than the target compressive strength of 6000 psi. This is particularly true for the concrete used in casting the deck of the two I-girders. This discrepancy between the actual and theoretical concrete strength in the deck is expected to have little impact on the results since the design moment and shear capacities were used as the threshold for assessing the bond behavior of the strands as will be discussed in the next subsection.

Table 6.8. Concrete Strength at Age of Flexural Tests

Batch	f_c (psi)
1	7330
2	9480
3	6820
4	-
5	8335
6	-
7	7491
8	7018

Girder	f_c (psi)
Box-1	8410
Box-2	8150
I-1	7491
I-2	7018
I-1 Deck	10416
I-2 Deck	9568

The effective prestress values determined using initial cracking moments from each test are shown in Table 6.9. The back-calculated f_{pe} values for the second and third test are significantly lower than those predicted by any of the codes described in Section 4.3; otherwise, the value calculated for the first and fourth tests show excellent correlation to predicted values. Results in the table may have been more accurate if explicit modulus of rupture tests were performed instead of using estimates based on compressive strengths. Back-calculated effective stresses may have varied between tests conducted on the same girder because of SCC batch distribution within the girder.

Table 6.9. Effective Prestress from Initial Cracking

Box Girders		
Test	M_{crack} (kip-ft)	f_{pe} (ksi)
1	709	165.9
2	687	158.6
3	683	158.5
4	703	165.0

I-Girders		
Test	M_{crack} (kip-ft)	f_{pe} (ksi)
5	1311	159.1
6	1241	147.6
7	1292	160.0
8	1278	160.0

6.3.2 Experimental vs. Design Shear and Moment Capacities

The critical loads observed in each box girder test are listed in Table 6.10; those observed in each I-girder test are listed in Table 6.11. Included are the loads at first flexural cracking, first shear cracking, and maximum sustained loads. Experimental cracking moments are compared to theoretical values in Table 6.12.

Table 6.10. Critical Loads for All Box Girder Tests

Test 1	Applied P (kip)	Total V (kip)	Total M (kip-ft)
1st Flexural Cracking	165	141	709
1st Shear Cracking	165	141	709
Maximum Load	197	167	841

Test 2	Applied P (kip)	Total V (kip)	Total M (kip-ft)
1st Flexural Cracking	155	109	687
1st Shear Cracking	218	152	957
Maximum Load	227	158	996

Test 3	Applied P (kip)	Total V (kip)	Total M (kip-ft)
1st Flexural Cracking	149	125	683
1st Shear Cracking	188	156	852
Maximum Load	217	179	978

Test 4	Applied P (kip)	Total V (kip)	Total M (kip-ft)
1st Flexural Cracking	161	104	703
1st Shear Cracking	235	151	1018
Maximum Load	253	162	1095

Table 6.11. Critical Loads for All I-Girder Tests

Test 5	Applied P (kip)	Total V (kip)	Total M (kip-ft)
1st Flexural Cracking	295	262	1316
1st Shear Cracking	179	161	813
Maximum Load	427	375	1882

Test 6	Applied P (kip)	Total V (kip)	Total M (kip-ft)
1st Flexural Cracking	290	254	1167
1st Shear Cracking	177	159	733
Maximum Load	484	421	1925

Test 7	Applied P (kip)	Total V (kip)	Total M (kip-ft)
1st Flexural Cracking	290	259	1254
1st Shear Cracking	150	138	671
Maximum Load	439	388	1874

Test 8	Applied P (kip)	Total V (kip)	Total M (kip-ft)
1st Flexural Cracking	295	259	1283
1st Shear Cracking	152	137	681
Maximum Load	426	370	1835

Table 6.12. Experimental vs. Design Cracking Moments

Test	$M_{cr\text{-}exp}$ (kip-ft)	$M_{cr\text{-}exp}/M_{cr\text{-}theory}$
1	709	1.04
2	687	1.01
3	683	1.01
4	703	1.04
5	1316	1.06
6	1167	0.94
7	1254	0.97
8	1283	1.00

The magnitude of the ultimate shear sustained in each box girder test is plotted against ACI and AASHTO design capacities in Figure 6.38; the same is plotted for I-girder tests in Figure 6.39. Within their respective shear spans, the girders consistently exceeded predicted values. Ratios between experimental and design shear capacities are presented in Table 6.7. Ratios were calculated using ACI design capacities since they remained essentially constant within the shear span regions. The impact of CFRP shear reinforcement is evident in the values presented in the table. Considering the box girder cases without external reinforcement, the average ratio $V_u/\Phi V_{n\text{-}design}$ was 1.12. Meanwhile, the externally-wrapped box girder in test three had a corresponding ratio of 1.23; thus, the CFRP was effective and resulted in an approximate 11% increase in shear capacity. For the I-girders, the average ratio $V_u/\Phi V_n$ was 2.49.

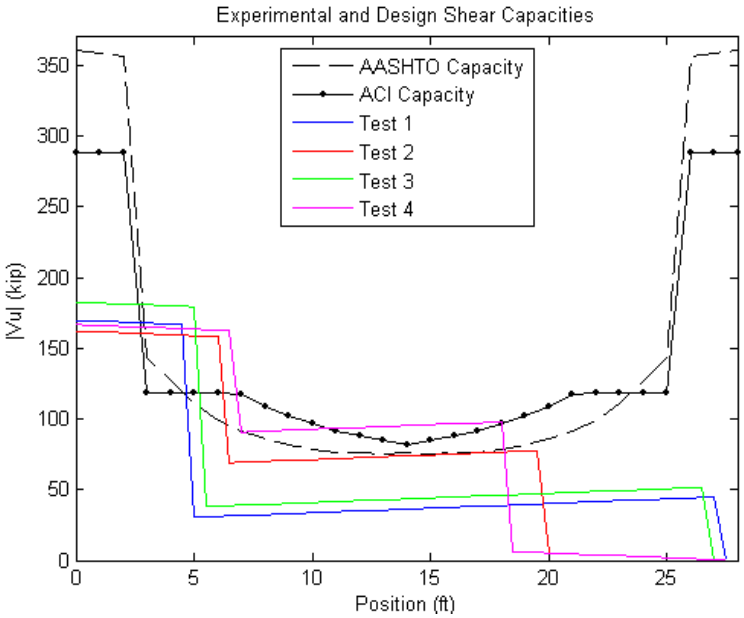

Figure 6.38. Magnitude of ultimate shear sustained in each box girder test

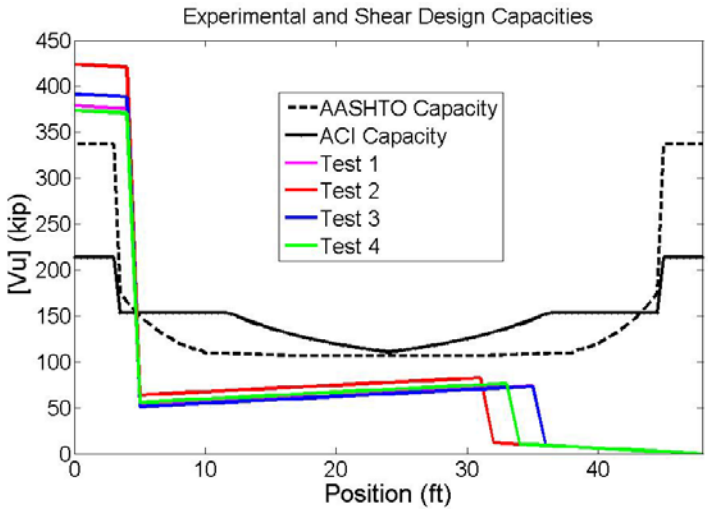

Figure 6.39. Magnitude of ultimate shear sustained in each I-girder test

Table 6.7. Experimental Ultimate Shear vs. Design Shear Capacities

Test	V_u (kip)	$V_u/\Phi V_n$
1	167	1.15
2	158	1.09
3	179	1.23
4	162	1.12
5	375	2.44
6	421	2.74
7	388	2.45
8	370	2.33

The experimental moment-deflection responses for all box and I-girder tests are shown in Figures 6.40 and 6.41, respectively. The response for embedment of 68.5 in. in Figure 6.40 is incomplete due to complications with the data acquisition system during the third test. Per the figures, the onset of nonlinear behavior correlated well with the predicted cracking moment. Yielding of the strands was reached in box girder tests with the two highest embedment lengths. Yielding of the strands was reached in all I-girder tests.

Ratios between experimental and design moment capacities for each test are presented in Table 6.8. The tests are listed in order of increasing embedment length. Test 1 utilized an embedment length of 62.8 in. and resulted in significant shear cracking followed by strand slip into the specimen. Only 81% of the design moment was achieved at maximum load. Test 2 utilized an embedment length of 77.5 in. and resulted in a combined flexure-shear failure with accompanying strand slip into the specimen. The specimen developed 96% of the design moment capacity. Test 3 utilized an embedment length of 68.5 in. and considered the effect of external CFRP shear reinforcement. The failure mode was similar to that observed in the second test, with significant shear cracks developing after substantial flexural cracks had already occurred. The specimen developed 94% of the design moment capacity before failing abruptly due to shear cracking and CFRP delaminating from the sides of the beam. The fourth and final box girder test utilized an embedment length of 83.5 in. and resulted in a flexural failure with negligible strand slip. The specimen developed 106% of the design moment capacity.

The I-girder Test 5 utilized an embedment length of 60.5 in. and resulted in shear cracking in the web and flexural cracks at progressively further distances from the load. Minimal strand slip was recorded as flexural cracks propagated. The specimen achieved 103% of the design moment at maximum load. Test 6 utilized an embedment length of 57.5 in. and resulted in a combined flexure-shear failure with minimal strand slip into the specimen. The specimen developed 107% of the design moment capacity. Test 7 utilized an embedment length of 63.5 in. The specimen developed 105% of the design moment capacity. Minimal end-slip was recorded. The fourth I-girder test (test 8) utilized an embedment length of 62 in. Minimal end slip was recorded with the progress of flexural cracks. The specimen developed 101% of the design moment capacity at the point of maximum loading.

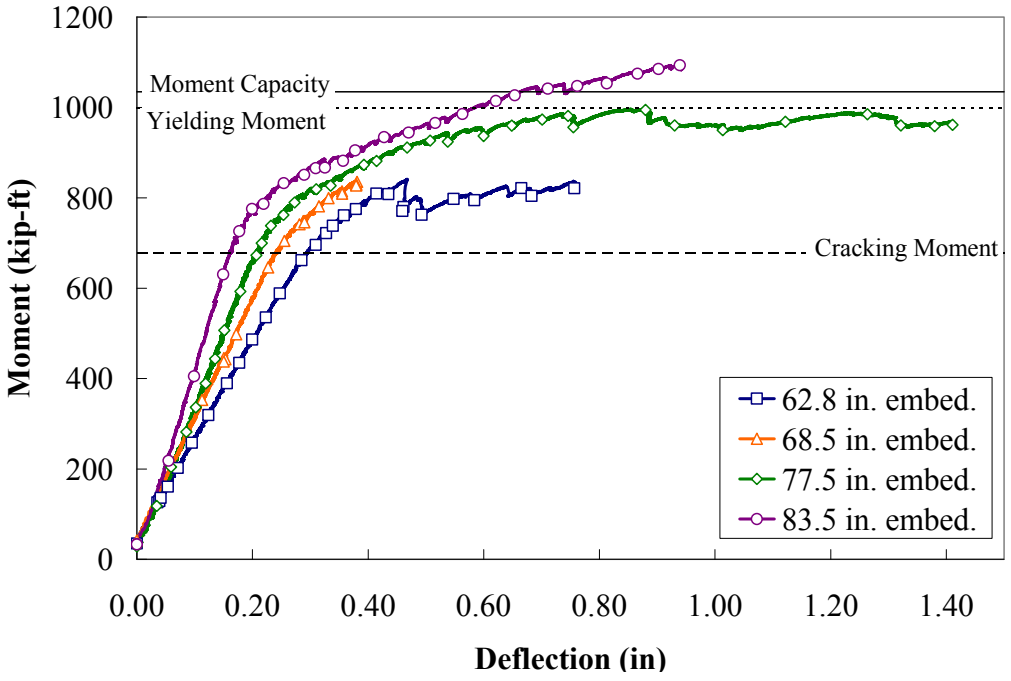

Figure 6.39. Moment-deflection responses for box girder tests.

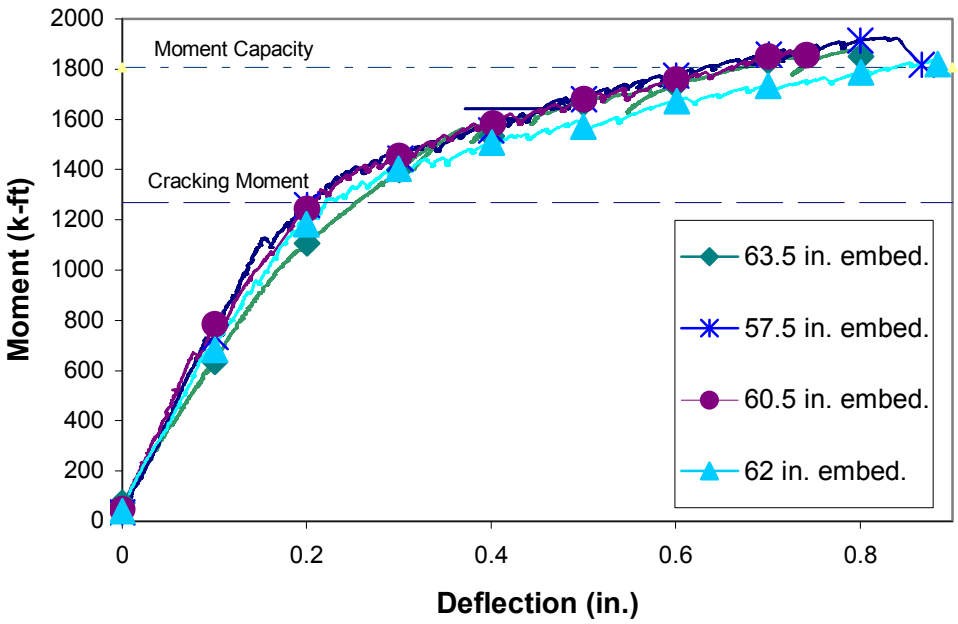

Figure 6.40. Moment-deflection responses for I-girder tests.

Table 6.8. Experimental vs. Design Moment Capacity

Box Girders			
Embedment (in)	**M_u (kip-ft)**	**$M_u/\Phi M_n$**	**Failure Mode**
62.8	841	0.81	Shear-Slip
68.5	978	0.94	Shear-Slip
77.5	996	0.96	Flexure-Shear
83.5	1095	1.06	Flexure
I-Girders			
Embedment (in)	**M_u (kip-ft)**	**$M_u/\Phi M_n$**	**Failure Mode**
60.5	1874	1.03	Flexure-Shear
57.5	1925	1.07	Flexure-Shear
63.5	1882	1.05	Flexure-Shear
62.0	1835	1.01	Flexure-Shear

In the first three tests of box girders, strand slip occurred only after shear cracks had propagated across the strands. On average, center strands slipped 24% further into the girders than outer strands. This is likely the result of higher strand concentration and less concrete cover in the center of the box girder cross-section. The structural behaviors observed in the second and third tests were comparable despite embedment lengths differing by 9 in. This suggests the box girders would perform adequately in flexure at embedment lengths of at least 68.5 in. if additional shear reinforcement were provided; this correlates well with predicted development values (Table 4.8), which ranged from 68.5 in. to 72.4 in. In the tests of I-girders, strand slip was observed only after the onset of flexural cracking. In the seventh test, strand slip was observed only after 80% of the peak load was

attained. The maximum average strand slip observed in girder I-1 was 39% greater than that of I-2. For sixth and seventh tests, the maximum strand slip occurred in the outer strands. For the fifth and eighth tests, the maximum slip occurred in the bottom and center strand locations respectively. The I-girders were found to perform adequately in both shear (Table 6.7) and flexure (Table 6.8) even when the embedment lengths were lower than the predicted development length values (Table 4.8) which ranged from 73.9 in. to 81 in.

It is important to recall that the specimens were designed for realistic AASHTO load conditions (see Section 4.5) and not the high concentrated loads applied during the experimental flexural tests. As such, it is reasonable to conclude that the SCC specimens in this study had sufficient bond between prestressing strands and concrete based on experimental flexural behavior.

CHAPTER 7 CONCLUSIONS

This report presented results of pullout, transfer length, and development length tests on steel strands in SCC specimens conducted from 2008-2010 at the University of Illinois at Urbana-Champaign. The primary goal of this research was to experimentally assess the bond behavior of prestressing strands in full-scale SCC members. Results were compared to design code requirements. The research presented in this report affords the following observations:

1. Pullout test results at various ages showed strand performance in SCC to be comparable with strand performance in NCC. Normalized pullout loads differed between the two concrete types by as little as 1% after three days of curing.
2. Normalized first slip loads were lower in SCC than in NCC for all tests except those conducted one day after casting. At 28 days, the average normalized first slip load in SCC was 4% below that in NCC.
3. Normalized peak pullout loads were higher in SCC than in NCC for all tests except those conducted seven days after casting. At 28 days, the average normalized peak pullout load in SCC was 6% higher than that in NCC.
4. The strands and SCC mixture utilized in pullout tests were deemed acceptable for use in large-scale prestressed specimens for transfer and development length testing.
5. Experimental transfer lengths at seven of the eight girder ends were below ACI and AASHTO required transfer lengths. Only at one end did experimental results consistently and significantly exceed code provisions (greater than $50d_b$ by up to 30%, greater than $60d_b$ by up to 8.3%). This end had the lowest concrete compressive strength of all locations and corresponded to the strand cutting location at prestress transfer.
6. Transfer lengths showed no correlation to casting location.
7. No correlation was observed between transfer length and girder type.
8. Overall, experimental transfer lengths were 86% of $50d_b$, 72% of $60d_b$, and 69% of $f_{pe}d_b/3$.
9. Experimental shear capacities of the as-built specimens were 112% of design ACI values. External CFRP shear reinforcement resulted in an approximate 11% increase in shear capacity of the box girder.
10. Strand embedment length of 62.8 in. resulted in shear-slip failure of the box girder specimen; the girder was able to develop 81% of the design moment.
11. The box girders were able to develop 94% and 96% of the design moment with strand embedment of 68.5 in. and 77.5 in., respectively. The failure mode for 68.5-in. embedment was primarily shear, while the failure mode for 77.5-in. embedment was primarily flexure.
12. In the first three development length tests, strand slip occurred only after shear cracks had propagated across the strands. On average, center strands slipped 24% further into the girders than outer strands, likely due to higher strand concentration and less concrete cover in the center of the box girder cross-section.
13. Strand embedment of 83.5 in. in the box girder resulted in flexural failure with negligible strand slip; the girder was able to develop 106% of the design moment capacity.
14. Results of the experimental development length tests suggest the SCC box girders in this study would perform adequately in flexure at embedment lengths of at least 68.5 in.; this correlates well with predicted development values, which ranged from 68.6 in. to 72.4 in.

15. I-girders were found to perform adequately in both shear and flexure even when the embedment lengths were lower than the predicted development length values which ranged from 73.9 in. to 81 in.
16. With satisfactory pullout behavior and adequate transfer and development lengths, it is reasonable to conclude that the SCC mixture in this study had sufficient bond to prestressing strands.

REFERENCES

AASHTO, *AASHTO LRFD Bridge Design Specifications*, 3rd Ed., American Association of State Highway and Transportation Officials, Washington, D.C., 2004.

ACI Committee 209, *Prediction of Creep, Shrinkage, and Temperature Effects in Concrete Structures (ACI 209R-92)*, American Concrete Institute, Farmington Hills, MI, 2008.

ACI Committee 318, *Building Code Requirements for Structural Concrete (ACI 318-08) and Commentary*, American Concrete Institute, Farmington Hills, MI, 2008.

ACI Committee 440, *Guide for the Design and Construction of Externally Bonded FRP Systems for Strengthening Concrete Structures (ACI 440.2R-08)*, American Concrete Institute, Farmington Hills, MI, 2008.

Andrawes, B., M. Shin, and A. Pozolo, "Transfer and Development Length of Prestressing Tendons in Full-Scale AASHTO Prestressed Concrete Girders using Self-Consolidating Concrete," Report ICT-09-038, Illinois Center for Transportation, Urbana, IL, 2009.

ASTM C143/C143M-10, "Standard Test Method for Slump of Hydraulic-Cement Concrete." ASTM International, West Conshohocken, PA, 2010.

ASTM C1611/C1611M-09b, "Standard Test Method for Slump Flow of Self-Consolidating Concrete," ASTM International, West Conshohocken, PA, 2009.

ASTM C1621/C1621M-09b, "Standard Test Method for Passing Ability of Self-Consolidating Concrete by J-Ring," ASTM International, West Conshohocken, PA, 2009.

Balazs, G., "Transfer Length of Prestressing Strand as a Function of Draw-In and Initial Prestress," *PCI Journal*, Vol. 38, No. 2, 1993, p. 86-93.

Bonen, D. and S. Shah, "The Effects of Formulation on the Properties of Self-Consolidating Concrete," *Concrete Science and Engineering: A Tribute to Arnon Bentur*, Proc. of the Int. RILEM Symposium, RILEM Publications, France, 2004, p. 43-56.

Buckner, C., "A Review of Strand Development Length for Pretensioned Concrete Members," *PCI Journal*, Vol. 40, No. 2, 1995, p. 84-105.

Burgueno, R. and M. Haq, "Effect of SCC Mixture Proportioning on Transfer and Development Length of Prestressing Strand," ACI, SP-247-9, 2007, p. 105-116.

Chan, Y., Y. Chen, and Y. Liu, "Development of Bond Strength of Reinforcement Steel in Self-Consolidating Concrete," *ACI Structural Journal*, Vol. 100, No. 4, 2003.

Cousins, T., D. Johnston, and P. Zia, "Bond of Epoxy Coated Prestressing Strand," Report No. FHWA-NC-87-05, Center for Transportation Engineering Studies, North Carolina State University, Raleigh, NC, 1986.

Darwin, D. et al. “Development Length Criteria for Conventional and High Relative Rib Area Reinforcing Bars.” *ACI Structural Journal*, Vol. 98, No. 5, 1996.

Esfahani, M., M. Lachemi, and M. Kianoush, “Top-Bar Effect of Steel Bars in Self-Consolidating Concrete (SCC),” *Cement and Concrete Composites*, Vol. 30, Issue 1, 2008.

Girgis, A. and C. Tuan, “Bond Strength and Transfer Length of Pretensioned Bridge Girders Cast with Self-Consolidating Concrete,” *PCI Journal*, Vol. 50, No. 6, 2005, p. 72-87.

Hanson, N. and P. Kaar, “Flexural Bond Tests of Pretensioned Prestressed Beams,” *ACI Journal*, Proceedings, Vol. 55, No. 7, 1959, p. 783-803.

IDOT, “Self-Consolidating Concrete for Precast Products (BDE),” Bureau of Materials and Physical Research, Illinois Dept. of Transportation, Springfield, IL, 2007.

Kachlakev, D. and D. McCurry, “Testing of Full-Size Reinforced Concrete Beams Strengthened with FRP Composites: Experimental Results and Design Methods Verification,” Report No. FHWA-OR-00-19, U.S. Department of Transportation Federal Highway Administration, 2000.

Labonte, T. and H. Hamilton, “Self-Consolidating Concrete (SCC) Structural Investigation,” Report No. BD545 RPWO #21, Florida Dept. of Transportation, Gainesville, FL, 2005.

Lange, D. et al. “Performance and Acceptance of Self-Consolidating Concrete: Final Report,” FHWA-ICT-08-020, Illinois Center for Transportation, Urbana, IL, 2008.

Larson, K., R. Peterman, and A. Esmaeily, “Evaluating the Time-Dependent Deformations and Bond Characteristics of a Self-Consolidating Concrete Mix and the Implication for Pretensioned Bridge Applications,” Final Report FHWA-KS-07-1, Kansas Department of Transportation, Topeka, KS, 2007.

Logan, D., “Acceptance Criteria for Bond Quality of Strand for Pretensioned Prestressed Concrete Applications,” *PCI Journal*, Vol. 42, No. 2, 1997, p. 52-90.

Marti-Vargas, J., C. Arbelaez, P. Serna-Ros, and C. Castro-Bugallo, “Reliability of Transfer Length Estimation from Strand End Slip,” *ACI Structural Journal*, Vol. 104, No. 4, 2007, p. 487-494.

Mitchell, D. and H. Marzouk, “Bond Characteristics of High-Strength Lightweight Concrete,” *ACI Structural Journal*, Vol. 104, No. 1, 2007.

Moustafa, S., “Pullout Strength of Strand and Lifting Loops,” Technical Bulletin 74-B5, Concrete Technology Associates, Tacoma, WA, 1974.

Naito, C. et al. “Performance of Bulb-Tee Girders Made with Self-Consolidating Concrete,” *PCI Journal*, Vol. 51, No. 6, 2006, p. 72-85.

Neville, A., *Properties of Concrete*, 4th Edition, John Wiley and Sons, Inc., New York, 1996.

Norris, T., H. Saadatmanesh, and M. Ehsani, “Shear and Flexural Strengthening of R/C Beams with Carbon Fiber Sheets,” *Journal of Structural Engineering*, Vol. 123, No. 7, 1997, p. 903-911.

Okamura, H. and M. Ouchi, “Self-Compacting Concrete,” *Journal of Advanced Concrete Technology*, Vol. 1, No. 1, 2003, p. 5-15.

Ouchi, M., S. Nakamura, T. Osterberg, and M. Lwin, “Applications of Self-Compacting Concrete in Japan, Europe, and the United States,” Proceedings of the International Symposium on High-Performance Concrete, Orlando, FL, 2003.

PCI, *Interim Guidelines for the Use of Self-Consolidating Concrete in Precast/Prestressed Concrete Member Plants,* Precast/Prestressed Concrete Institute, Chicago, IL, 2003a.

PCI, *PCI Bridge Design Manual,* Precast/Prestressed Concrete Institute, Chicago, IL, 2003b.

PCI, *PCI Design Handbook: Precast and Prestressed Concrete,* Sixth Edition, Precast/Prestressed Concrete Institute, Chicago, IL, 2004.

Rose, D. and B. Russell, “Investigation of Standardized Tests to Measure the Bond Performance of Prestressing Strand.” Research Report, Fears Structural Engineering Laboratory, University of Oklahoma, Norman, OK, 1996.

Russell, B. and N. Burns, “Design Guidelines for Transfer, Development and Debonding of Large Diameter Seven Wire Strands in Pretensioned Concrete Girders,” Research Report 1210-5F, Center for Transportation Research, University of Texas at Austin, Austin, TX, 1993.

Schindler, A., R. Barnes, J. Roberts, and S. Rodriguez, “Properties of Self-Consolidating Concrete for Prestressed Members,” *ACI Materials Journal*, 2007, p. 53-61.

Staton, B., N. Do, E. Ruiz, and W. Hale, “Transfer Lengths of Prestressed Beams Cast with Self-Consolidating Concrete,” *PCI Journal*, Vol. 54, No. 2, 2009, p. 64-83.

Trent, J., “Transfer Length, Development Length, Flexural Strength, and Prestress Losses Evaluation in Pretensioned Self-Consolidating Concrete Members,” M.S. Thesis, Virginia Polytechnic Institute and State University, Blacksburg, VA, 2007.

Wehbe, N., A. Sigl, Z. Gutzmer, and C. Stripling, “Structural Performance of Prestressed Self-Consolidating Concrete Bridge Girders Made with Limestone Aggregates,” Upper Great Plains Transportation Institute at North Dakota State Univ., 2009.

W.R. Grace & Co., “Test Methods for Self-Consolidating Concrete,” Technical Bulletin TB-1506, Cambridge, MA, 2005.

Zia, P., R. Nunez, and L. Mata, “Implementation of Self-Consolidating Concrete for Prestressed Concrete Girders,” FHWA-NC-2006-30 Final Report, North Carolina Department of Transportation, Raleigh, NC, 2005.

APPENDIX A: FORCE-DISPLACEMENT RESPONSES FOR PULLOUT TESTS

This appendix contains figures of the force-displacement responses generated during the pullout tests described in Chapter 3, as well as the first slip and peak pullout loads obtained for all pullout specimens. Figures A.1-A.4 show responses for strands embedded in normally-consolidated blocks at various curing ages, while Figures A.5-A.8 show responses for stands embedded in SCC blocks at various curing ages. No data is presented for strand N3-E in Figure A.2 because the LVDT became dislodged during testing, requiring an abrupt stop to the servo-controlled loading mechanism; the LVDT and load cell were recalibrated prior to testing the next strand. Displacement values in the figures are those measured by the pullout apparatus LVDT (see Figure 3.5) at a position 20 in. above the upper surface of the pullout blocks; the figures do not account for strand elongation and, thus, are not force-slip responses. Table A.1 summarizes the first slip and peak pullout loads for all pullout test specimens.

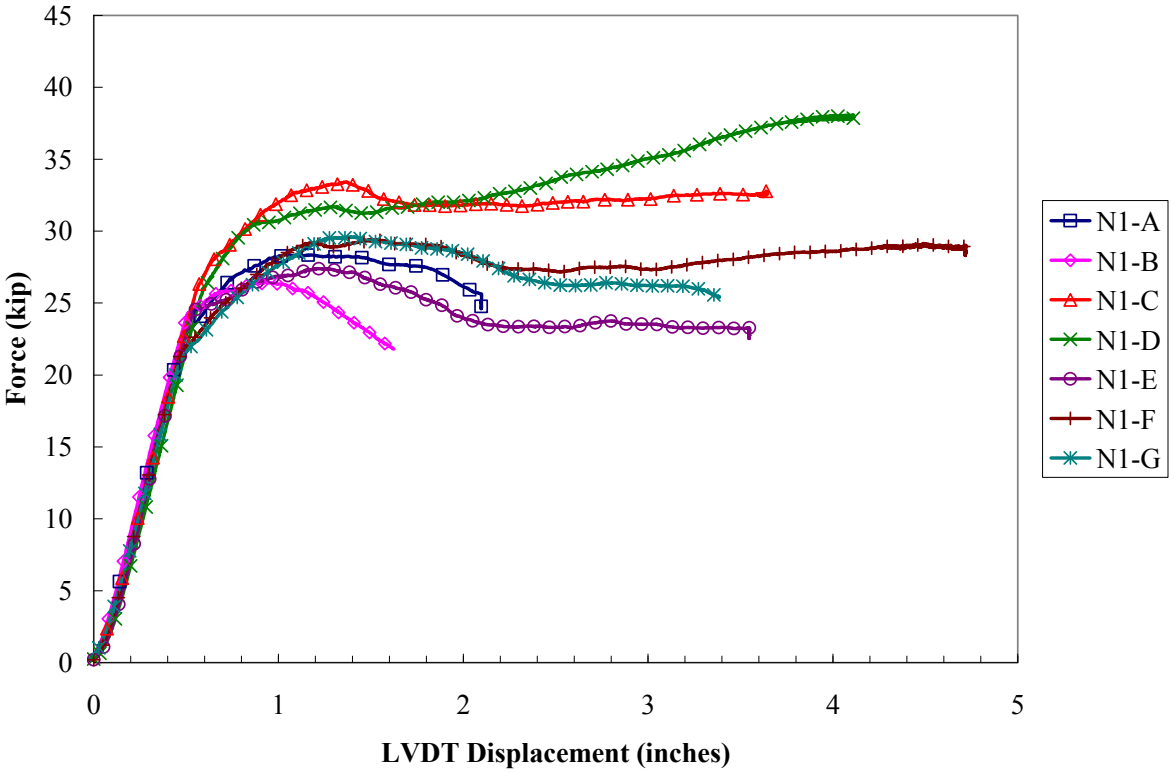

Figure A.1. Force-displacement responses for strands in NCC 1 day after casting

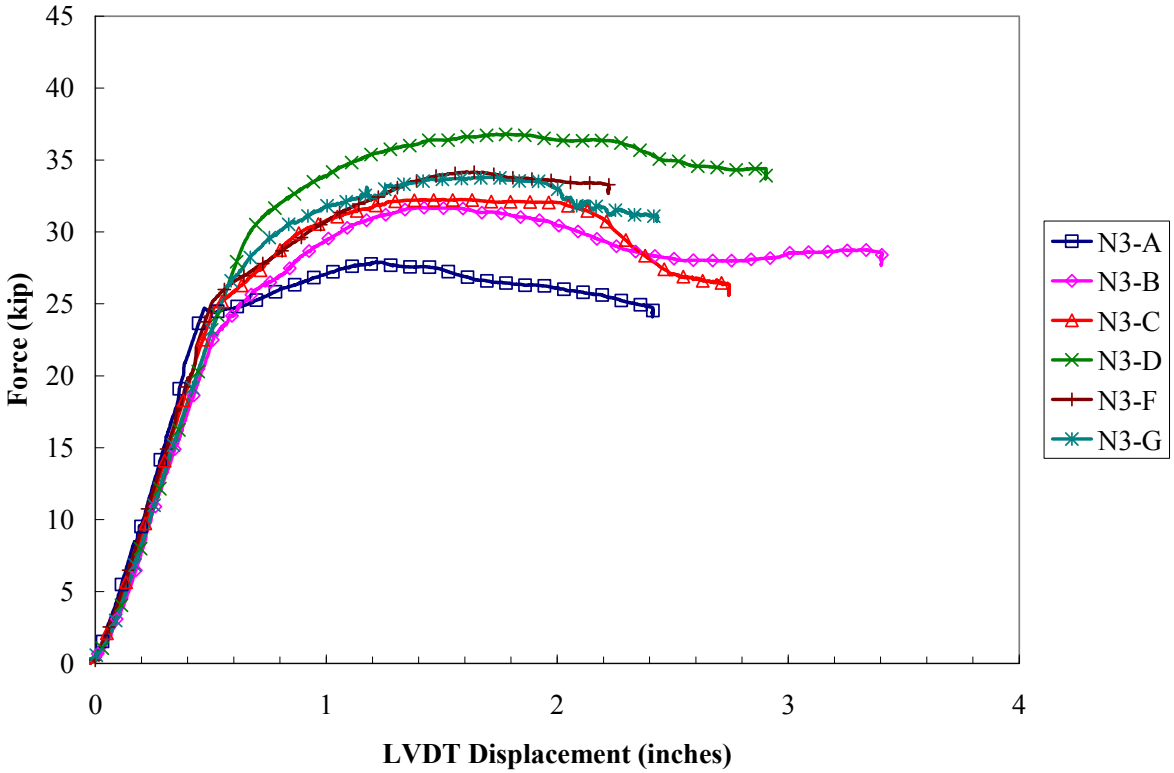

Figure A.2. Force-displacement responses for strands in NCC 3 days after casting

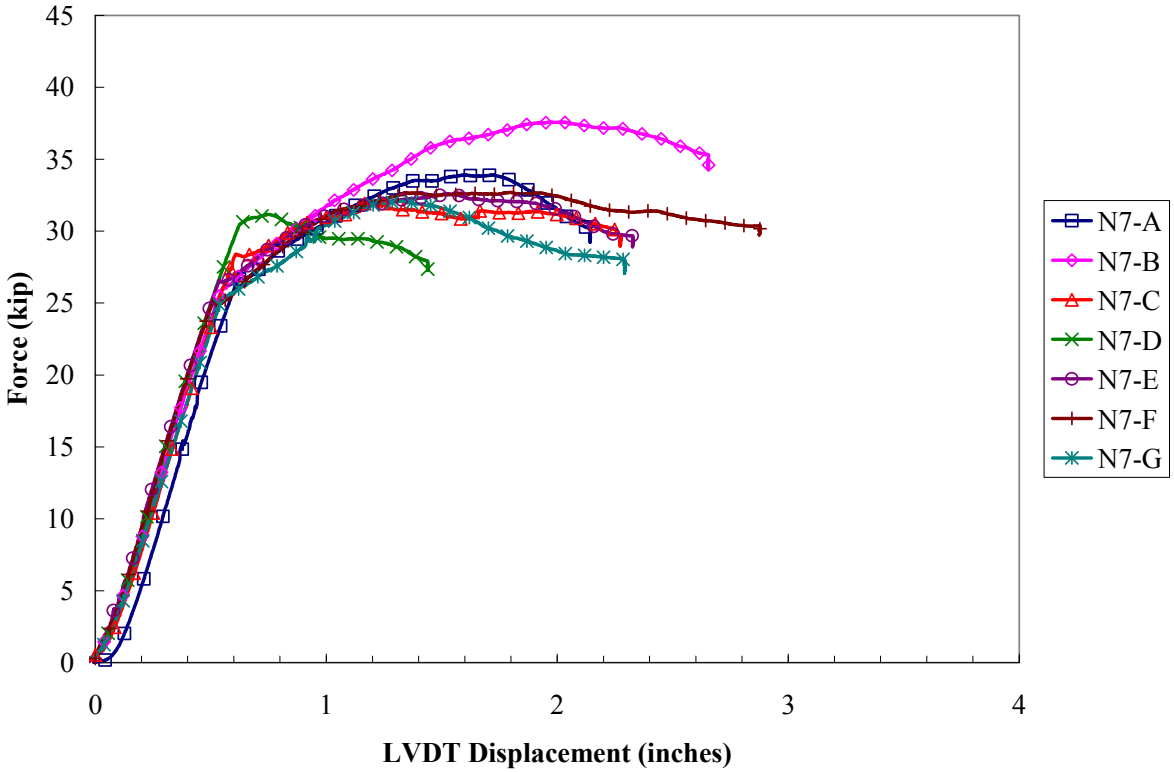

Figure A.3. Force-displacement responses for strands in NCC 7 days after casting

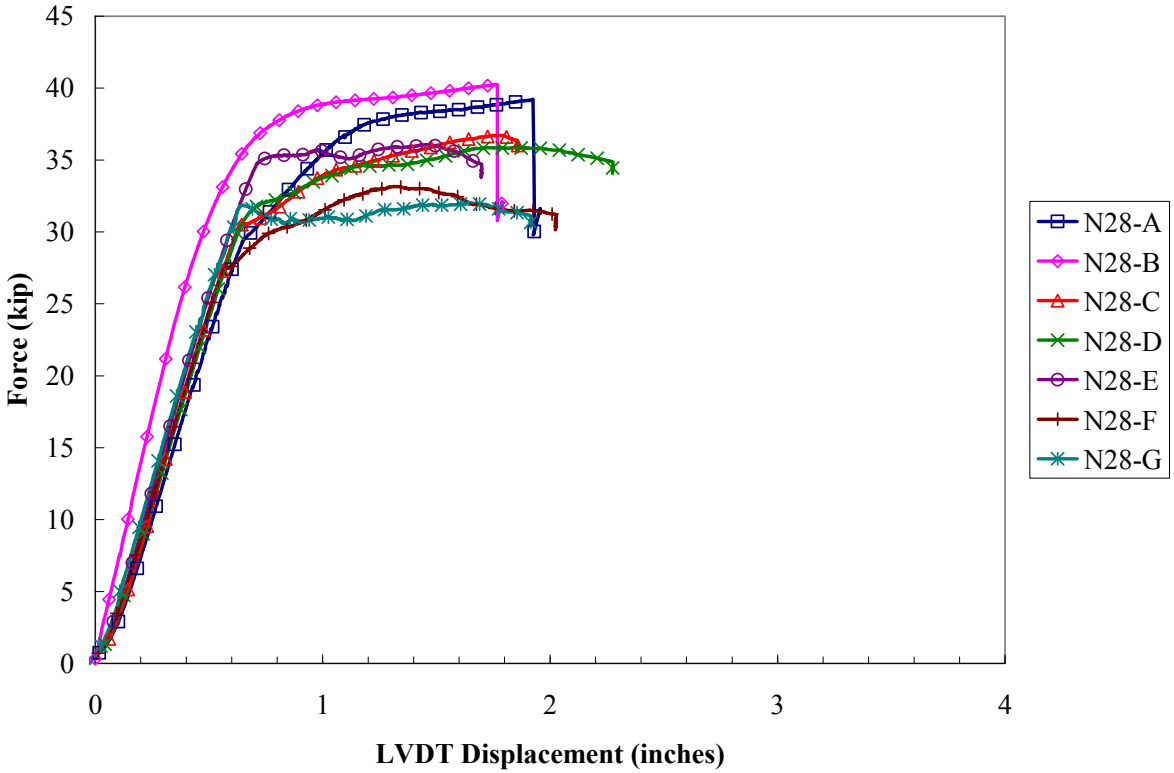

Figure A.4. Force-displacement responses for strands in NCC 28 days after casting

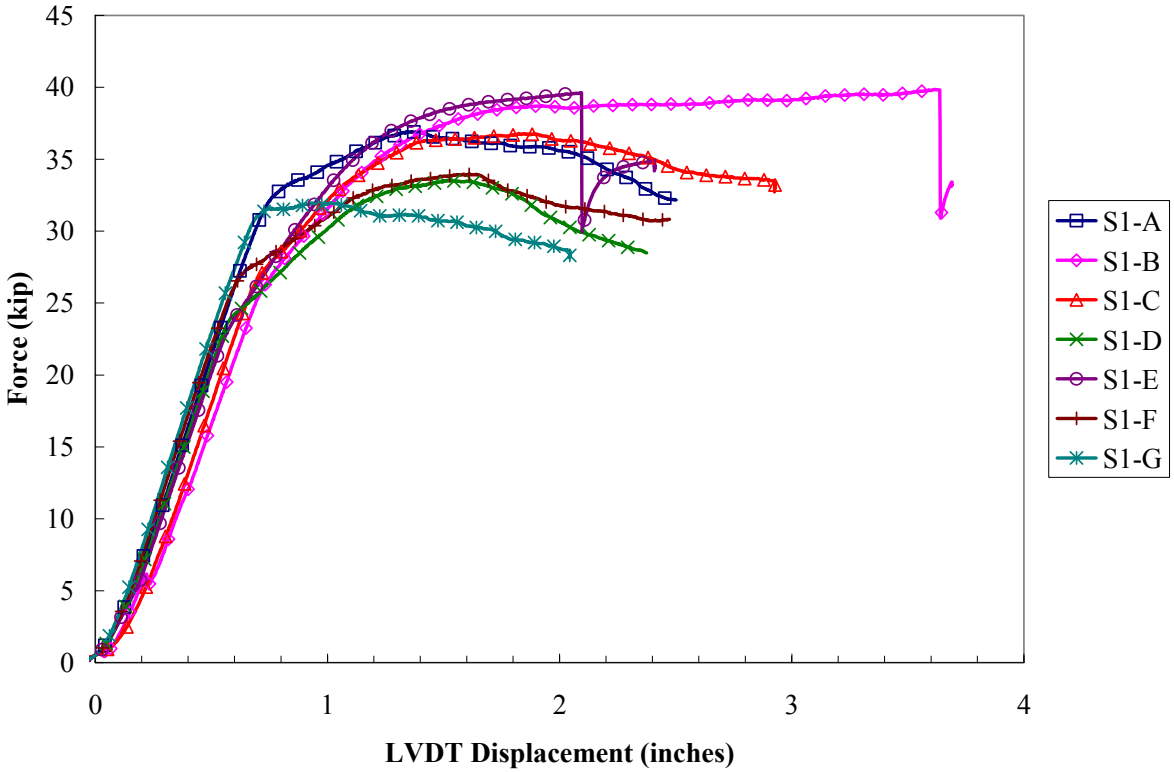

Figure A.5. Force-displacement responses for strands in SCC 1 day after casting

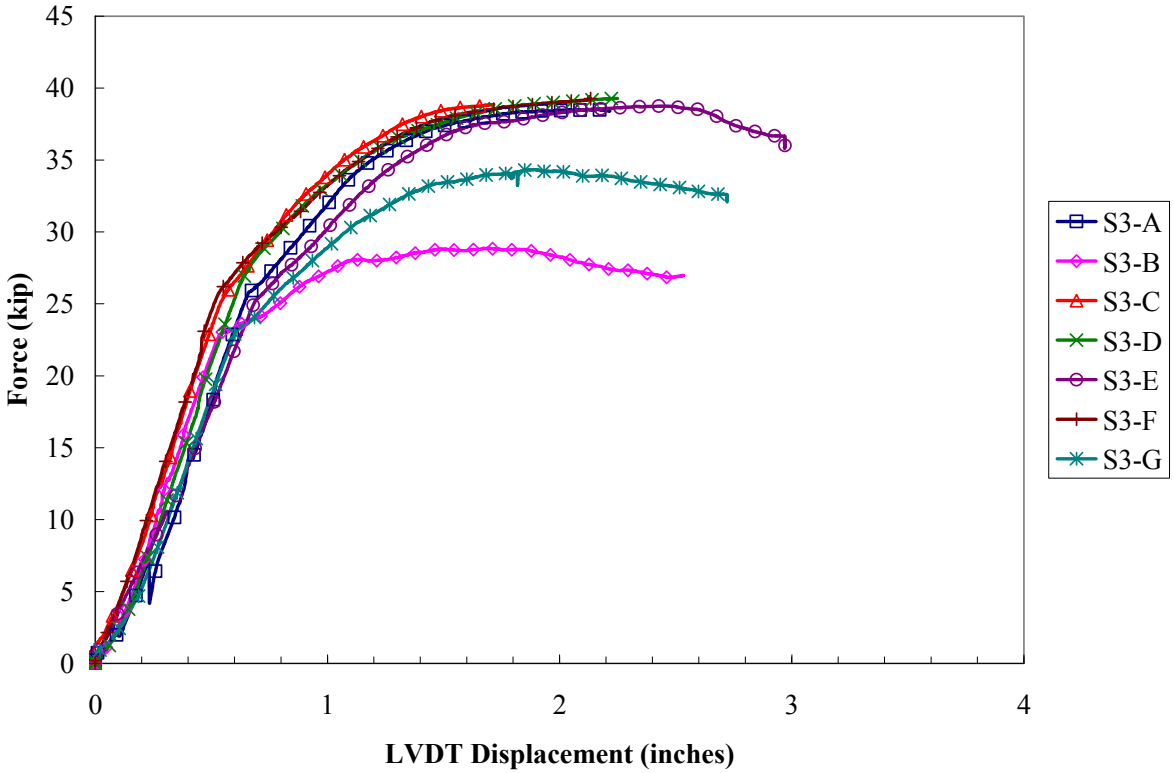

Figure A.6. Force-displacement responses for strands in SCC 3 days after casting

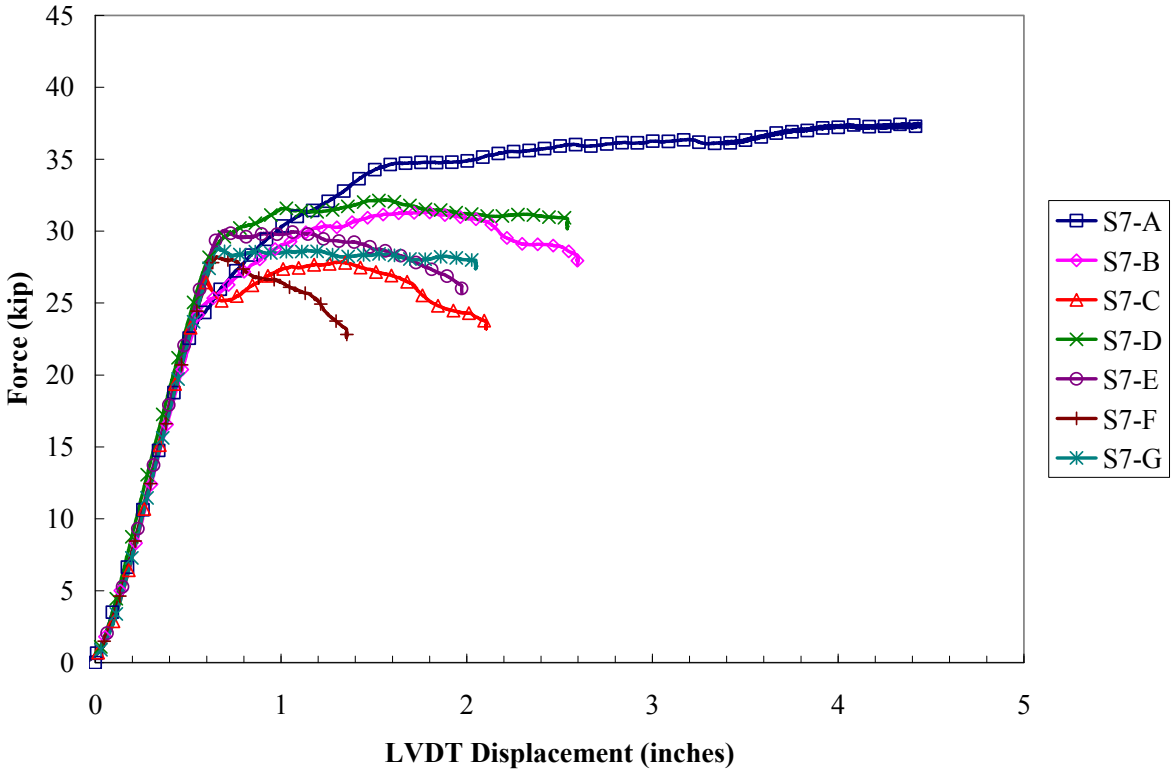

Figure A.7. Force-displacement responses for strands in SCC 7 days after casting

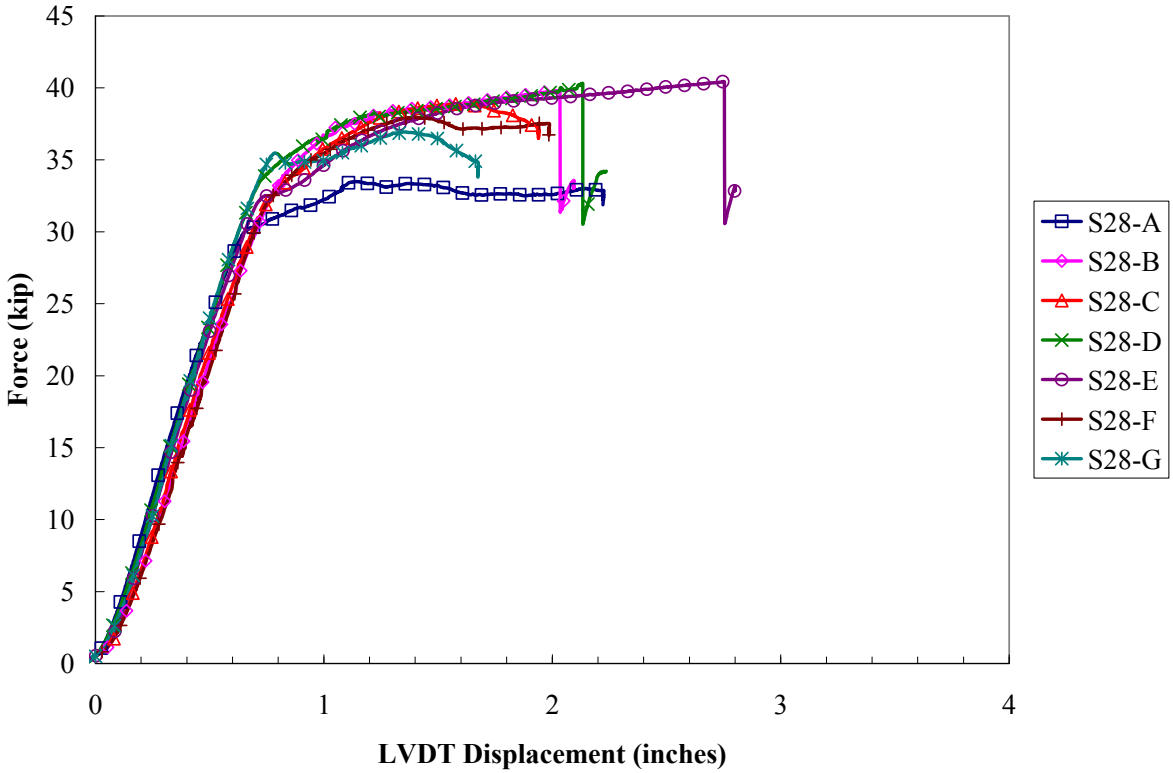

Figure A.8. Force-displacement responses for strands in SCC 28 days after casting

Table A.1. First Slip and Peak Pullout Loads for all Pullout Tests

	First Slip Loads (kip)				Peak Pullout Loads (kip)			
NCC	**1 Day**	**3 Day**	**7 Day**	**28 Day**	**1 Day**	**3 Day**	**7 Day**	**28 Day**
A	22.8	24.5	26.6	24.0	28.4	27.9	33.9	39.2
B	24.3	23.1	26.1	27.0	26.5	31.7	37.6	40.3
C	25.8	24.5	26.5	23.0	33.4	32.3	32.0	36.7
D	25.4	28.5	21.7	27.5	38.1	36.8	31.2	35.9
E	23.2	-	26.4	27.0	27.4	-	32.6	36.1
F	21.8	25.0	24.9	28.0	29.4	34.2	32.7	33.2
G	21.1	25.1	25.5	27.5	29.6	33.8	32.1	32.0
Average	**23.5**	**25.1**	**25.4**	**26.3**	**30.4**	**32.8**	**33.2**	**36.2**
Stdev	**1.8**	**1.8**	**1.7**	**2.0**	**4.1**	**3.0**	**2.1**	**3.0**

	First Slip Loads (kip)				Peak Pullout Loads (kip)			
SCC	**1 Day**	**3 Day**	**7 Day**	**28 Day**	**1 Day**	**3 Day**	**7 Day**	**28 Day**
A	28.5	25.7	23.4	23.5	36.9	38.5	37.5	33.5
B	23.5	23.1	24.9	25.5	39.8	29.5	31.3	39.8
C	24.1	25.5	25.9	26.0	36.8	38.9	27.8	38.9
D	23.1	25.6	26.1	23.0	33.6	39.3	32.2	40.3
E	21.9	25.6	26.9	24.0	39.6	38.8	30.1	40.4
F	22.3	25.4	23.2	28.0	34.0	39.4	28.2	38.0
G	23.3	23.5	26.4	27.0	32.0	34.3	28.8	36.9
Average	**23.8**	**24.9**	**25.3**	**25.3**	**36.1**	**36.9**	**30.8**	**38.3**
Stdev	**2.2**	**1.1**	**1.5**	**1.9**	**3.0**	**3.7**	**3.4**	**2.5**

APPENDIX B

FABRICATION DRAWINGS FOR FULL-SCALE GIRDERS

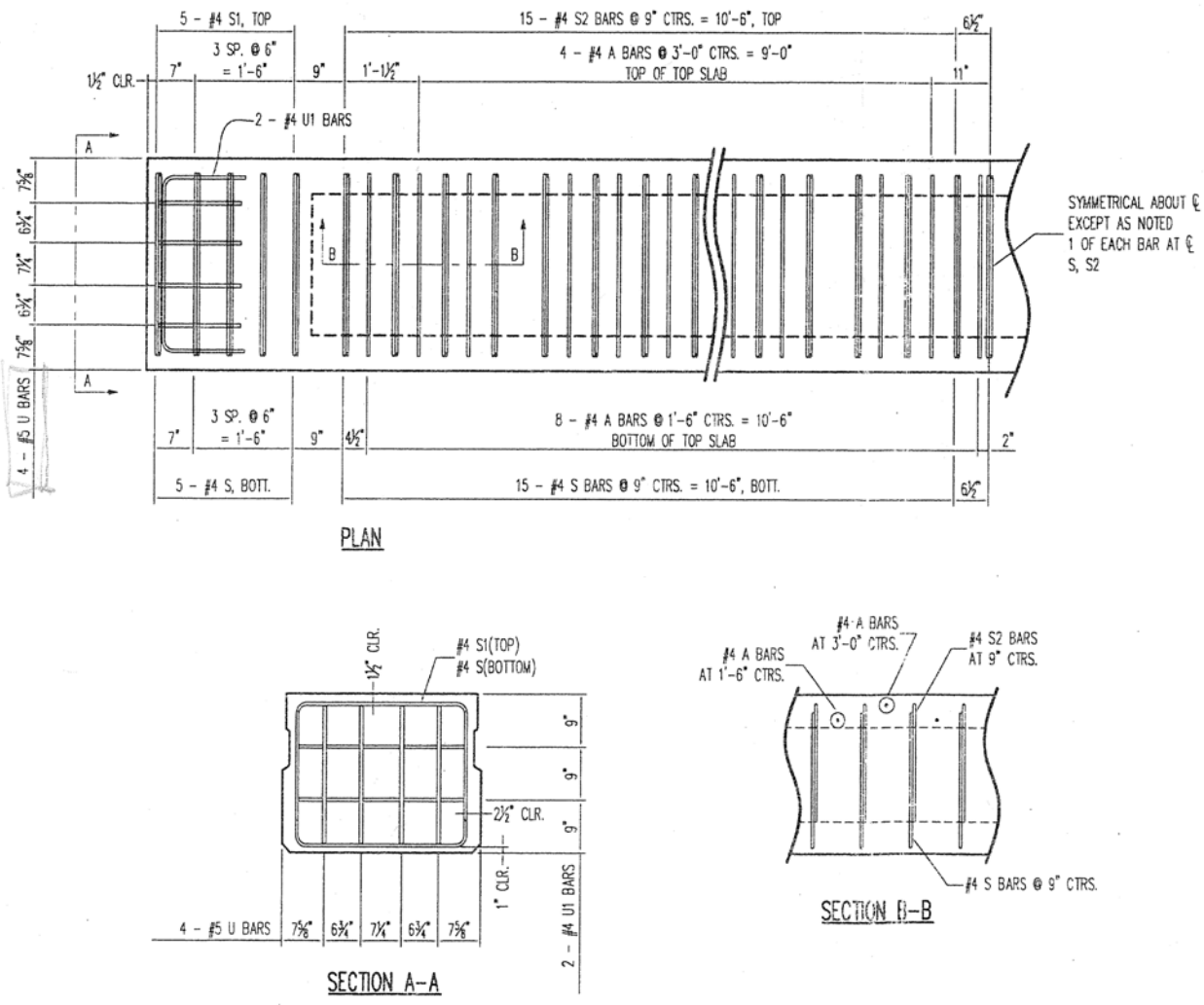

Figure B.1: Reinforcement layout for hollow box girders

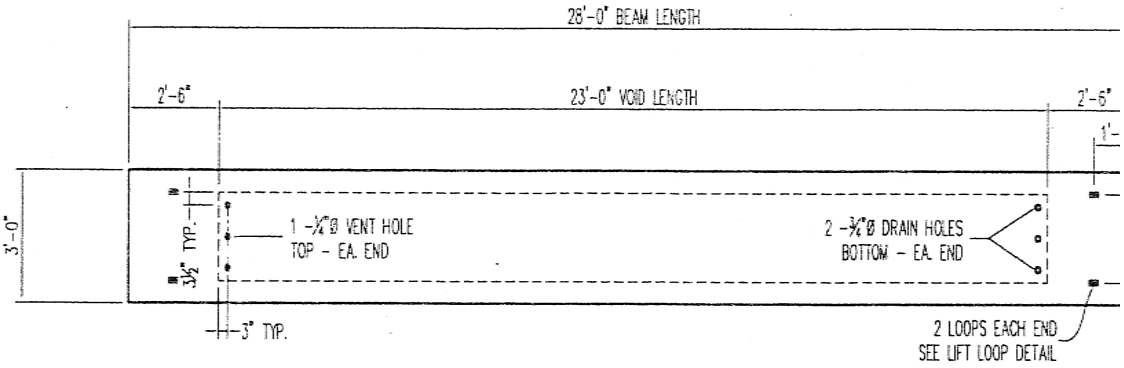

Figure B.2: Plan for hollow box girders showing center void

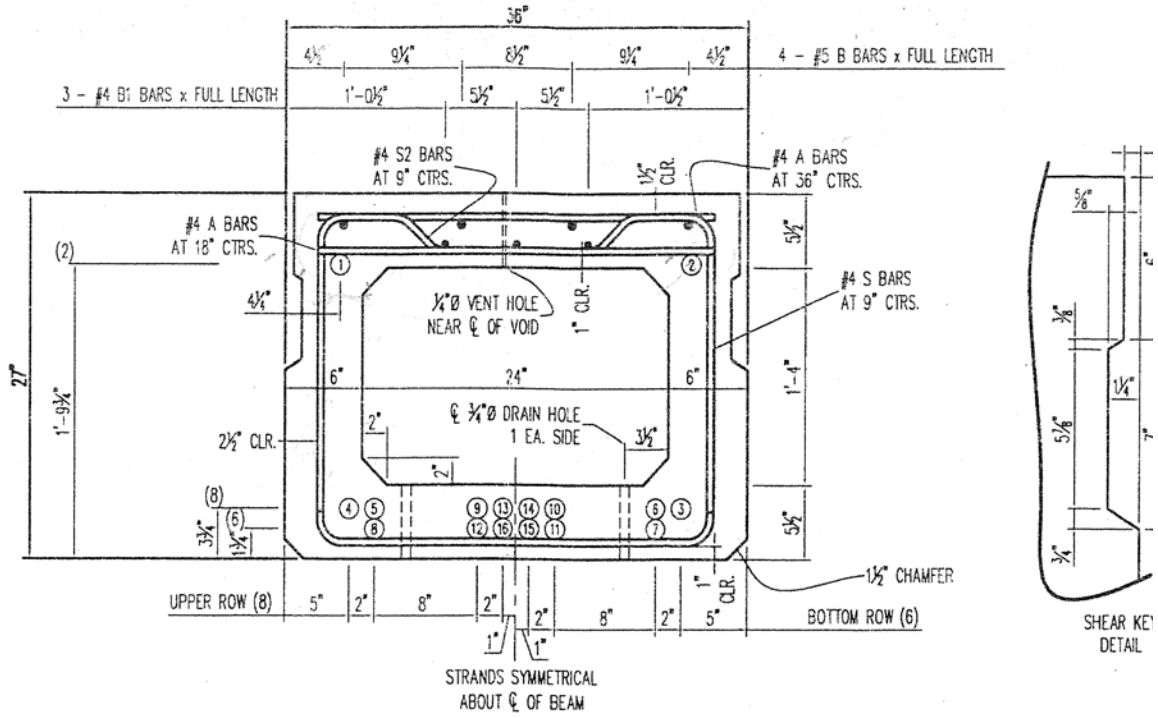

Figure B.3: Strand pattern and cross-section geometry for hollow box girders

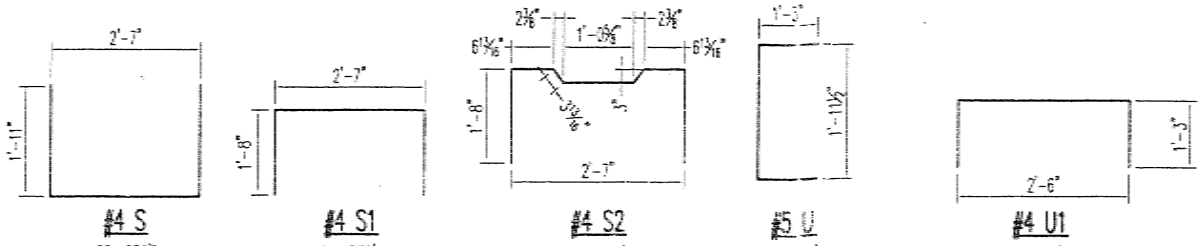

REINFORCEMENT BARS						
BAR	SIZE	NO. / BM.	LENGTH	SHAPE	T. REQ'D	LBS.
A	#4	8	2'-7"	——	16	28
B	#5	4	27'-9"	——	8	232
B1	#4	3	27'-9"	——	6	111
S	#4	41	6'-5"	⊔	82	351
S1	#4	10	5'-11"	⊓	20	79
S2	#4	31	6'-2"	⊓	62	255
U	#5	8	4'-6"	⊏	16	75
U1	#4	4	5'-0"	⊓	8	27

Figure B.4: Reinforcement specifications for hollow box girders

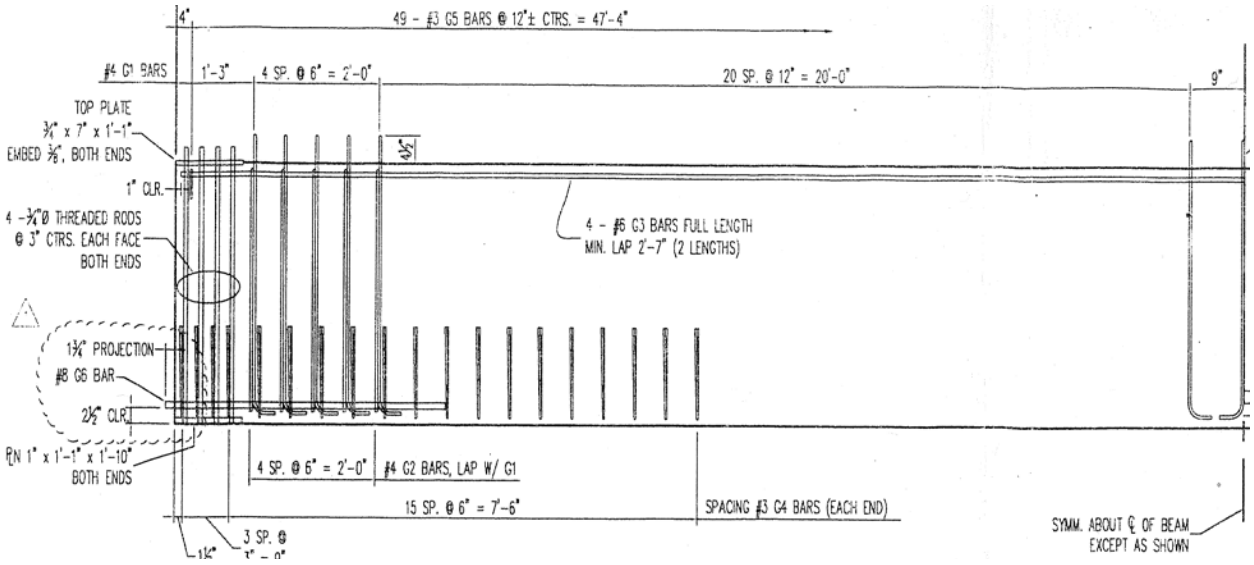

Figure B.5: Reinforcement layout for I-girders

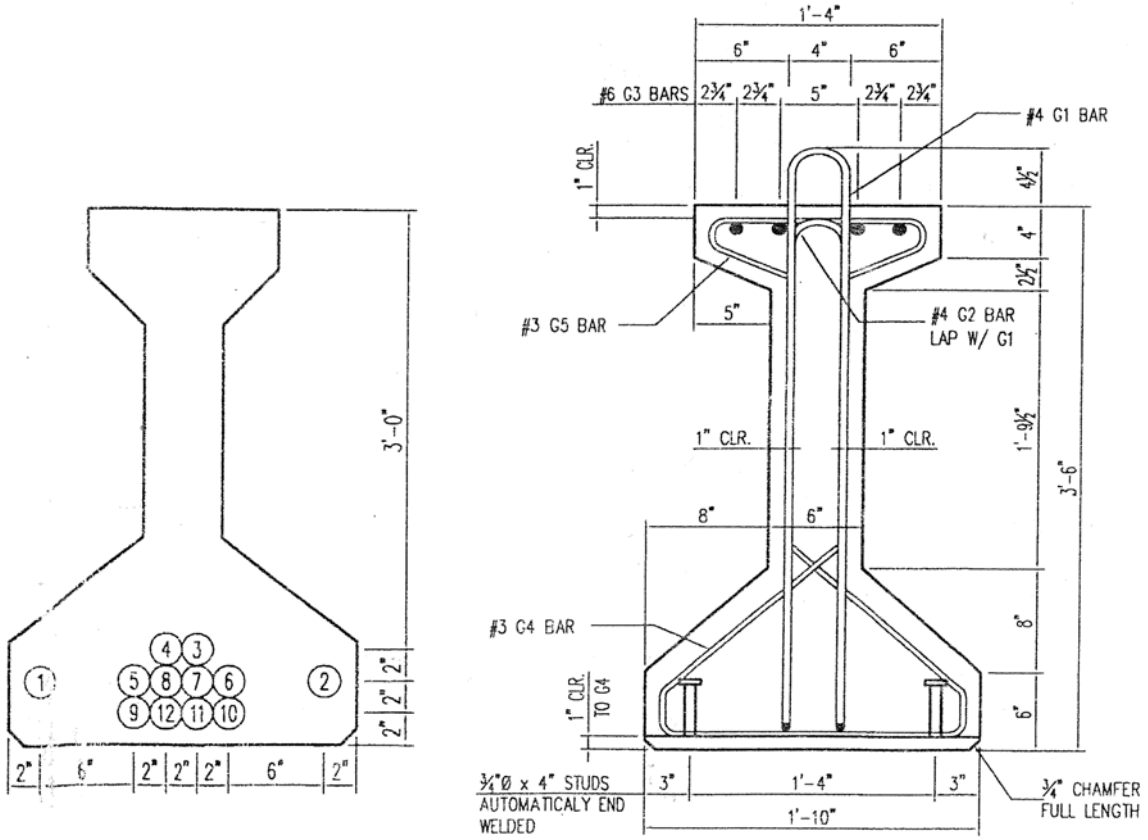

Figure B.6: Strand pattern and cross-section geometry for I-girders

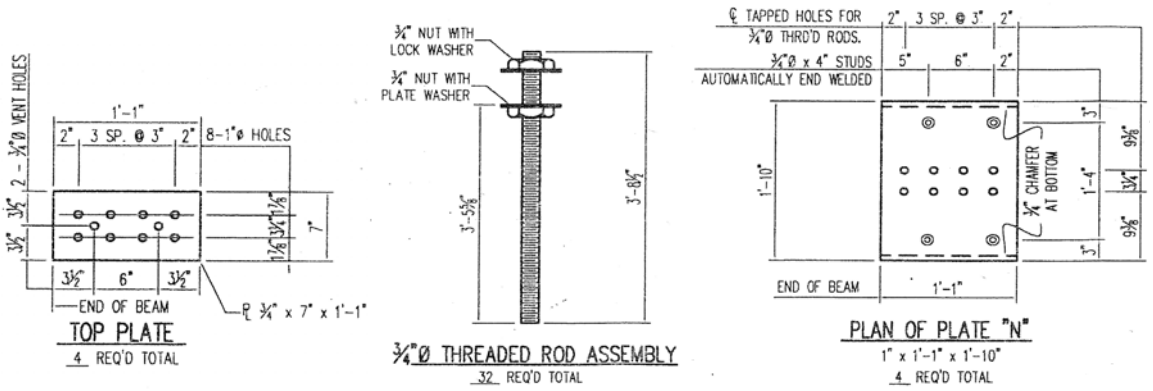

Figure B.7: Hardware details for I-girders

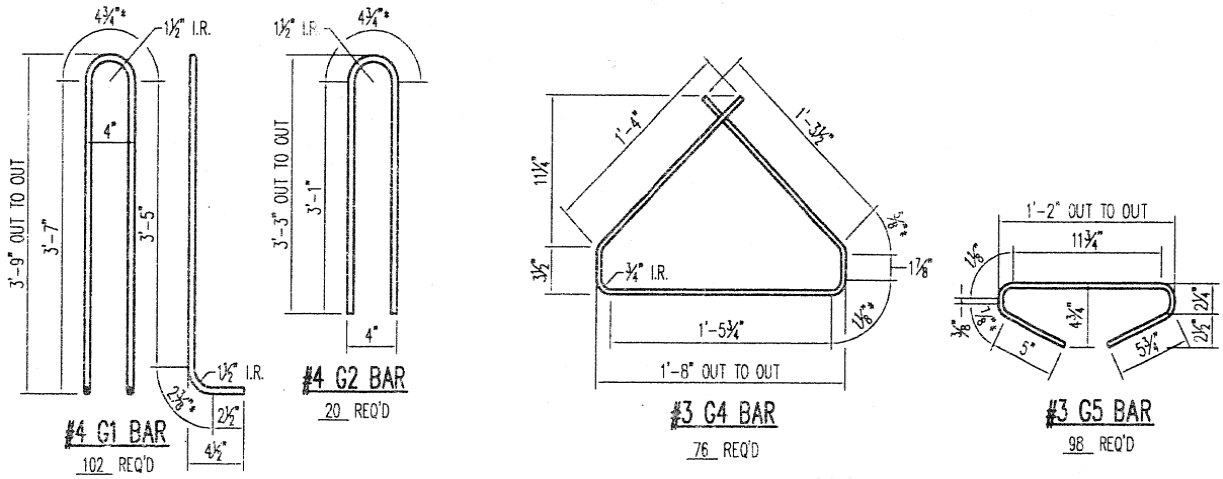

REINFORCEMENT BARS – ALL BEAMS						
BAR	SIZE	REQ'D	*LENGTH	SHAPE	REQ'D	LBS.
G1	#4	51	8'-1"	⊓L	102	551
G2	#4	10	6'-7"	⊓	20	88
G3	#6	8	25'-3"	—	16	607
G4	#3	38	4'-8"	⌂	76	133
G5	#3	49	2'-3"	⊐	98	83
G6	#8	4	4'-6"	—	8	96

Figure B.8: Reinforcement specifications for I-girders

APPENDIX C: STRAIN PROFILES FOR 95% AMS TRANSFER LENGTH

This appendix contains all strain readings recorded for the transfer length measurements described in Chapter 5. Each of the following figures contains the smoothed strain profiles generated for one location of one specimen at all testing ages. Figures C.1-C.4 show profiles for specimen Box-1; Figures C.5-C.8 show profiles for specimen Box-2; Figures C.9-C.12 show profiles for specimen I-1; Figures C.13-C.16 show profiles for specimen I-2.

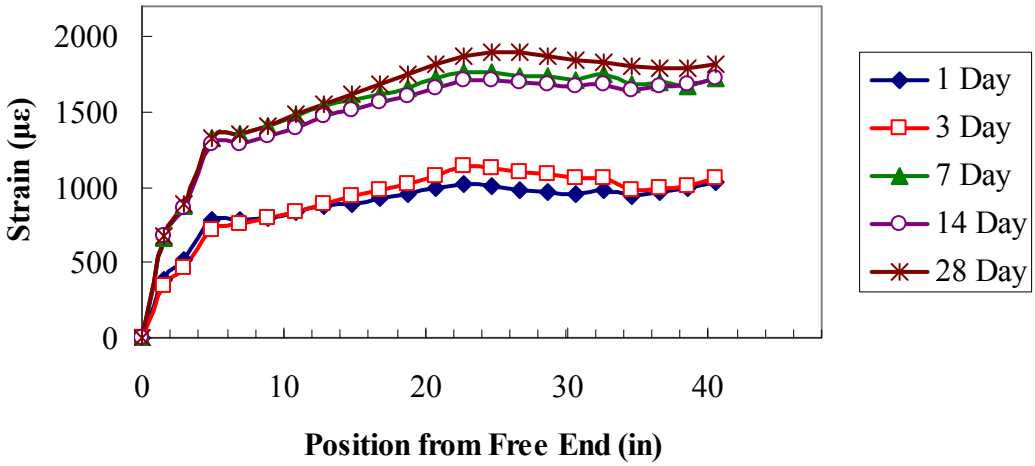

Figure C.1: Strain readings at Box-1, Starting End, Side A

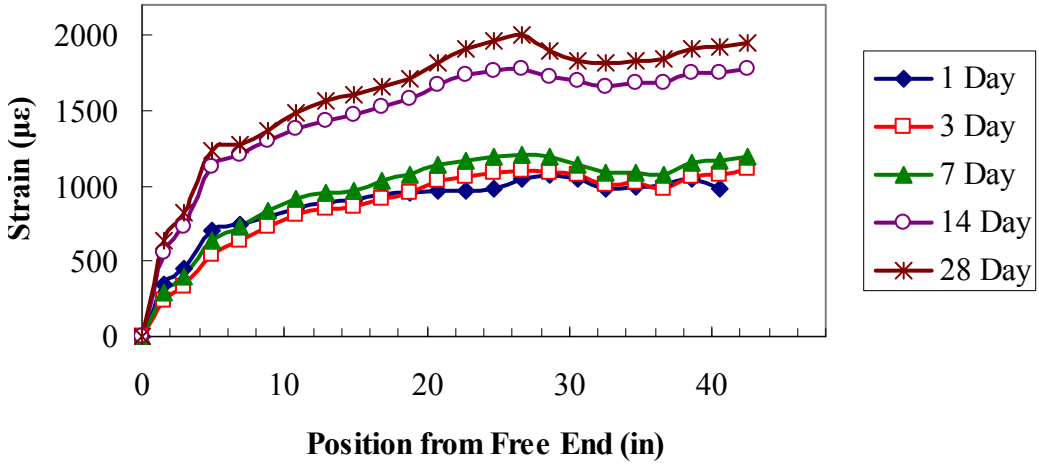

Figure C.2: Strain readings at Box-1, Starting End, Side D

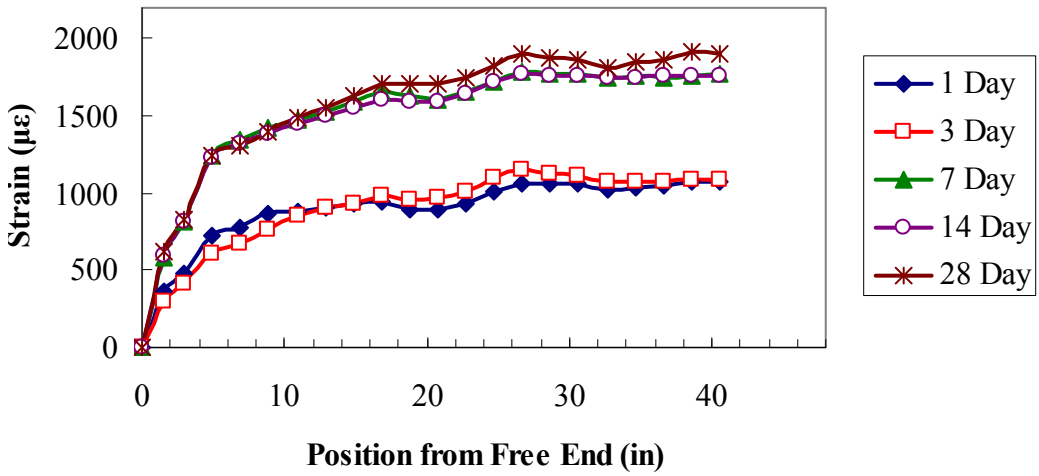

Figure C.3: Strain readings at Box-1, Far End, Side B

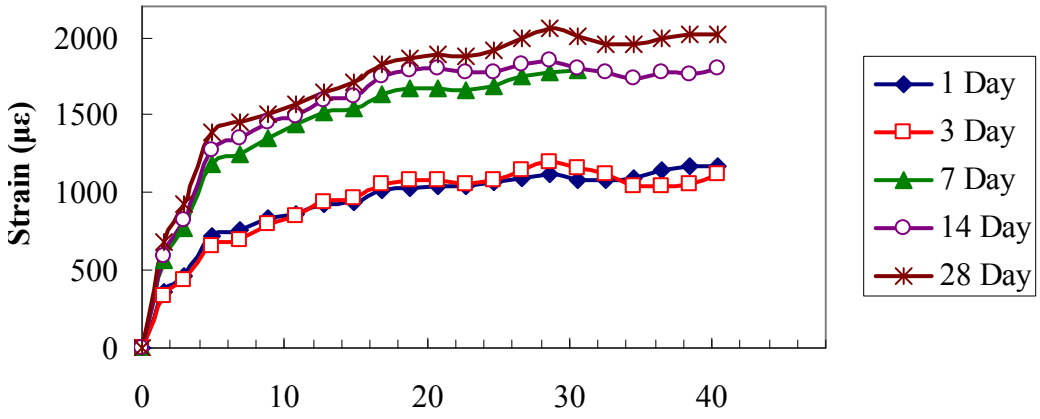

Figure C.4: Strain readings at Box-1, Far End, Side C

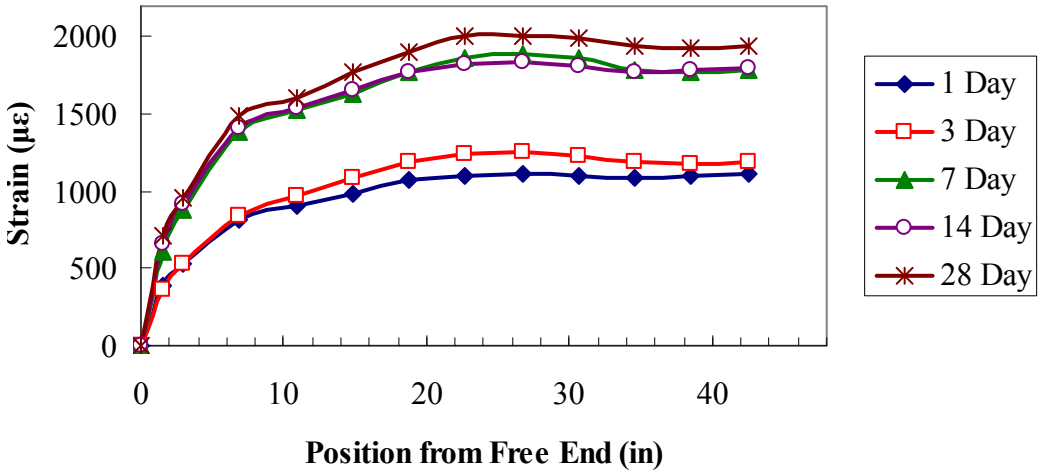

Figure C.5: Strain readings at Box-2, Starting End, Side A

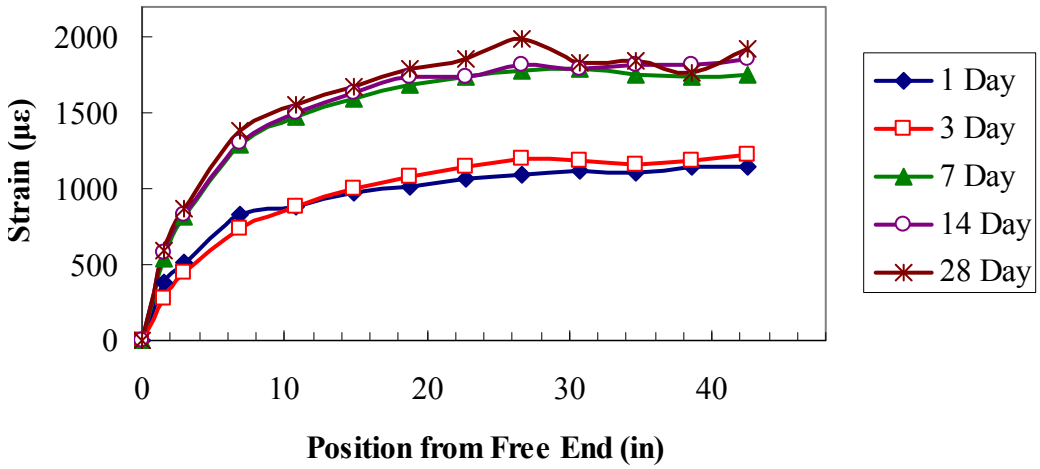

Figure C.6: Strain readings at Box-2, Starting End, Side D

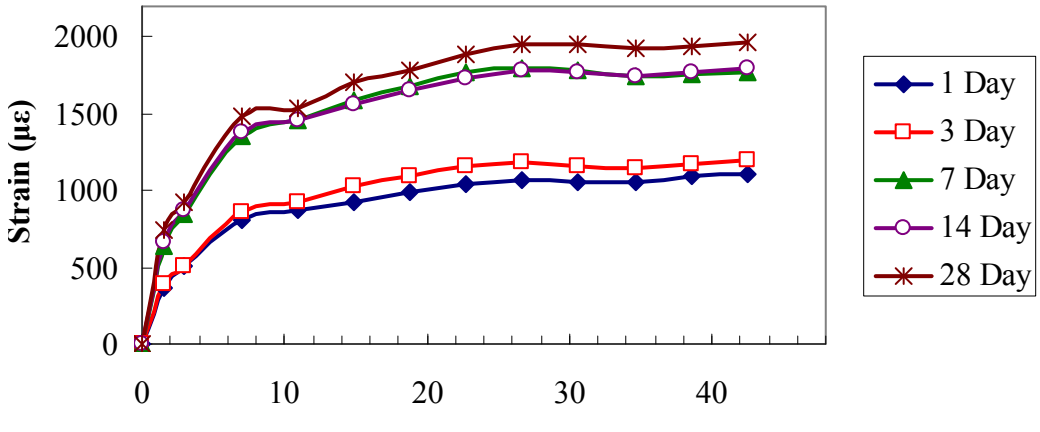

Figure C.7: Strain readings at Box-2, Far End, Side B

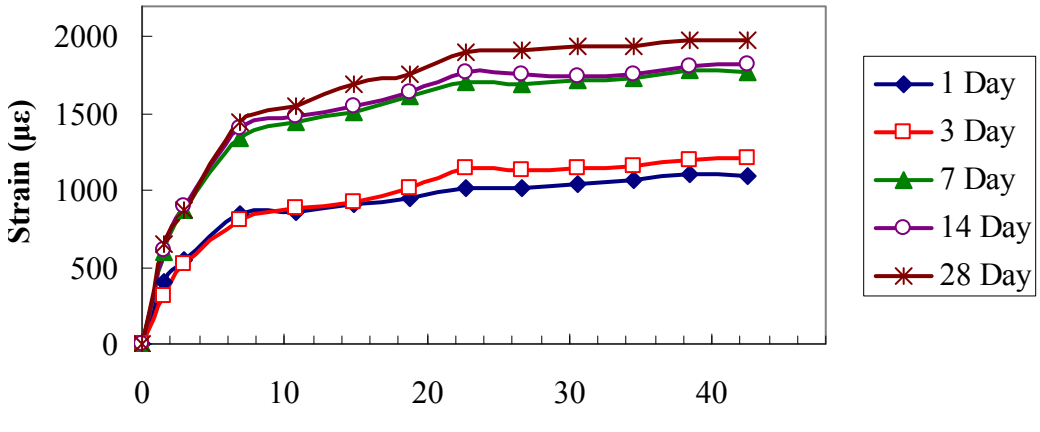

Figure C.8: Strain readings at Box-2, Far End, Side C

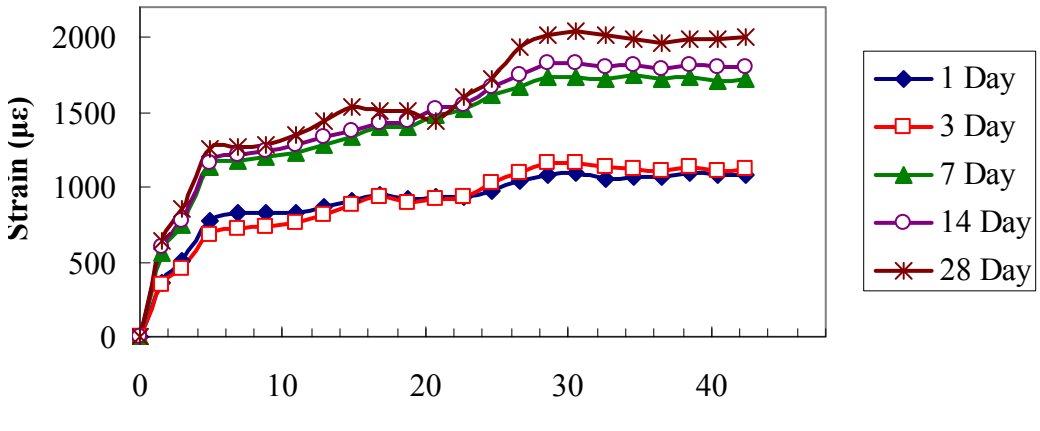

Figure C.9: Strain readings at I-1, Starting End, Side B

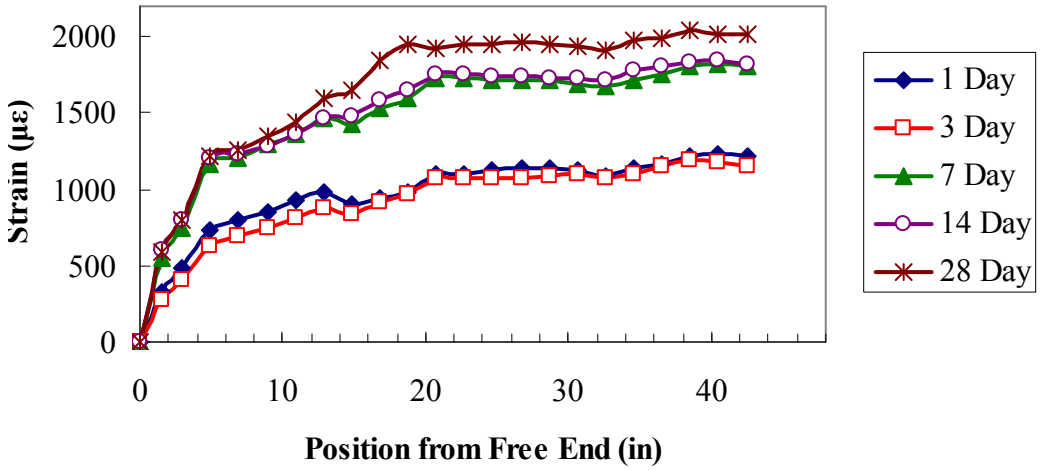

Figure C.10: Strain readings at I-1, Starting End, Side C

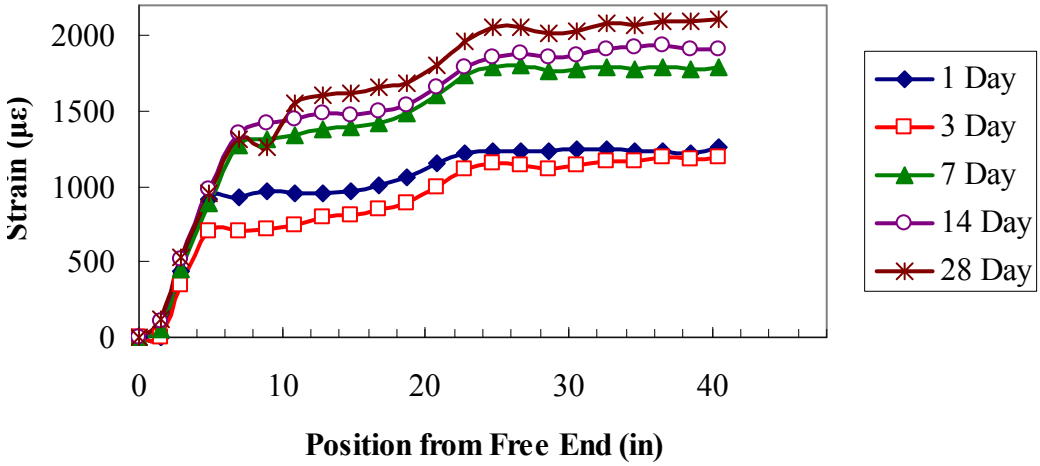

Figure C.11: Strain readings at I-1, Far End, Side A

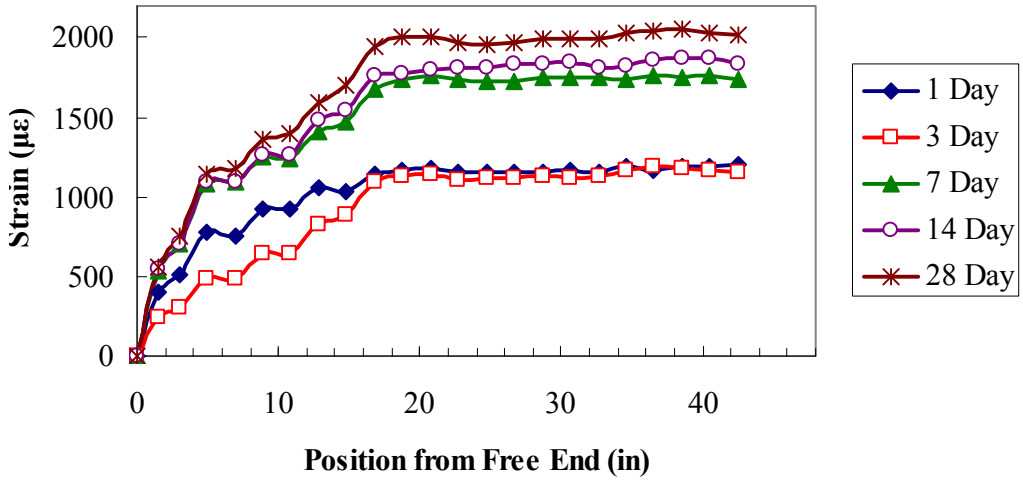

Figure C.12: Strain readings at I-1, Far End, Side D

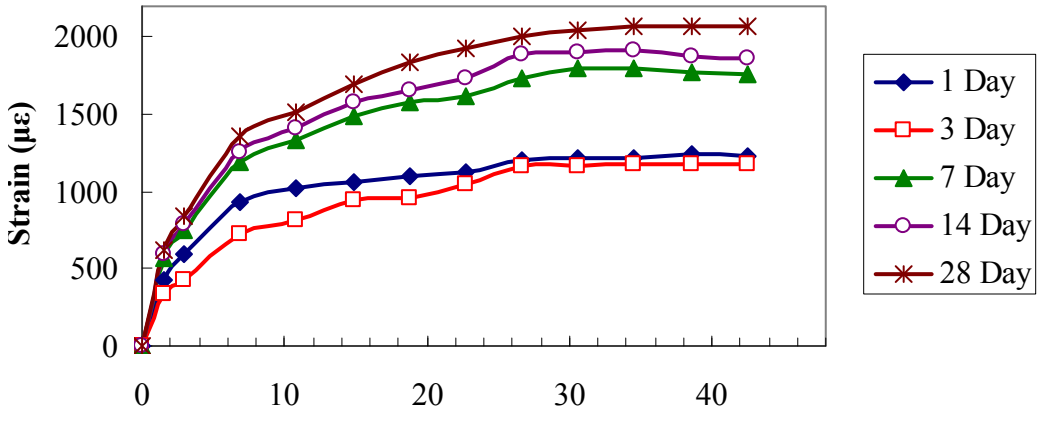

Figure C.13: Strain readings at I-2, Starting End, Side B

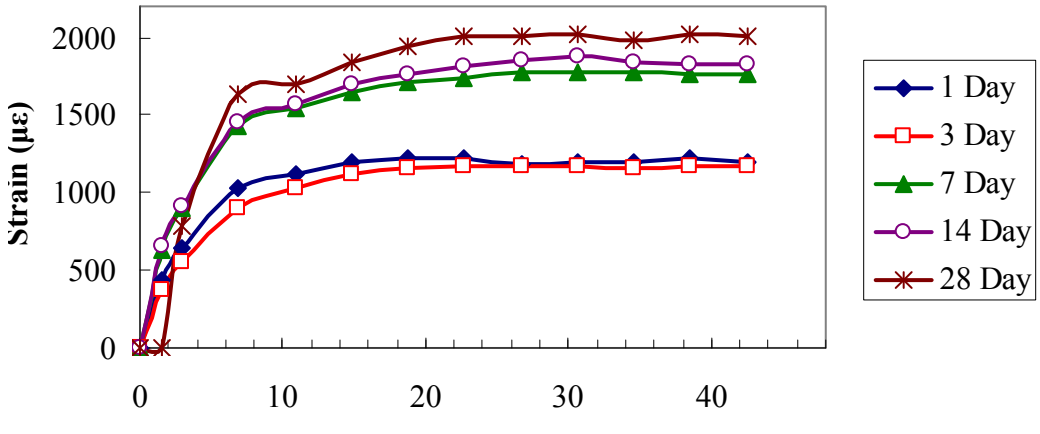

Figure C.14: Strain readings at I-2, Starting End, Side C

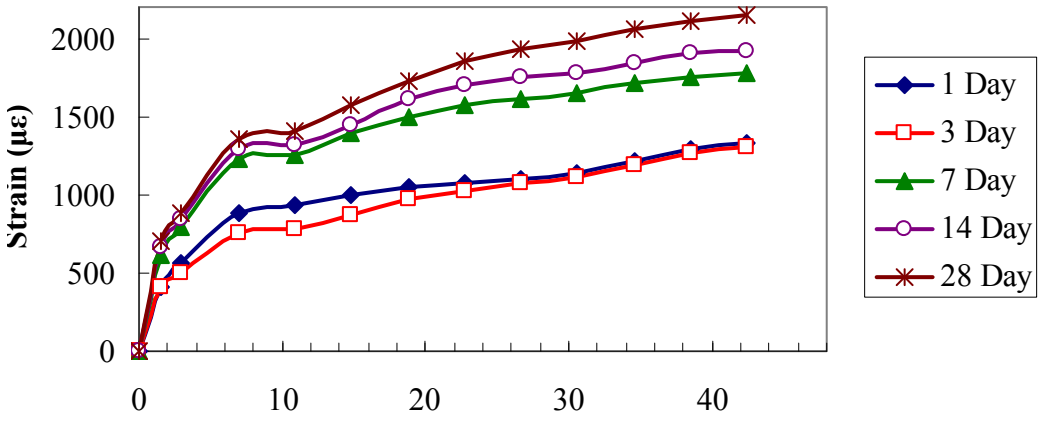

Figure C.15: Strain readings at I-2, Far End, Side A

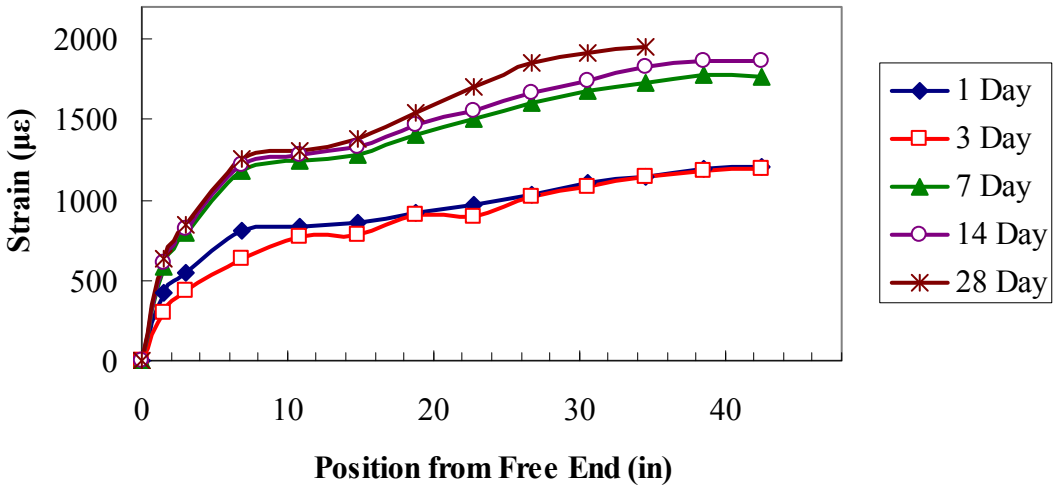

Figure C.16: Strain readings at I-2, Far End, Side D

APPENDIX D: CRACK PATTERNS FOR FLEXURAL TESTS

Figure D.1. Crack pattern for Box-1, South End, Side A.

Figure D.2. Crack pattern for Box-1, South End, Side D.

Figure D.3. Crack pattern immediately prior to failure for Box-1, North End, Side C.

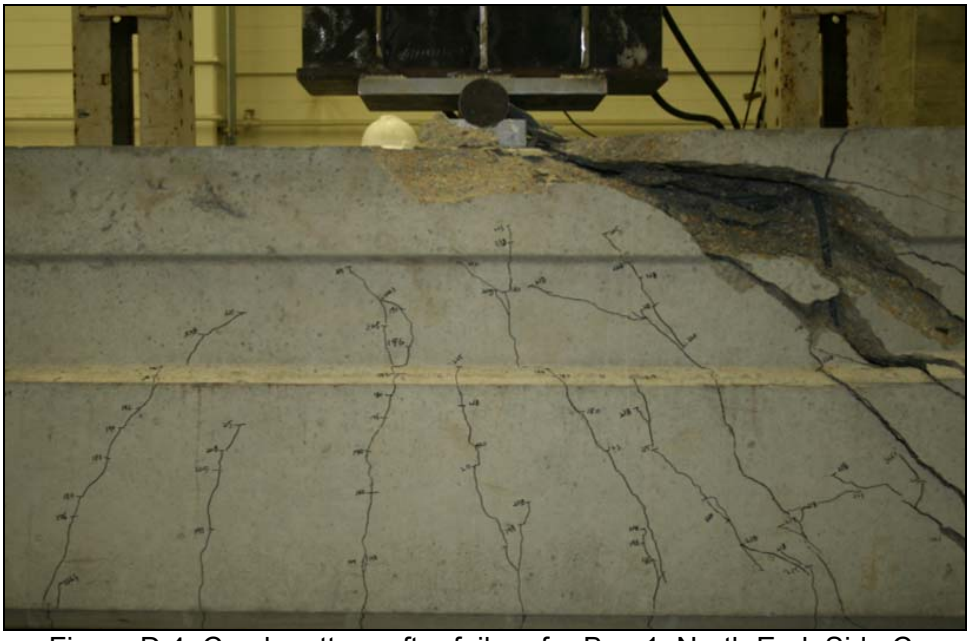

Figure D.4. Crack pattern after failure for Box-1, North End, Side C.

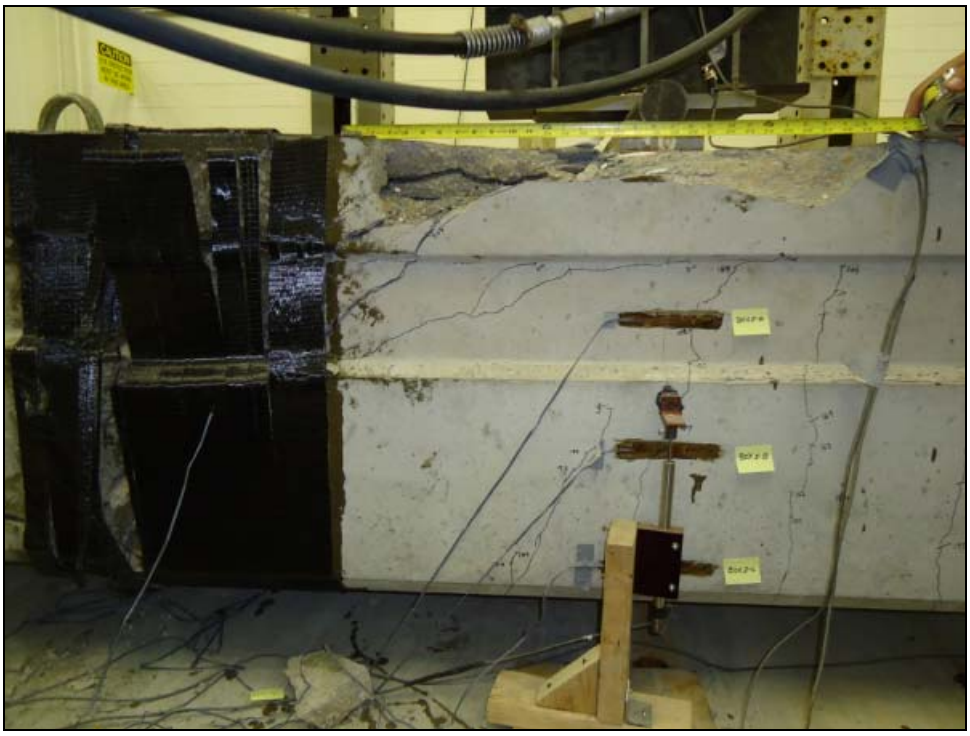

Figure D.5. Crack pattern after failure for Box-2, South End, Side D.

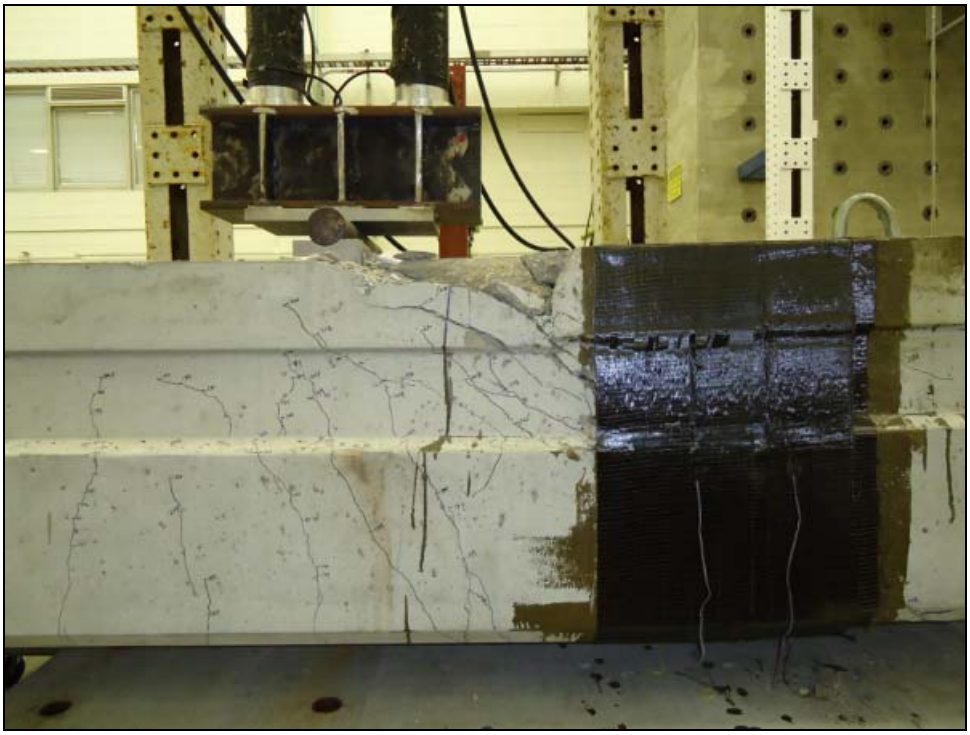

Figure D.6. Crack pattern after failure for Box-2, South End, Side A.

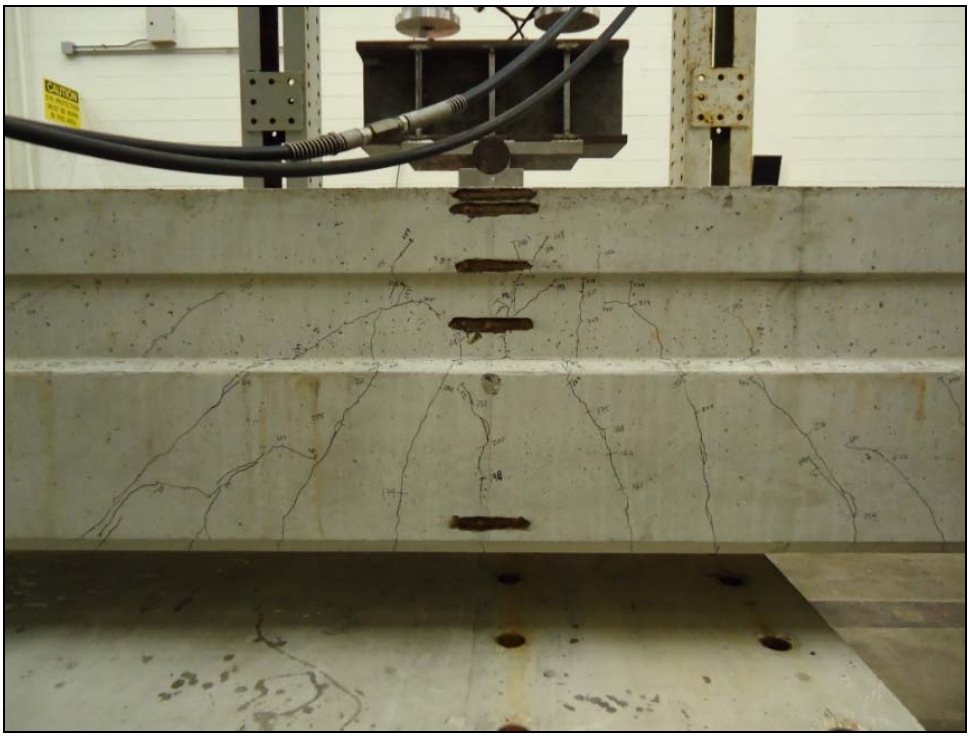

Figure D.7. Crack pattern for Box-2, North End, Side B.

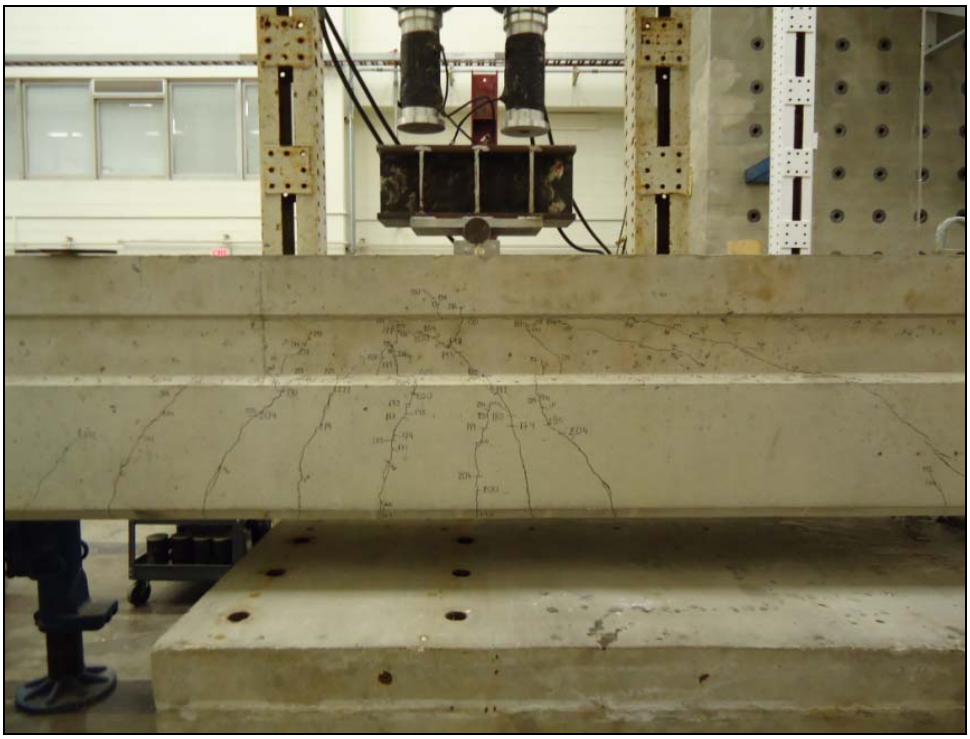

Figure D.8. Crack pattern for Box-2, North End, Side C.

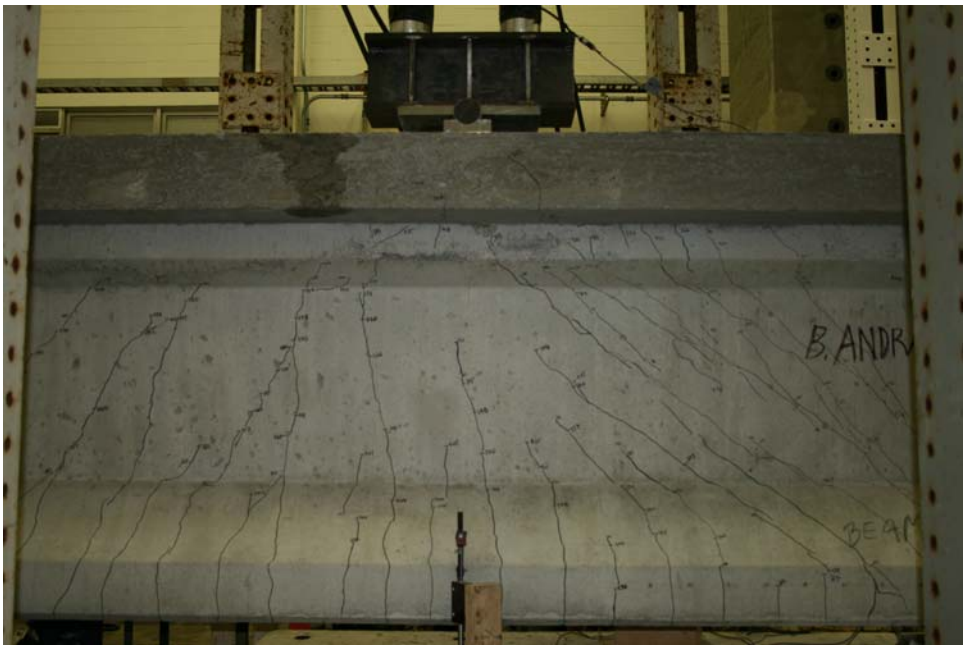

Figure D.9. Crack pattern for I-2, South End, Side A.

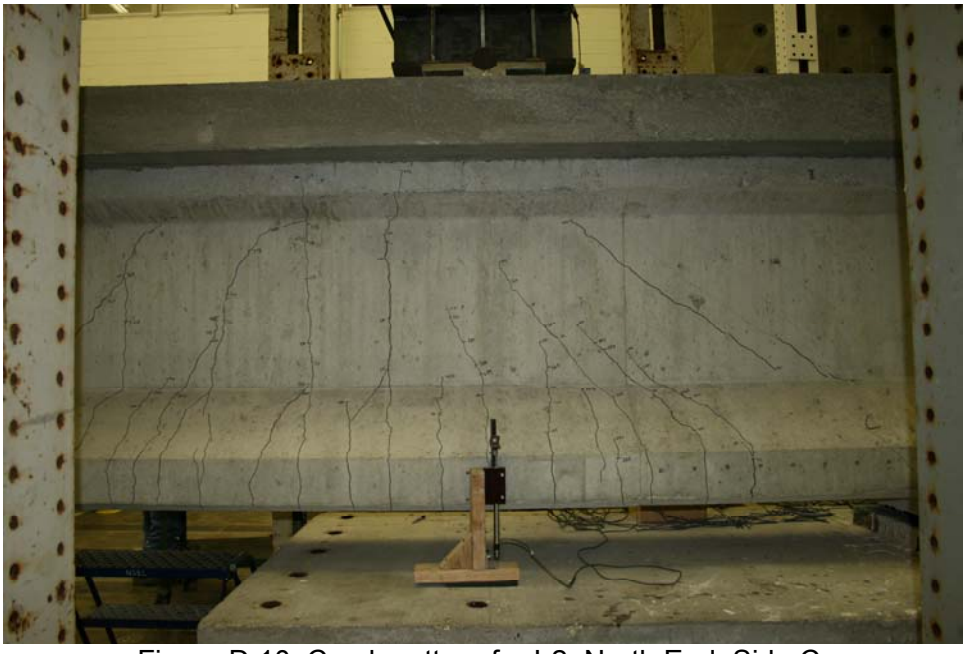
Figure D.10. Crack pattern for I-2, North End, Side C.